FORMATION PORE PRESSURE PREDICTION BY SEISMIC

DATA IN SAN SAI OILFIELD, FANG BASIN

Adisorn Sridej

A Thesis Submitted in Partial Fulfillment of the Requirements for the

Degree of Master of Engineering in Geotechnology

Suranaree University of Technology

Academic Year 2011

การคาดการณ์ความดันของชั้นหินจากข้อมูลที่ได้จากการสำรวจ
คลื่นไหวสะเทือนในแหล่งน้ำมันสันทราย แอ่งฝาง

นายอดิศร ศรีเดช

วิทยานิพนธ์นี้เป็นส่วนหนึ่งของการศึกษาตามหลักสูตรปริญญาวิศวกรรมศาสตรมหาบัณฑิต
สาขาวิชาเทคโนโลยีธรณี
มหาวิทยาลัยเทคโนโลยีสุรนารี
ปีการศึกษา 2554

FORMATION PORE PRESSURE PREDICTION BY
SEISMIC DATA IN SAN SAI OILFIELD, FANG BASIN

Suranaree University of Technology has approved this thesis submitted in partial fulfillment of the requirements for a Master's Degree.

Thesis Examining Committee

_____

(Assoc. Prof. Kriangkrai Trisarn)

Chairperson

_____

(Dr. Akkhapun Wannakomol)

Member (Thesis Advisor)

_____

(Dr. Chongpan Chonglakmani)

Member

_____   _____

(Prof. Dr. Sukit Limpijumnong)   (Assoc. Prof. Flt. Lt. Dr. Kontorn Chamniprasart)

Vice Rector for Academic Affairs   Dean of Institute of Engineering

อดิศร ศรีเดช : การคาดการณ์ความดันของชั้นหินจากข้อมูลที่ได้จากการสำรวจคลื่น
ไหวสะเทือนในแหล่งน้ำมันสันทราย แอ่งฝาง (FORMATION PORE PRESSURE
PREDICTION BY SEISMIC DATA IN SAN SAI OILFIELD, FANG BASIN)
อาจารย์ที่ปรึกษา : อาจารย์ ดร. อัฆพรรค์ วรรณโกมล, 165 หน้า.

ความดันภายในช่องว่างของเนื้อหินนั้นสัมพันธ์กับแรงกดทับของตัวหิน ซึ่งสามารถ
คำนวณได้จากค่าความเร็วของคลื่นตามยาวจากข้อมูลการสำรวจคลื่นไหวสะเทือน การศึกษานี้มี
วัตถุประสงค์เพื่อคาดการณ์ความดันของชั้นหินในแอ่งฝาง จังหวัดเชียงใหม่ ประเทศไทย โดยใช้
ข้อมูลจากการสำรวจคลื่นไหวสะเทือน ขั้นตอนการศึกษาหลักของการศึกษานี้คือ 1.) การรวบรวม
ข้อมูลที่เกี่ยวข้อง ประกอบด้วย ข้อมูลเวลาที่ใช้ในการเดินทางผ่านชั้นหินของคลื่นเสียง ข้อมูล
ความดันอันเนื่องมาจากน้ำหนักกดทับด้านบน และข้อมูลความดันของของไหลในหลุมเจาะ ของ
แหล่งน้ำมันสันทราย ซึ่งอยู่ในแอ่งฝาง 2.) การสร้างเส้นแนวโน้มของการอัดตัวปกติของชั้นหิน
จากข้อมูลเวลาที่ใช้ในการเดินทางผ่านชั้นหินของคลื่นเสียง ซึ่งได้จากการสำรวจคลื่นไหวสะเทือน
และ 3.) การคาดการณ์ความดันของชั้นหินโดยใช้วิธีของอีตัน ผลที่ได้จากการคำนวณหาความดัน
ภายในช่องว่างของเนื้อหินพบว่า ค่าความดันภายในช่องว่างของเนื้อหินต่อความลึกของพื้นที่ศึกษา
อยู่ในช่วงระหว่าง 0.434 ถึง 0.452 ปอนด์/ตารางนิ้ว/ฟุต และค่าความคลาดเคลื่อนเฉลี่ยของการ
คำนวณด้วยวิธีนี้ เมื่อคิดเป็นเปอร์เซ็นต์เฉลี่ยอยู่ที่ 1.24 ถึง 4.87 เปอร์เซ็นต์ ซึ่งข้อมูลการคาดการณ์
ความดันชั้นหินที่ได้จากการศึกษานี้สามารถนำไปใช้เพื่ออ้างอิงสำหรับการวางแผนการขุดเจาะใน
บริเวณพื้นที่แอ่งฝางในอนาคตได้ต่อไป

สาขาวิชา __เทคโนโลยีธรณี__   ลายมือชื่อนักศึกษา _____
ปีการศึกษา 2554   ลายมือชื่ออาจารย์ที่ปรึกษา _____

ADISORN SRIDEJ : FORMATION PORE PRESSURE PREDICTION

BY SEISMIC DATA IN SAN SAI OILFIELD, FANG BASIN.

THESIS ADVISOR : AKKHAPUN WANNAKOMOL, Ph.D., 165 pp.

PORE PRESSURE PREDICTION/SEISMIC DATA/SAN SAI OILFIELD/FANG BASIN

Pore pressure is related to the stress of formation which can be calculated by compressional wave velocity from seismic exploration data. The objective of this study is to predict formation pore pressure in San Sai oilfield, Fang basin, located in Chiang Mai Province, Northern Thailand, by using seismic data. The main activities in this study are: (1) required data collecting, including seismic travel time data, overburden pressure data and hydrostatic pressure of San Sai oilfield located in Fang basin, (2) normal compaction trend generating from p-wave transit time, and (3) formation pore pressure predicting by using the Eaton's method of pressure prediction. Result from calculated pore pressure indicated that pore pressure gradient in study area is in range between 0.434 and 0.452 psi/ft and erroneous percentage of this method is in range between 1.24% and 4.87%. Thus the predicted formation pore pressure data that obtained from this study will be informatively supported for drilling plan in Fang basin in the future.

School of Geotechnology   Student's Signature _____

Academic Year 2011   Advisor's Signature _____

ACKNOWLEDGEMENTS

TABLE OF CONTENTS

Page

TABLE OF CONTENTS (Continued)

LIST OF TABLES

LIST OF TABLES (Continued)

LIST OF TABLES (Continued)

LIST OF TABLES (Continued)

LIST OF TABLES (Continued)

LIST OF TABLES (Continued)

LIST OF TABLES (Continued)

Table   **Page**

LIST OF FIGURES

LIST OF FIGURES (Continued)

LIST OF FIGURES (Continued)

LIST OF FIGURES (Continued)

LIST OF FIGURES (Continued)

LIST OF FIGURES (Continued)

LIST OF FIGURES (Continued)

LIST OF FIGURES (Continued)

LIST OF FIGURES (Continued)

Figure   **Page**

SYMBOLS AND ABBREVIATIONS

%	=	Percent
^{o}C	=	Degree Celsius
^{o}F	=	Degree Fahrenheit
$	=	US Dollar
1-D	=	One dimensional
2-D	=	Two dimensional
ft	=	Foot
gal	=	Gallon
Ibm	=	Pound (mass)
m	=	Meter
NNE	=	North-Northeast
P-wave	=	Primary wave
PFG	=	Fluid pressure gradient
psi	=	Pounds per square inch
RFT	=	Repeat Formation Test
sec	=	Second
msec	=	Millisecond
µsec	=	Microsecond
Sh	=	Shale
SSW	=	South-Southwest

CHAPTER I

INTRODUCTION

1.1   Rationale and background

Pore pressure is defined as the fluid pressure in the pore space of the rock matrix. In a geologic setting with perfect communication between the pores, the pore pressure is the hydrostatic pressure due to the weight of the fluid. Hydrostatic pressure is often referred to normal pressure conditions. Conditions that deviate from normal pressure are said to be either overpressured or underpressured, depending on whether the pore pressure is greater than or less than the normal pressure. The term "geopressure" is often used to describe abnormally high pore fluid pressures. Knowledge of the pore pressure in an area is important for several reasons. In overpressured zones, there is often little difference between the fluid pressure and the reservoir fracture pressure. In order to maintain a safe and controlled drilling, the mud weight must lie in this interval (i.e. between fluid pressure and fracture pressure). If a too low mud weight is used (underbalanced drilling) while drilling through high pressure zones, well kick is normally occurred and it is danger. In rare cases one might encounter dangerous blowouts, although the risk of this is significantly reduced during the last decade thanks to modern equipment. If the mud weight is too high, the formation fracture pressure is exceeded, and the drill pipe may be stuck. In either case, valuable operation time is lost.

1.2   Research objective

The objective of this thesis is to calculate pore pressure gradient by using seismic data which had been run in Fang basin, Chiang Mai Province (Figure 1.1). The result from this study can be used for pore pressure predicting and apply to the drilling program for new well drilling in the study area.

1.3   Scope and limitation of the study

The Scope and limitations of this thesis are listed as follows;

1.3.1   The data used in this thesis based only on seismic data run in Fang basin.

1.3.2   A calculated pore pressure can specifically predict pore pressure gradient only in Fang basin.

1.3.3   Due to limitation in sonic velocity data available, calculated pore pressure can predicted only on the normal pressure trend.
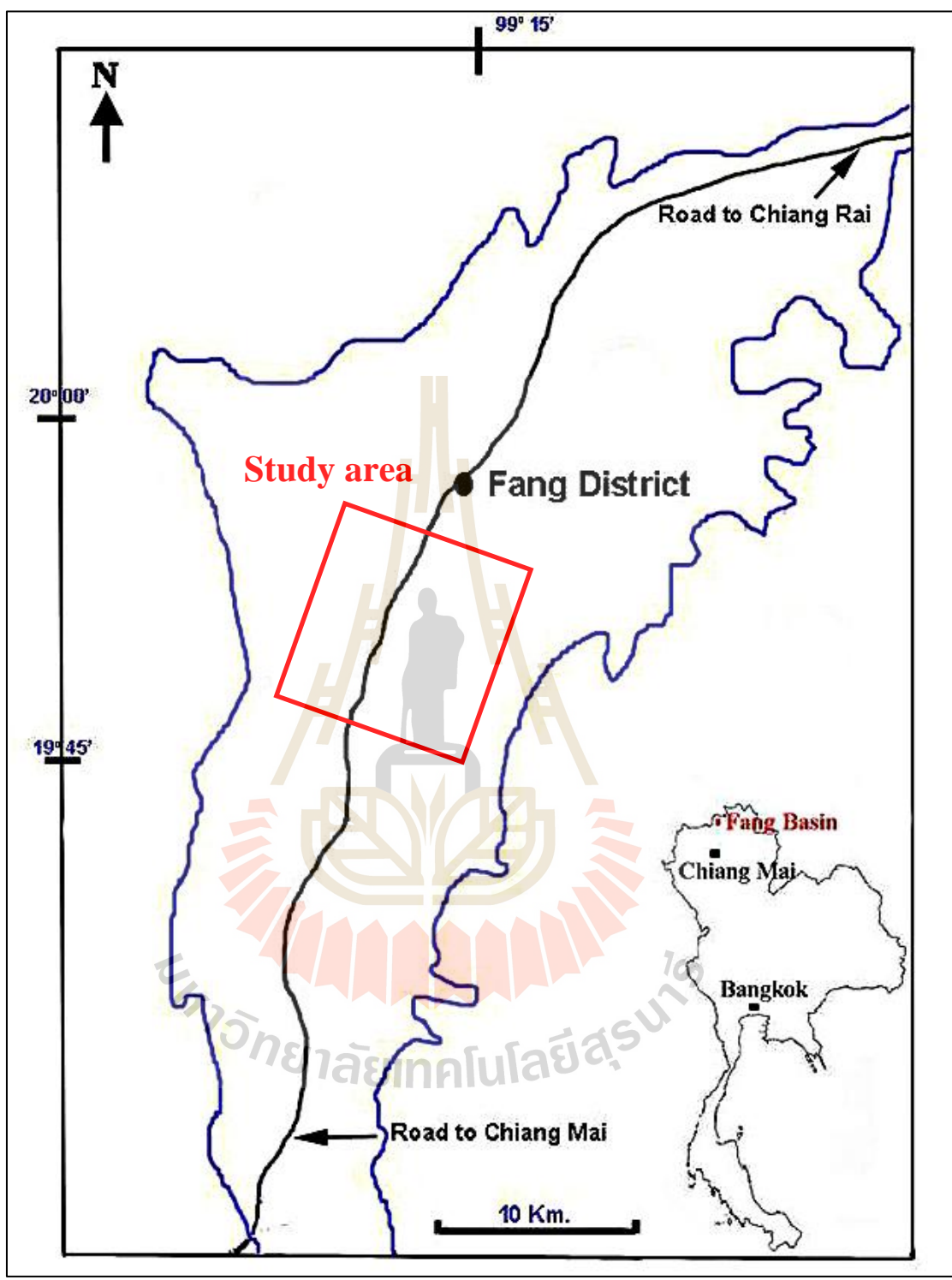
Figure 1.1 Location of study area in Fang basin, Chiang Mai, Thailand

CHAPTER II

LITERATURE REVIEW

2.1   Pore pressure

Pore pressure is defined as the fluid pressure in the pore space of the rock matrix. In a geologic setting with perfect communication between the pores, the pore pressure is the hydrostatic pressure due to the weight of the fluid. The pore pressure at depth z can then be computed as (Bourgoyne $et\ al.$, 1986):

$$p(z) \quad = \quad \int_{z_0}^{z} \rho(z)gzdz + p_0 \tag{2.1}$$

where $\rho(z)$ = fluid density (Ibm/gal),

g = gravitational acceleration (ft/s^2)

p_0 = pressure at depth z_0, usually atmospheric pressure (psi).

Hydrostatic pressure is often referred to as normal pressure conditions. Conditions that deviate from normal pressure are said to be either overpressured or underpressured, depending on whether the pore pressure is greater than or less than the normal pressure. The term "geopressure" is often used to describe abnormally high pore fluid pressures.

The concept of abnormal pressure, especially geopressure, is most important in hydrocarbon exploration and production. Drilling through geopressure zones is

challenging, and requires extra care. As fields have matured, there is a rising demand in the industry to explore areas that previously were regarded as too technically challenging. This includes deepwater areas, which are often associated with high pore pressures. Dutta (2002b) reports that the industry will spend about $100 billion in hydrocarbon exploration and production in deepwater areas over a five-year period, beginning in 2001. In the North sea it is estimated that each deep-drilled well (high-temperature, high-pressure well) on average gives 2 kicks related to high pore pressures.
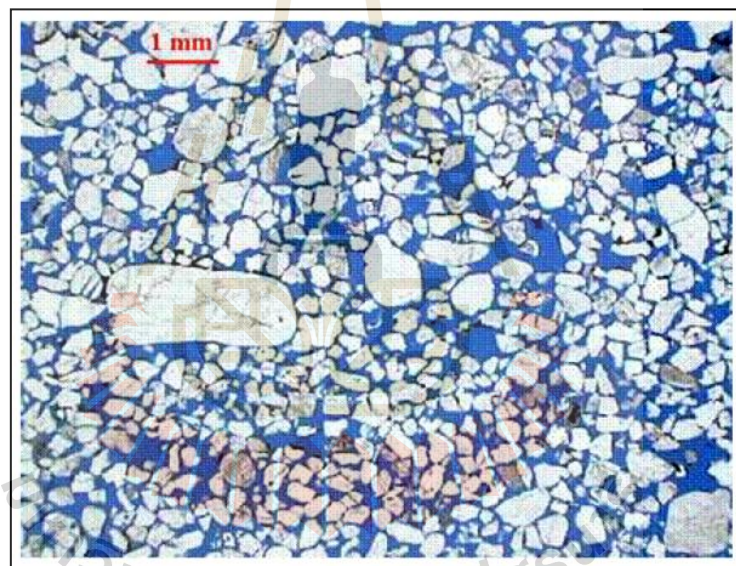
Figure 2.1 Pore space in sandstone (blue color) (Øyvind Kvam, 2005)

High pore pressures have been observed at drilling sites all over the world, both on- and offshore. The frequently encountered overpressures in the Gulf of Mexico have been particularly well studied and observed, since this is an important area of hydrocarbon production, but the phenomenon have been observed in many other places, including the North Sea, the Caspian Sea, Pakistan and the Middle East

(Fertl, 1976). The nature and origin of pore pressures are manifold and complex. The demands for better understanding and pre-drill prediction of pore pressure are substantial. The industry spends considerable sums on research, and the efforts have paid off.

In order to investigate the nature of abnormal pore pressures some practical definitions have been made. The overburden pressure is defined as the combined weight of sediments and fluid overlying a formation. Mathematically, the overburden pressure can be defined as (Bourgoyne *et al.*, 1986):

$$S(z) = \int_{z_0}^{z} \rho(z) g \, dz \tag{2.2}$$

and

$$\rho(z) = \phi(z) \rho_f(z) + (1 - \phi(z)) \rho_m(z) \tag{2.3}$$

where ϕ = porosity,

ρ_f = fluid density (Ibm/gal)

ρ_m = rock matrix density (Ibm/gal).

If the density is known, the overburden pressure can be measured.

The effective pressure is defined as (Fjær, *et al.*, 1989):

$$P_e \quad = \quad S - nP \tag{2.4}$$

where P_e =   effective pressure (psi),

       P =   pore fluid pressure (psi)

       n =   Biot coefficient.

For static compression of the rock frame, the Biot coefficient is defined as (Fjær, *et al.*, 1989):

$$n \quad = \quad 1 - \frac{K_{fs}}{K_s} \tag{2.5}$$

where K_{fs} is the bulk modulus of the rock frame (psi) and K_s is the bulk modulus of the mineral that the rock is composed of (psi). For soft materials, $n = 1$

It is also convenient to define the pressure gradient G, which strictly speaking is not really a gradient, but an engineering term. The pressure gradient is simply defined as the ratio of pressure to depth. Pressure gradients can describe overburden, fluid and effective pressures. As an example, in the Gulf of Mexico, the overburden gradient is found to be very close to 1 psi/ft, while normal pressure conditions (i.e. hydrostatic pressure) correspond to a fluid pressure gradient of about 0.465 psi/ft (Dutta, 1987).

From the definitions above it is clear that a high pore pressure will give a correspondingly low effective pressure. The degree of overpressure may in extreme cases be such that the effective pressure equals zero, and in some rare cases even is less than zero. Table 2.1 summarizes degrees of pressures encountered based on experience from the Gulf of Mexico, as given in Dutta (1987).

Table 2.1 Geopressure characterization according to Dutta (1987).

Fluid pressure gradient (Psi/ft)	Geopressure characterization
$0.465 < G < 0.65$	soft or mild
$0.65 < G < 0.85$	intermediate or moderate
$G > 0.85$	hard

According to Fertl (1976) all occurrences of overpressure in the subsurface are associated with a permeability barrier that simultaneously acts as a pressure barrier. This barrier prevents fluid to flow along a pressure gradient. The nature of such a seal can differ greatly at different localities. Low permeability shales have often been observed to act as pressure barriers, but also faults can form such barriers.

The processes in which high pressures develop in the vicinity of the pressure barriers are complex. Smith (1971) described how high pressures can develop in areas where there have been rapid depositions of sediments, allowing seals to form before excess fluid has escaped from deeper layers. The increasing weight of the overburden will tend to decrease the porosity, and hence the pore space. However, if the formation is sealed, the fluid has nowhere to escape and starts to carry some of the weight of the overburden. The result is that the fluid pressure is increased. This process is often termed "undercompaction" or "compaction disequilibrium", and is one of the major causes of abnormally high pore pressures (Dutta, 2002).

Tectonic activity may also cause high pressures. Physical deformation of geological formations may for instance change the volume in which the sealed-off pore fluid exists, thus changing the pressure. Salt diapirism is an example of physical deformation of the subsurface. Areas where salt tectonism is frequent are often associated with high pore pressures (e.g., Gulf of Mexico).

2.2 Pore pressure prediction strategies

Bourgoyne *et al.* (1986) clearly summarized four mechanisms for generating abnormal pore pressures, or overpressures; Compaction, Diagenesis, Differential Density and Fluid Migration. The most common overpressure generating mechanism is compaction. When sediments are deposited in a deltaic depositional environment (the most common depositional environment) the sediments are initially unconsolidated and remain in suspension with the carrying fluid, typically sea water. As the depositional process continues, the sediments come into contact with each other and are able to support the weight of the sediments being deposited above them by the grain-to-grain contact points. Throughout this process, the formation continues to remain in hydraulic communication with the fluid source above. As the depositional process continues, the weight of the overlying sediments begins to compact the sediments, causing the sediments to realign, resulting in a reduced porosity and expulsion of fluid from the formation. As long as the pore fluid can escape as quickly as required by the natural compaction process, the formation pore space will remain in hydraulic communication with the fluid source and the pore pressure is solely the hydrostatic pressure generated from the density of the pore fluid. However, if the natural compaction process is faster than the rate of the pore fluid expulsion, abnormal formation pressures will be generated due to some of the load being placed upon the sediments being supported by the pressure in the pore fluids.

The second overpressure generating mechanism explained by Bourgoyne et al is diagenesis. Diagenesis is defined as the physical, chemical or biological alteration of sediments into sedimentary rock at relatively low temperatures and pressures that

can result in changes to the rock's original mineralogy and texture. It includes compaction, cementation, recrystallization, and perhaps replacement, as in the development of dolomite. In Gulf of Mexico sedimentary basins, one diagenetic process is the conversion of montmorillonite clays to illites, chlorites and kaolinite clays during compaction when in presence of potassium ions. Water is present in clay deposits as both free water and bound water. The bound water has significantly higher density. During diagenesis, as the bound water becomes free water, the higher density bound water must undergo a volume increase as it desorbs. If the free water is not allowed to escape (i.e. rapid compaction, precipitates caused from diagenesis, caprock, etc.), then the pore pressure will become abnormally pressured. Diagenesis typically occurs under bottomhole temperatures of at least 200 °F.

The third overpressure generating mechanism described by Bourgoyne *et al* is differential density. This mechanism occurs when a formation contains a pore fluid with a density significantly less than the normal pore fluid density for the area. If the structure has significant dip, then the extension of the structure up dip will result in higher pore pressure gradients than experienced down dip where the pressure gradient is known. Although the up dip pore pressure will be lower in absolute pressure, the pressure gradient will be higher requiring a higher hydrostatic gradient to control the pore pressure.

The fourth and final overpressure generation mechanism elucidated by Bourgoyne *et al* is fluid migration. This mechanism occurs when overpressured formations have a communication path to a normally pressured formation and the normally pressure formation becomes charged. The hydraulic communication path can be man-made or naturally occurring.

Karl Terzaghi (1943) developed a simple relationship between pore pressure and the effective stress of the rock. Even though his relationship was determined empirically, it was proven later that it can be derived analytically from 1-D compaction theory. Terzaghi noted: The stresses in any point of a section through a mass of soil can be computed from the total principal stresses σ_1, σ_2, σ_3, which act in this point. If the voids of the soil are filled with water under a stress μ, the total principal stress consists of two parts. One part, μ, acts in the water and in the solid in every direction with equal intensity. It is called the neutral stress (or the porewater pressure). The balance $\sigma_i = \sigma_i - \mu$ represents an excess over the neutral stress μ, and it has its seat exclusively in the solid phase of the soil. This fraction of the principal stress will be called the effective principal stress. A change in the neutral stress μ produces practically no volume change and has practically no influence on the stress conditions for failure. Porous materials (such as sand, clay and concrete) react to a change of μ as if they were incompressible and as if their internal friction were equal to zero. All the measurable effects of a change of stress, such as compression, distortion and a change of shearing resistance are exclusively due to changes in the effective stress σ'_i.

The above statement indicates that this is a conceptual stress. Only the effects of an effective stress change are measurable, not the effective stress itself. Terzaghi determined the following mathematical relationship: $\sigma_{ei} = \sigma_i - P_f$.

where P_f is the formation pressure (psi), σ_i is the principal stress (psi) and σ_{ei} is the effective vertical stress (psi)

Therefore, pore pressure can be calculated from the difference between principal and effective stresses acting in a given direction. In the case of drilling for oil and gas, the principal stress in the vertical direction is the overburden stress, which can be determined by a number of published correlations or by integration of the bulk density log data. The unknown variable is the corresponding conceptual effective stress. In general, overpressuring during the compaction process is associated with a slower porosity decrease with depth. If the assumption is made that vertical strains dominate during the compaction process, then Terzaghi's principle would imply that the effective vertical stress is the exclusive cause of shale porosity variations. Therefore, pore pressure is determined from the effective vertical stress and the overburden stress by the following relationship (Terzaghi, 1943):

$$P_f \quad = \quad \sigma_{OB} - \sigma_{EV} \quad\quad\quad (2.6)$$

where P_f =   formation pressure (psi)

σ_{OB} =   overburden stress (psi)

σ_{EV} =   effective vertical stress (psi)

One of the early papers published on pore pressure interpretation was authored by Hottman and Johnson. The authors included a description of the pore pressure, overburden stress and effective vertical stress relationship described by Terzaghi. They recognized the 10 significance of Terzaghi's relationship and developed an empirical relationship between fluid pressure gradient (FPG) and the electrical log properties. The data sets used for the development of the techniques were taken from Tertiary sediments located in Southern Louisiana and the Upper

Texas Gulf Coast. The geologic age of the acquired data set was Miocene and Oligocene.

The pore pressure and acoustic data used in the interpretation technique is included in Table 2.2.

Table 2.2 Pressure and acoustic log data – overpressured Miocene-Oligocene

Formations, South Louisiana and Upper Texas Gulf Coast per Hottman

and Johnson.

County and State	Well	Depth (ft)	Pressure (psi)	FPG (psi/ft)	$dT_{ob(sh)}$ - $dT_{n(sh)}$ (microsec/ft)
Terrebonne, La	1	13387	11647	0.87	22
Offshore Lafourche, La	2	11000	6820	0.62	9
Assumption, La	3	10820	8872	0.82	21
Offshore Vermillion, La	4	11900	9996	0.84	27
Offshore Terrebonne, La	5	13118	11281	0.86	27
East Baton Rouge, La	6	10980	8015	0.73	13
St. Martin, La	7	11500	6210	0.54	4
Offshore St. Mary, La	8	13350	11481	0.86	30
Calcasieu, La	9	11800	6608	0.56	7
Offshore St. Mary, La	10	13010	10928	0.84	23
Offshore St. Mary, La	11	13825	12719	0.92	33
Offshore Placquemines, La	12	8874	5324	0.60	5
Cameron, La	13	11115	9781	0.88	32
Cameron, La	14	11435	10292	0.90	38
Jefferson, Tx	15	10890	9910	0.91	39
Terrebonne, La	16	11050	8951	0.81	21
Offshore Galveston, Tx	17	11750	11398	0.97	56
Chambers, Tx	18	12080	9422	0.78	18

Data presented in Table 2.2 was plotted and showed in Figure 2.2. Figure 2.2 illustrates the relationship of the difference between the interval transit time of the observed shale and the interval transit time of the normally pressured shale section ($dT_{ob(sh)}$ - $dT_{n(sh)}$) values and Formation Pressure Gradient (FPG).
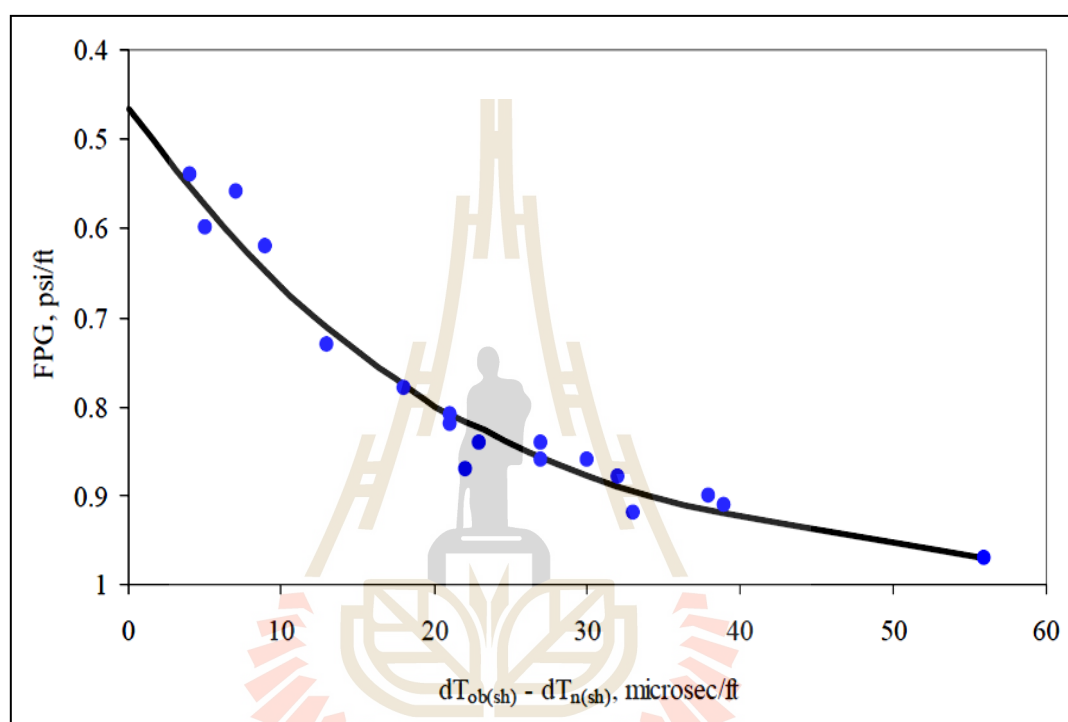
Figure 2.2 Relationship between shale acoustic parameter $dT_{ob(sh)}$ - $dT_{n(sh)}$ and reservoir FPG per Hottman and Johnson

To estimate pore pressure the following procedures had been developed when acoustic travel time data were known for shale formations.

1. The "normal compaction trend" for the area of interest is established by plotting the logarithm of $dT_{(sh)}$ vs. depth as showed in figure 2.3.

2. A similar plot is made for the well in question.

3. The top of the overpressured formation is found by noting the depth at which the plotted points diverge from the trendline.

4. The fluid pressure gradient of a reservoir at any depth is found as follows:

   4.1 The divergence of adjacent shales from the extrapolated normal line is measured.

   4.2 The fluid pressure gradient (FPG) corresponding to the ($dT_{ob(sh)}$ - $dT_{n(sh)}$) value is found using the solid black line in Figure 2.2.

5. The FPG value is multiplied by the depth to obtain reservoir pressure.
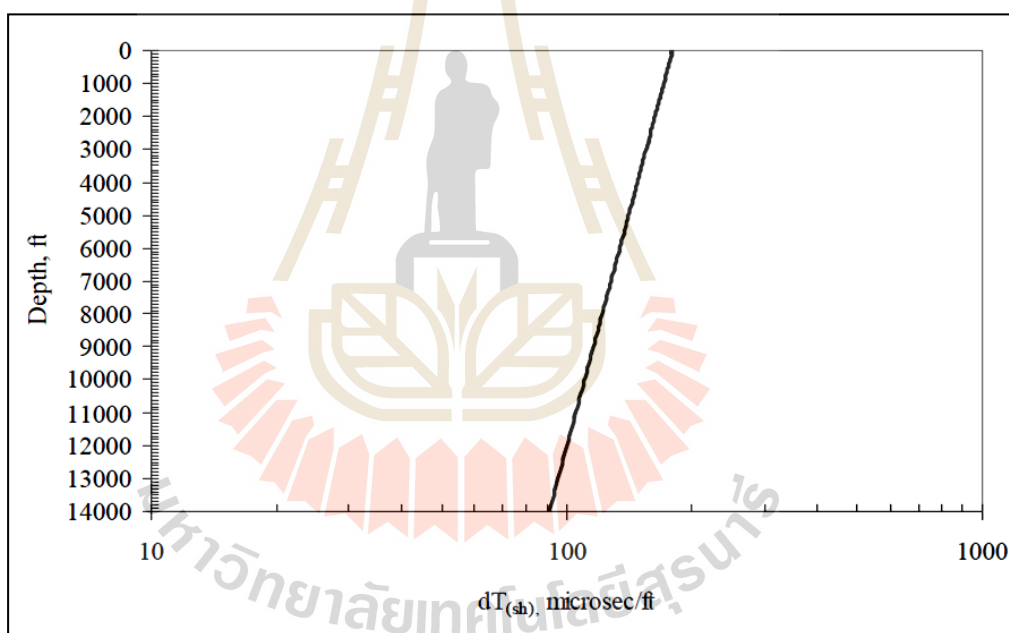
Figure 2.3 Shale travel time vs burial depth for Miocene and Oligocene Shales, South Louisiana and Upper Texas Gulf Coast per Hottman and Johnson

In 1972 Eaton published a technique for pore pressure prediction. Eaton recognized that Hottman and Johnson's basic relationship is correct, but can be improved. Hottman and Johnson's relationships, in the simplest terms, are as follows:

$$P_f / D \quad = \quad f(dT_{ob(sh)} - dT_{n(sh)}) \tag{2.7}$$

where P_f =   formation pore pressure (psi)

       D =   depth (ft)

       $dT_{ob(sh)}$ =   observed shale transit time (millisecond)

       $dT_{n(sh)}$ =   normal shale transit time (millisecond), obtained from normal

                          compaction trend

After rearrangement of the terms, the relationships are as follows:

$$\frac{dT_{ob(sh)}}{dT_{n(sh)}} = f\left(P_f / D\right) \tag{2.8}$$

Though Hottman and Johnson recognized Terzaghi's relationship to be true, their relationship did not follow the same form. Specifically, there was no way to distinguish the effects of the three variables in Terzaghi's pore pressure relationship. Their relationship related pore pressure to just one petrophysical parameter, whether it was formation resistivity or interval transit time.

Eaton noted that the technique developed by Hottman and Johnson utilized just a single line drawn through the FPG versus the petrophysical parameter data and that data was considerably scattered. This led Eaton to expand on Hottman and Johnson's relationships. Eaton combined Terzaghi's and Hottman and Johnson's relationships by solving Terzaghi's relationship for pressure and dividing all of the variables by depth as follows:

$$\frac{P_f}{D} \quad = \quad \left(\left(\frac{\sigma_{OB}}{D}\right) - \left(\frac{\sigma_{EV}}{D}\right)\right) \tag{2.9}$$

where σ_{OB} = overburden stress (psi)

σ_{EV} = effective vertical stress (psi)

Eaton postulates that the parameters derived from petrophysical log data are dependent variables primarily controlled by the pore pressure gradient and overburden stress gradient groups. He believed that Hottman and Johnson's relationships should be expanded to account for the effect of the overburden stress gradient. Up to this point, it was argued that the overburden stress gradient is constant for a given area and of no significance. Eaton refutes this argument saying that overburden stress gradients are functions of burial depth in areas where compaction and abnormal pressures are caused by increasing overburden loads with deeper burial. The overburden stress is a function of burial depth and formation bulk density by the following relationship:

$$\sigma_{ob} = \int \rho_b dD \tag{2.10}$$

where ρ_b is the formation bulk density (Ibm/gal)

Eaton (1972) presented a mathematical expression which related sonic travel times to pore pressure. Reynolds (1970) described how velocities derived from seismic data could be used for pore pressure prediction. All methods take advantage of the fact that sonic velocities depend on the effective pressure, and hence the pore pressure.

Travel time and pore pressure relationship proposed by Ben Eaton (1972):

$$P_{pore} = OB_Z - [OB_Z - Pn_Z] \times \left(\frac{\Delta t_n}{\Delta t_O}\right)^\alpha \quad\quad (2.11)$$

where P_{pore} = Predicted pore pressure (psi)

OB = Overburden pressure (psi)

Pn = Normal pressure (psi)

Z = Depth to point of measurement (ft)

Δt_n = The assumed normal sonic slowness at depth Z calculated

from the Normal compaction trend line (µsec/ft)

Δt_o = The observed (measured) sonic slowness at depth Z (µsec/ft)

α = Pore Pressure transformation exponent variable with

age/basin location (no unit),

The relationship between effective pressure and velocity depend heavily on the texture and mineral composition of the rock. For instance, for unconsolidated sandstones, the P-wave velocity varies significantly with effective pressure (Domenico, 1977). The mechanism thought to be important here is the strengthening of grain contacts with increasing effective pressure. When applying external load to unconsolidated sand, the contacts between the individual grains become stronger. Thus the stiffness of the sand is increased. This leads to an increased P-wave velocity (Mindlin and Deresiewicz, 1953). On the other hand, velocities in consolidated rocks may also vary significantly with pressure. This is not due to strengthening of grain contacts, but rather to microscopic cracks in the rock. When applying external pressure, these cracks tend to close, thus creating contacts at the crack surfaces. As a

result, the P-wave velocity increases. However, for consolidated rocks with little cracks, the velocities may not vary very much with pressure. In fact it can be shown (Dvorkin, *et al.*, 1991) that the granular rock with cemented grain contacts have no pressure dependence at all.

The cause of geopressuring may be significant for discriminating between normal and high pore pressure based on seismic velocities. In the previous section, undercompaction was mentioned as one of the most important geological processes for buildup of abnormally high pore pressures. A consequence of undercompaction is that the porosity of the sediments is preserved. This means that undercompacted sediments are more porous than compacted sediments. The porosity is one of the key factors determining the velocity of a rock. Both theoretical considerations and experiments show that seismic velocities in general decrease with increasing porosity. Thus, undercompacted sediments tend to have lower velocities than compacted sediments. In cases where the cause of geopressuring is due to other geological processes, the porosity does not have to be abnormally high. However, the mechanisms mentioned above (contact stiffness and microcracks) may still influence the velocity.

2.3   Fang basin

2.3.1   General geology of Fang basin

Fang Basin is a NNE-SSW trending, small intracratonic basin. It formed in the Early Tertiary and evolved in the Middle Tertiary in a transtensional regime followed by Pliocene to Pleistocene compression in a transtensional /transpressional left-lateral tectonic system (Zollner and Moller, 1996). The

depositional environment in the Tertiary was fluvial-lacustrine and changed to fluvial and alluvial in the Quaternary (Settakul, 1985). It is on the western margin of the Sokhothai fold belt, which comprises Paleozoic and Triassic strata and volcanic rocks that accumulated on the eastern margin of the Shan-Thai craton prior to the Indosinian orogeny. This fold belt is complex and deformed by granitic intrusions during the collision of the Indochina and Shan-Thai cratons (Bunopas and Vella, 1983).

2.3.2 Structure of Fang basin

Fang basin is a half-graben that has a steep faulted western flank and a gently dipping eastern flank. The basin can be divided in three sub-basins. These are Huai Pasang, Huai Ngu, and Pa Ngew sub-basins, the three being separated by saddles formed by older rocks. The deepest part of Fang basin is the central Huai Ngu sub-basin, which has a sedimentary fill of 3,000 m (Settakul, 1985). Fang basin now produces oil from five structures, all of which are in the Huai Ngu sub-basin. The order of oil production, from high to low, is the Mae Soon, San Sai, Nong Yao, Ban Thi, and Sam Jang structures.

2.3.3 Stratigraphy and sedimentological overview of Fang basin

The Pre-Tertiary basement rocks consist of sedimentary, metamorphic and igneous rocks. On the western side of the basin, the rocks are Cambrian-Permian in age, and include Carboniferous granite. On the eastern side of the basin, the rocks are Silurian-Devonian and Jurassic, with Triassic granite. The Tertiary rocks of the Fang basin are conglomerate, sandstone, claystone and shale. The Quaternary deposits are silt, clay, sand and gravel and occur as stream channels, terrace deposits and alluvial fans. These sediments are covered by recent soil and lateritic sand.

Depth (ft.)	Formation	Age	Sand Unit	Lithology	Description
735	Mae Fang	Pleistocene to Recent			Loose arkosic sandstone-gravel sandstone, grey, fine-coarse, angular-subangular, interbedded with thin layer of grey claystone and carbonized wood.
1,000 / 2,000 / 2,200	Upper Mae Sod	Late Miocene to Pliocene	D E F G		Blackish grey siltstone intercalated with grey sandstone, medium - coarse, subangular locally conglomeratic sandstone.
3,000 / 3,700	Middle Mae Sod	Oligocene to Miocene	H		Most darkish brown, grey and reddish brown shale, claystone, mudstone interbedded with fine - very coarse sandstone, subangular-subround, moderately sorted with fossil gastropods, leaves and fish fragments.
4,000 / 5,000	Lower Mae Sod	Late Eocene			Most greyish brown, grey and reddish brown shale interbedded with grey, medium-course sandstone, siltstone, conglomerate and coal.
	Basement ?	Pre-Tertiary			Weathered andesite and Permian Ratburi Limestone.

Legend

Shale, Clay.

Sandstone.

Oil Sand, Sandstone.

Figure 2.4 Stratigraphy of the Fang basin (modified after Buravas (1973); Sethakul (1984); Settakul (1985))

2.3.4 Petroleum system of the Fang basin

Zollner and Moller (1996) described the hydrocarbon system of Fang basin and suggested that the source rocks were deposited in a lacustrine environment. Potential source rocks include bituminous shale and lignite of the Lower Mae Sod formation. Reservoir rocks in the Mae Soon and the San Sai structures are infill sands of the Upper Mae Sod formation, whereas in the Pong Nok area they are westward prograding sandstone that pinches out towards the east. Mostly intra-formation shale layers are interpreted to act as seals. The generation of structures was related to the compression during the Pliocene to Pleistocene. Source rocks were within the oil window during this time. Top of the oil window is interpreted to be located at a depth of approximately 2,750 ft (Temperature gradient: 7.2 $^{\circ}$C / 100 m). Migration pathways are interpreted to have been updip and along faults.
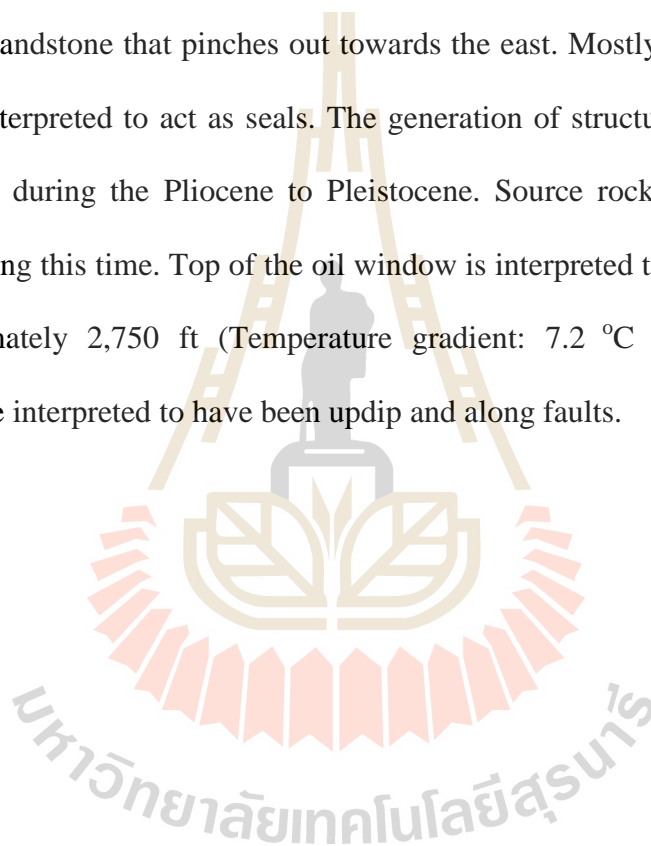
CHAPTER III

RESEARCH METHODOLOGY

Prediction of pore pressure within study area had been conducted by using seismic velocities. The steps that used to calculate pore pressure in this research are: 1.) Seismic data collecting and preparing, 2.) Normal compaction trend generating, and 3.) Pore pressure calculation

3.1 Seismic data collecting and preparing

Seismic data from eight 2D Seismic lines including Line S-2, Line S-3, Line F-89-031, Line F-1, Line F-2, Line F-3, Line F-89-038 and Line F-89-040 were collected and analyzed to calculate pore pressure gradient. Location of studied seismic survey lines are presented in Figure 3.1. All of seismic lines had to prepare in to time – depth relationship form by using Dix's equation as showed below:

$$
h_n = \frac{V_n\left(t_{0(n)} - t_{0(n-1)}\right)}{2} \tag{3.1}
$$

where h_n =   thickness of layer n (ft)

      V_n =   Interval velocity at laver n (ft/sec)

      $t_{0(n),(n-1)}$ =   zero offset reflection time at reflector n and $n-1$ respectively

                 (sec)

and

$$H_n = \sum_1^n h_i \qquad\qquad (3.2)$$

where H_n is depth to layer n (ft)
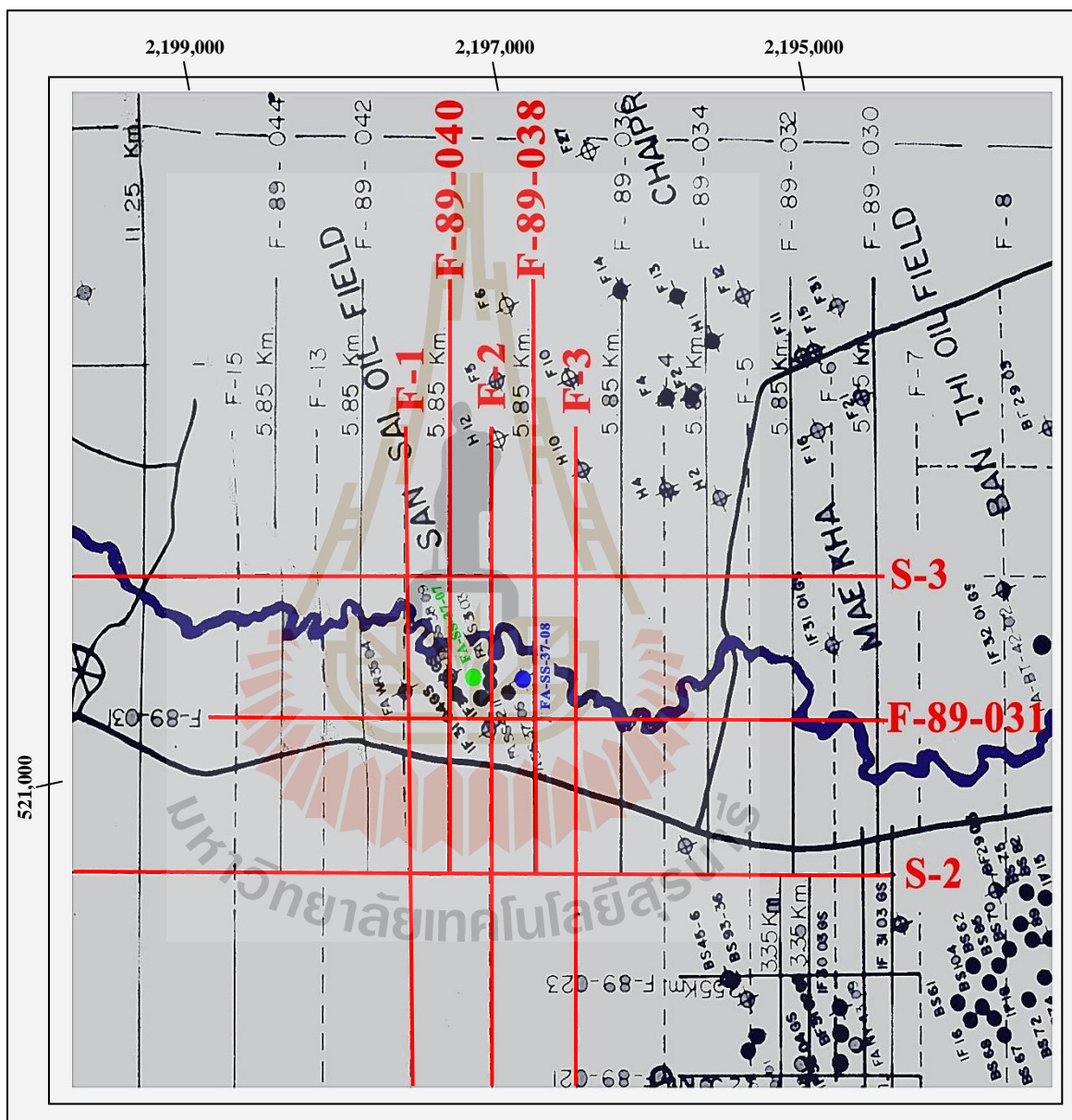
Figure 3.1 Location of studied seismic survey lines and reference well

FA-SS-37-07 (green) and well FA-SS-37-08 (blue)

3.2   Normal compaction trend generating

Normal compaction trend can be generated by making a transit time–depth plot on semi-log paper. The normal compaction trend can be determined by drawing a straight line through the average of transit time value in the relative depth.

In this research twenty four of normal compaction trend lines were created, three data sets from each seismic line were used to create normal compaction trend lines.

3.3   Pore pressure calculation

The pore pressure had been calculated from travel time and pore pressure relationship proposed by Ben Eaton (1972) in equation 2.11:

$$P_{pore} \quad = \quad OB_Z - [OB_Z - Pn_Z] \times \left(\frac{\Delta t_n}{\Delta t_O}\right)^{\alpha} \tag{2.11}$$

where OB =   Overburden pressure at depth z (psi)

Pn =   Normal pressure at depth z (psi)

According to the theory, overburden pressure gradient and normal pressure gradient (hydrostatic pressure gradient) that used in this research were set as 1 psi/ft and 0.433 psi/ft respectively and used pore pressure transformation exponent variable(α) as 0.3 (This value was obtained from fitting curve between RFT and sonic log data from well FA-SS-37-08).

Therefore, equation 2.11 had been transformed to:

$$P_{pore_z} = (1 \times D_z) - [(1 \times D_z) - (0.433 \times D_z)] \times \left(\frac{\Delta t_n}{\Delta t_O} \right)^{0.3} \qquad (3.3)$$

where D   =   depth at interesting depth z (ft)

α   =   0.3 (This value obtained from filling curve between RFT and

sonic log data of well FA-SS-37-08)

In this study, Equation 3.3 had been used to calculate the pore pressure throughout the study.

In order to check the accuracy of the calculated pore pressure from this study, pressure data obtained from Repeat Formation Test (RFT) of well FA-SS-37-08 and from deriving from pressure gradient of well FA-SS-37-07 were used for comparison. Locations of well FA-SS-37-07 and well FA-SS-37-08 are depicted in Figure 3.1.

CHAPTER IV

RESULTS AND DISCUSSION

In order to study the relationship among pore pressure, depth, and seismic wave travel time, these data were each other cross-plotted and some results can be summarized as follows.

4.1   Normal compaction trend lines

Normal compaction trend lines were generated from plotting transit time versus depth in semi-logarithmic scale and generated trend lines by using Microsoft Excel 2010.

Normal compaction trend lines of first data set which were collected from shot point numbers closed to reference drilling well (well FA-SS-37-07 and FA-SS-37-08) including Line S-2 SPN 1560, Line S-3 SPN 1476, Line F-89-031 SPN 1257, Line F-1 SPN 1231, Line F-2 SPN 1227, Line F-3 SPN 1266, Line F-89-038 SPN 1127, and Line F-89-040 SPN 1131 are showed in Figure 4.1 – Figure 4.8.

Normal compaction trend lines of second data set which were located next to the first data set, including Line S-2 SPN 1524, Line S-3 SPN 1440, Line F-89-031 SPN 1189, Line F-1 SPN 1174, Line F-2 SPN 1192, Line F-3 SPN 1228, Line F-89-038 SPN 1079, and Line F-89-040 SPN 1085 were results in Figure 4.9 – Figure 4.16.

Normal compaction trend lines of third data set which were located next to the first data in the opposite side of second data set including Line S-2 SPN 1596, Line S-3 SPN 1512, Line F-89-031 SPN 1313, Line F-1 SPN 1286, Line F-2 SPN

1271, Line F-3 SPN NULL, Line F-89-038 SPN 1127, and Line F-89-040 SPN 1167
were results in Figure 4.17 – Figure 4.24.
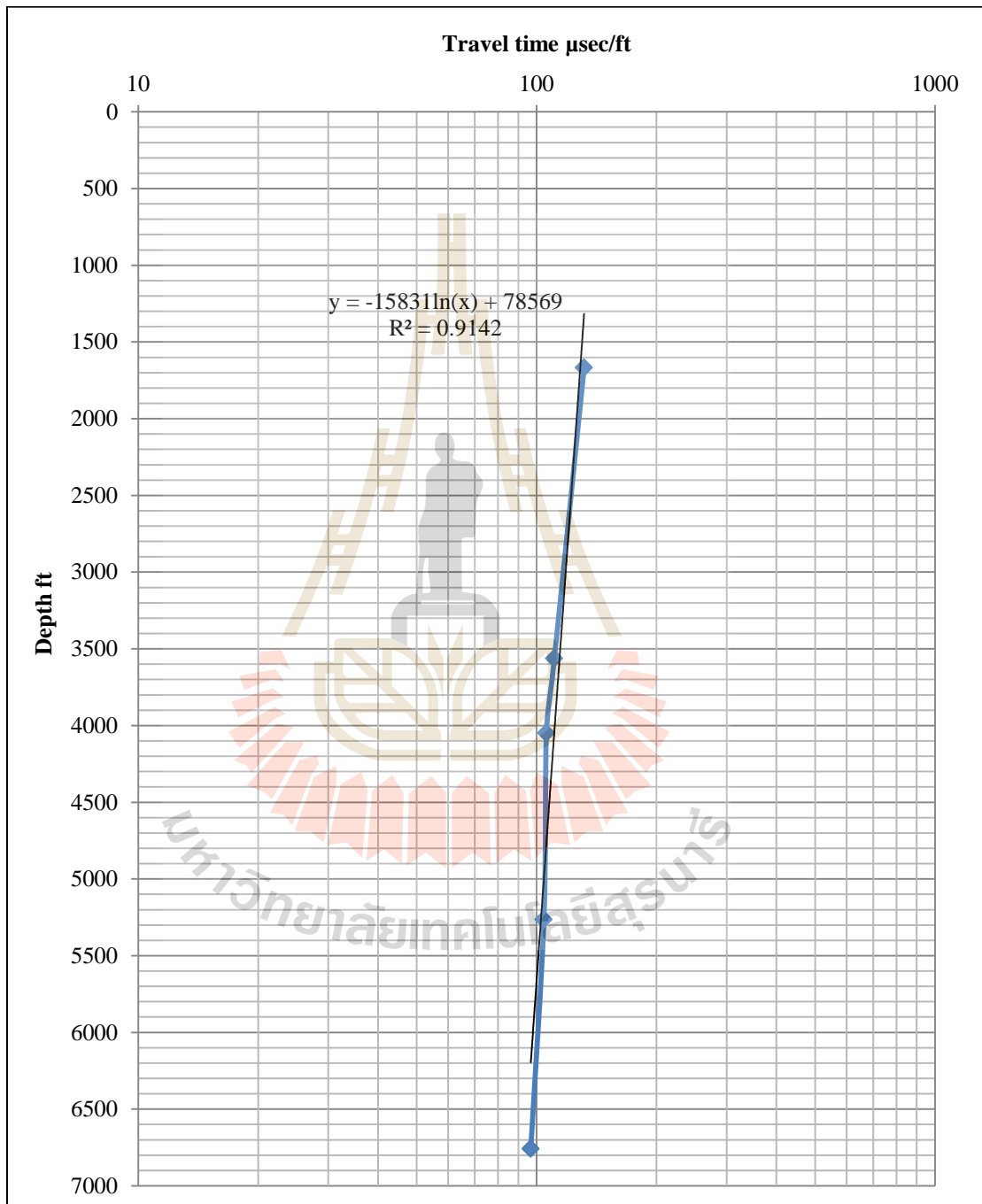
Figure 4.1 Normal compaction trend line with its corresponding linear equation
generated from seismic line S-2 shot point number 1560 data
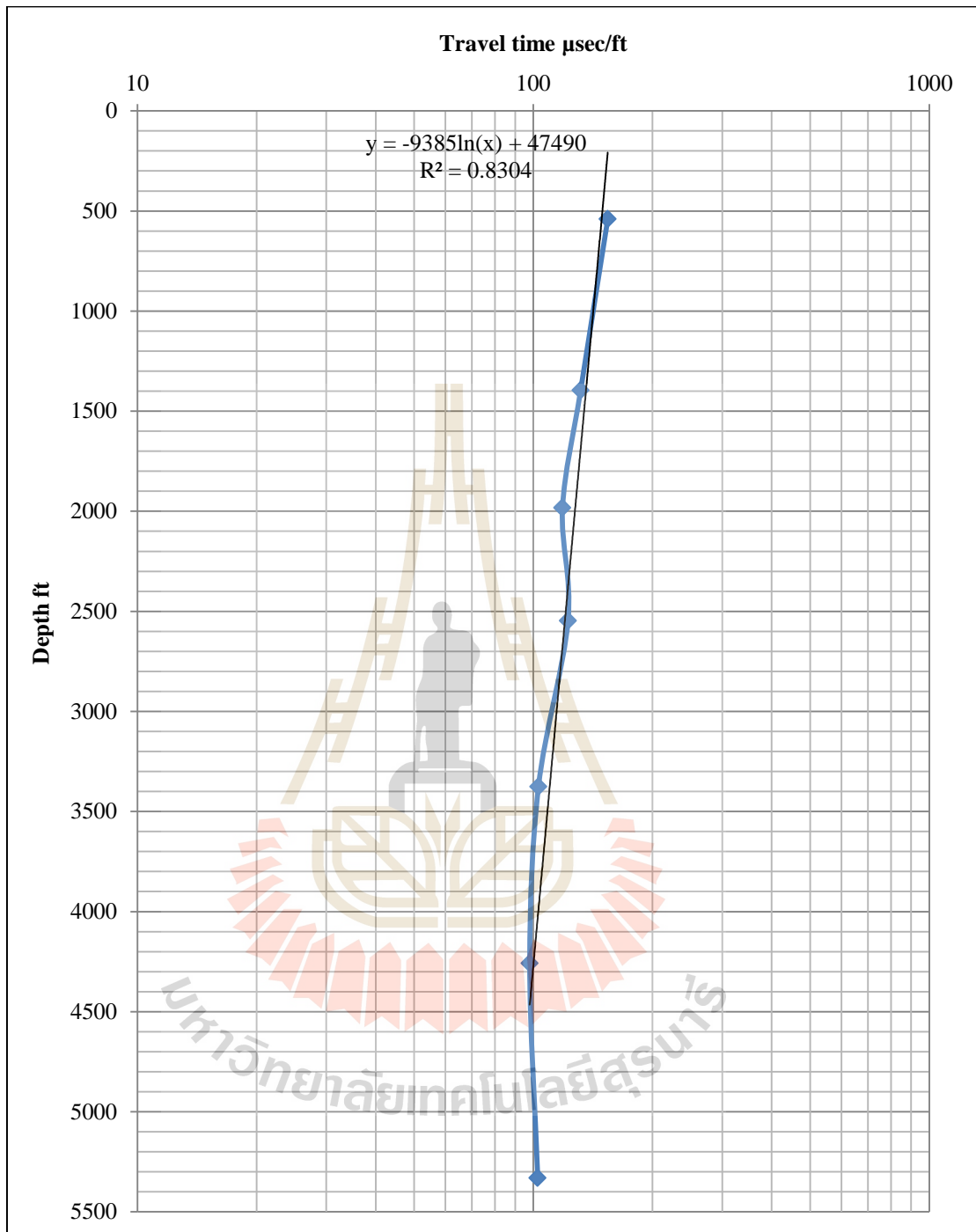
Figure 4.2 Normal compaction trend line with its corresponding linear equation

generated from seismic line S-3 shot point number 1476 data
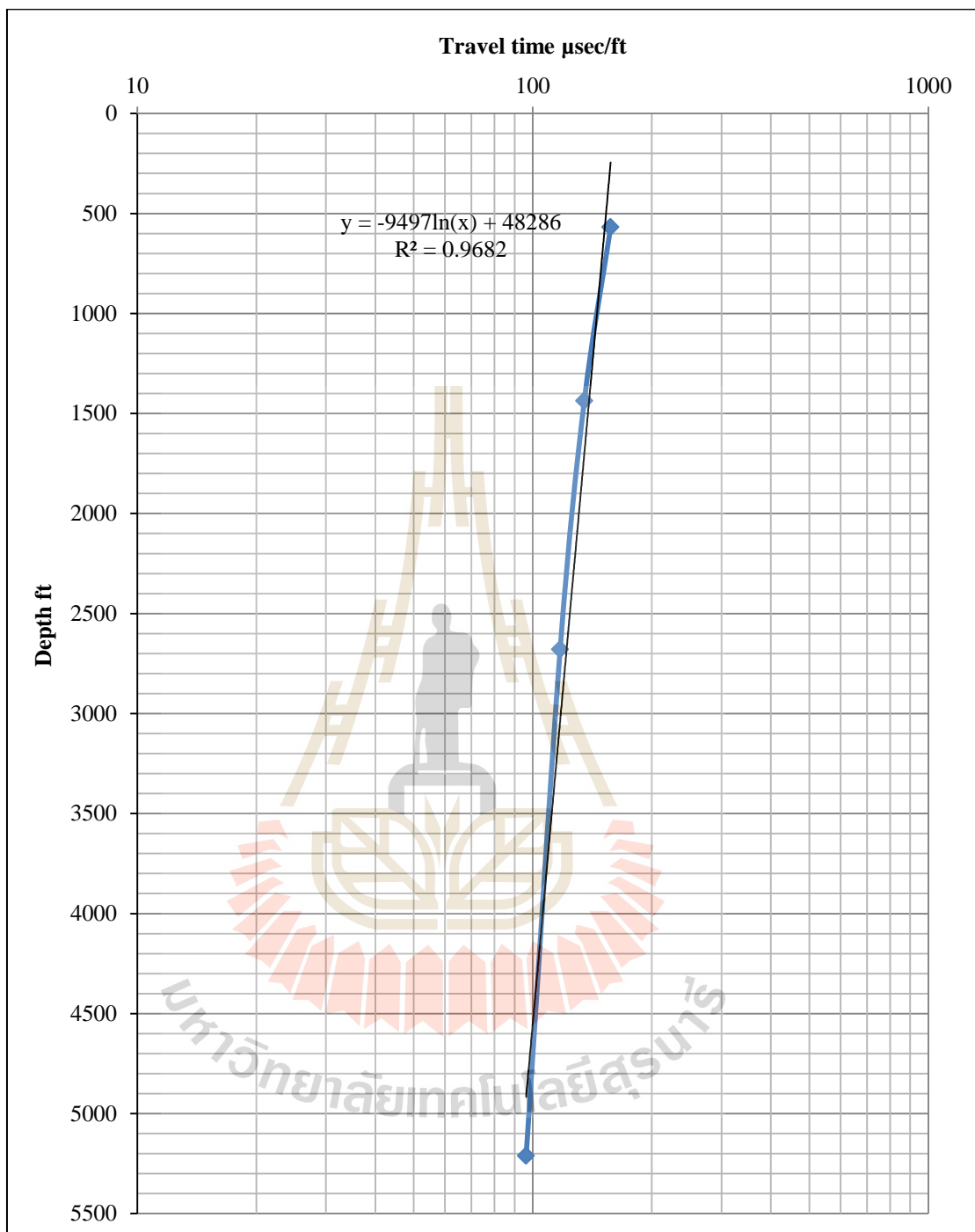
Figure 4.3 Normal compaction trend line with its corresponding linear equation

generated from seismic line F-89-031 shot point number 1257 data
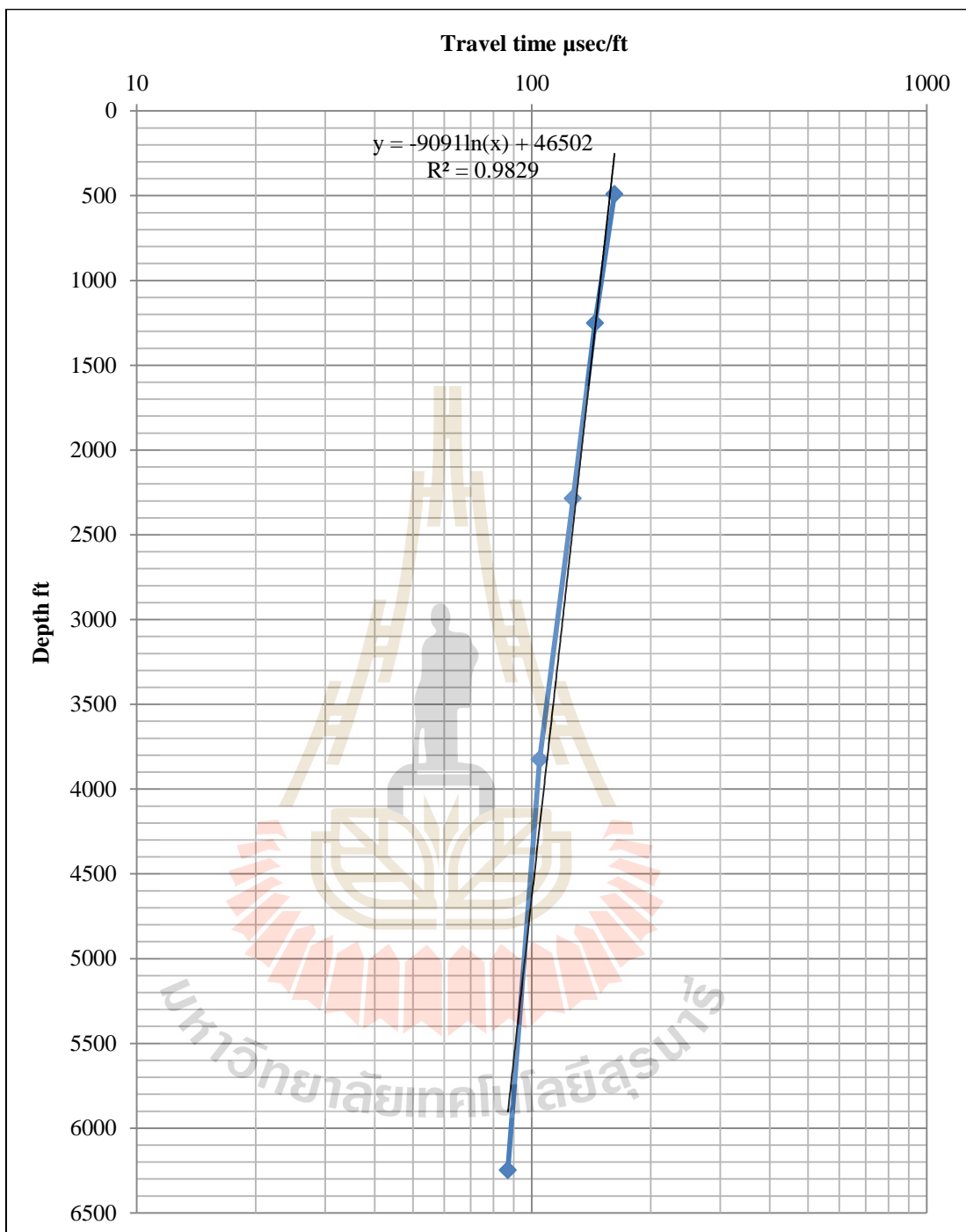
Figure 4.4   Normal compaction trend line with its corresponding linear equation

generated from seismic line F-1 shot point number 1231 data
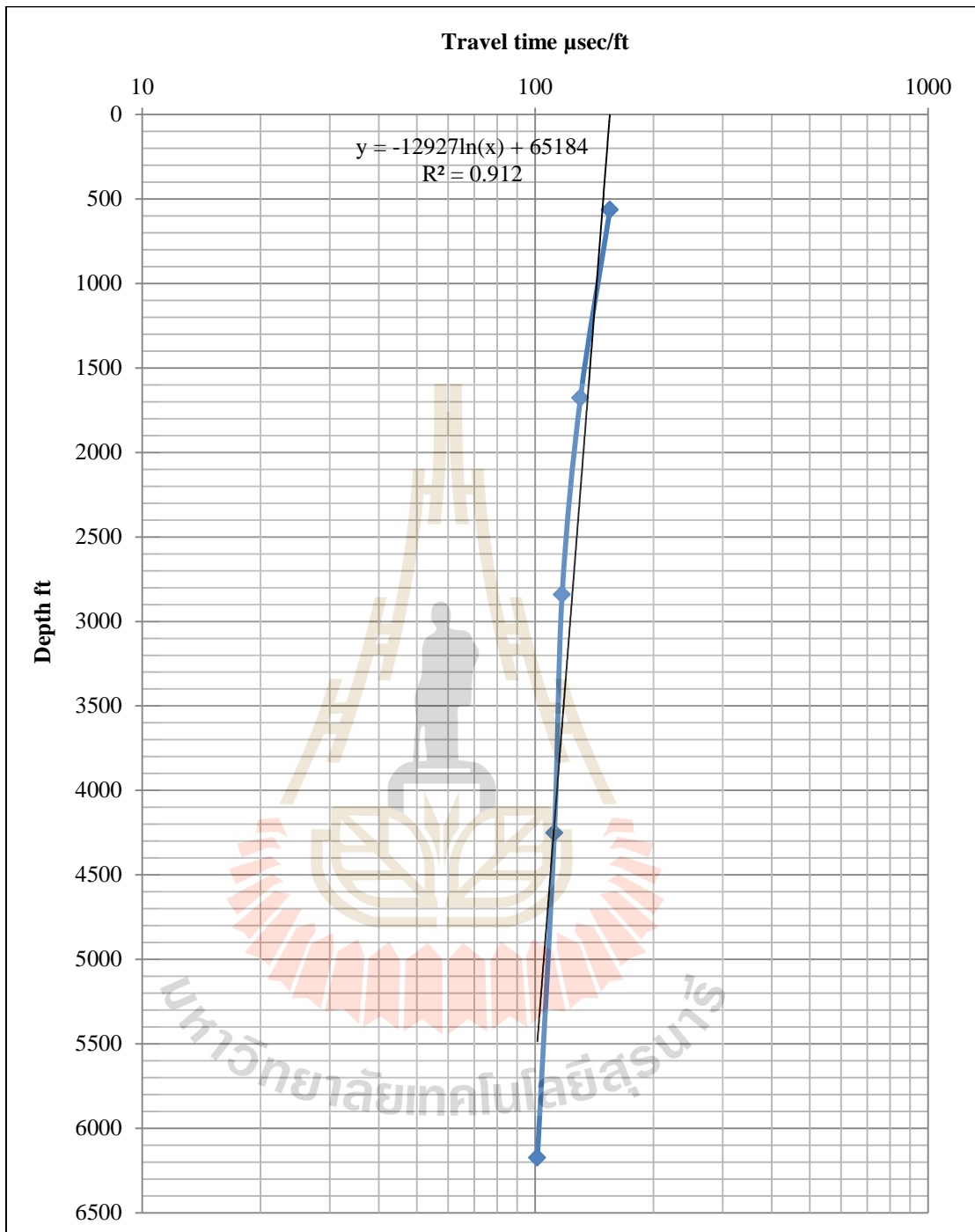
Figure 4.5   Normal compaction trend line with its corresponding linear equation

generated from seismic line F-2 shot point number 1227 data
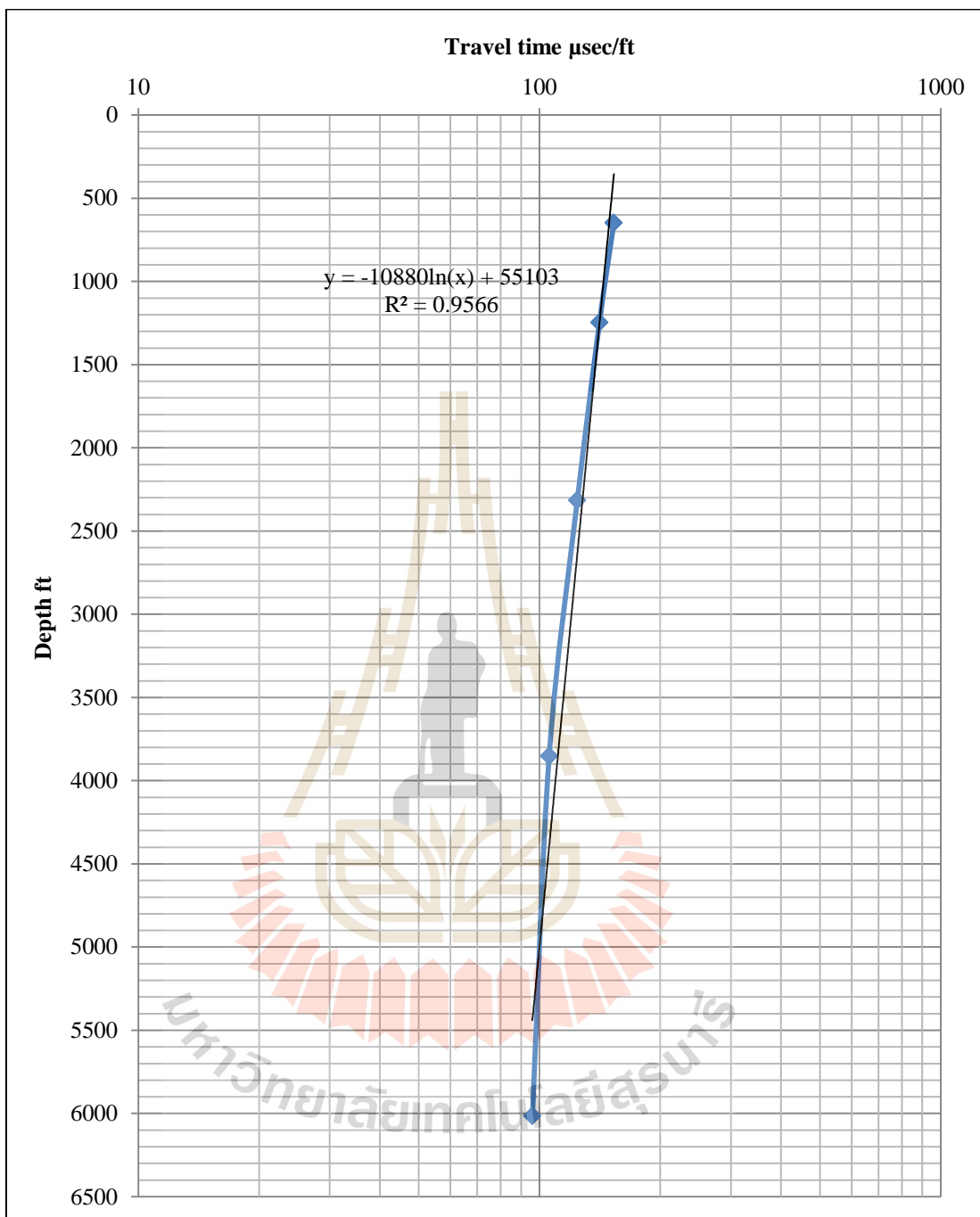
Figure 4.6 Normal compaction trend line with its corresponding linear equation

generated from seismic line F-3 shot point number 1266 data
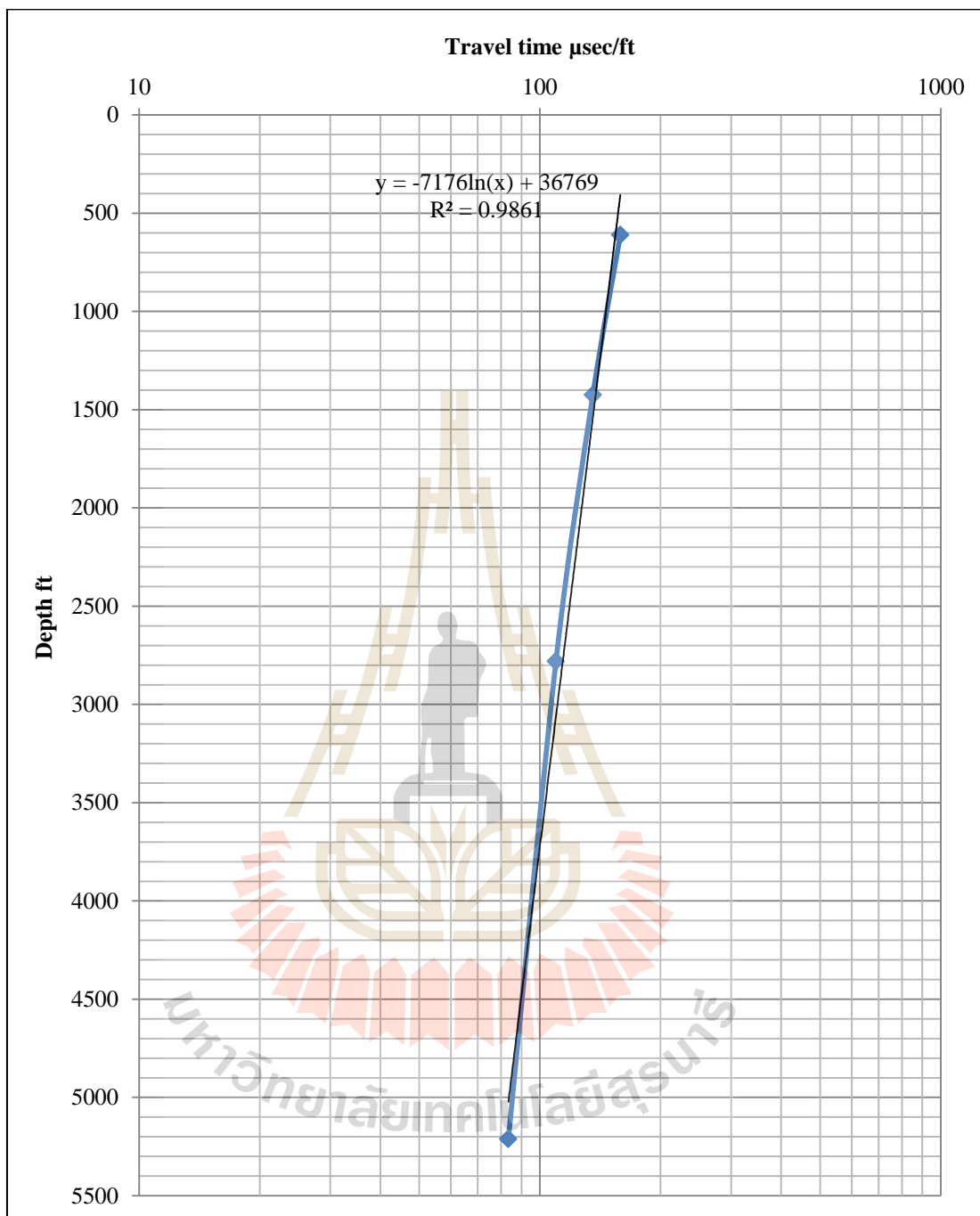
Figure 4.7   Normal compaction trend line with its corresponding linear equation

generated from seismic line F-89-038 shot point number 1127 data
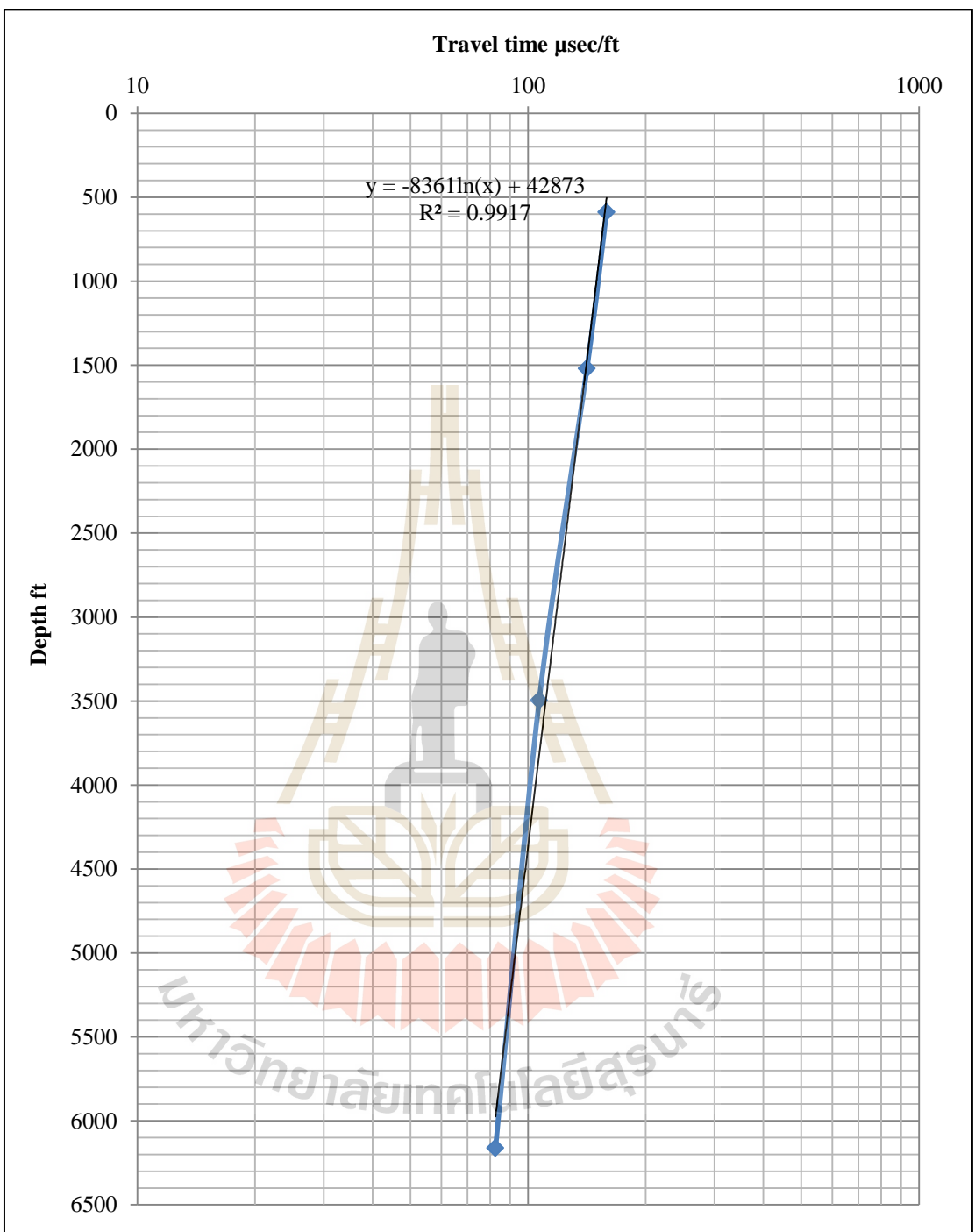
Figure 4.8 Normal compaction trend line with its corresponding linear equation

generated from seismic line F-89-040 shot point number 1131 data
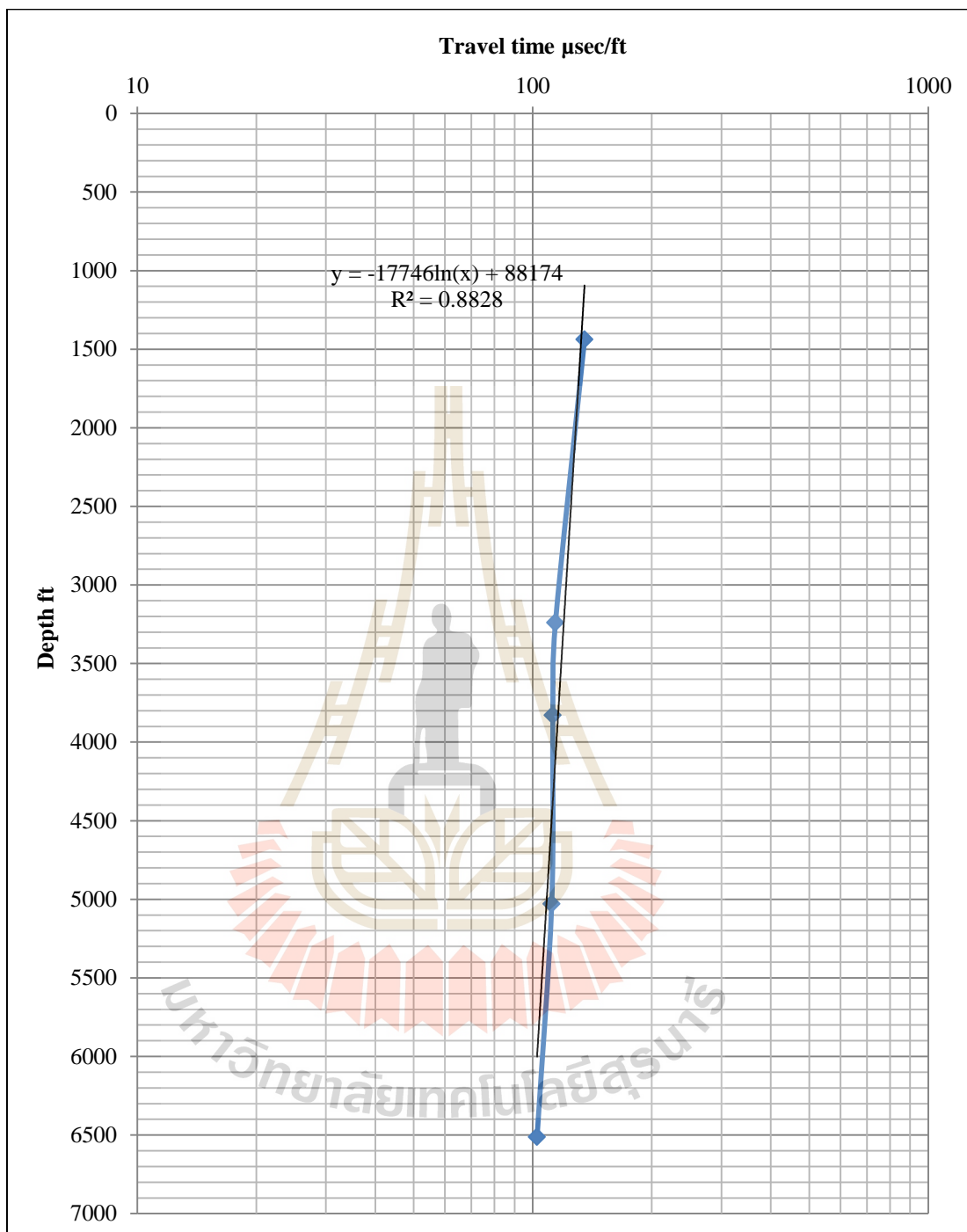
Figure 4.9 Normal compaction trend line with its corresponding linear equation

generated from seismic line S-2 shot point number 1524 data

Travel time μsec/ft

$$y = -10256\ln(x) + 51632$$
$$R^2 = 0.8506$$
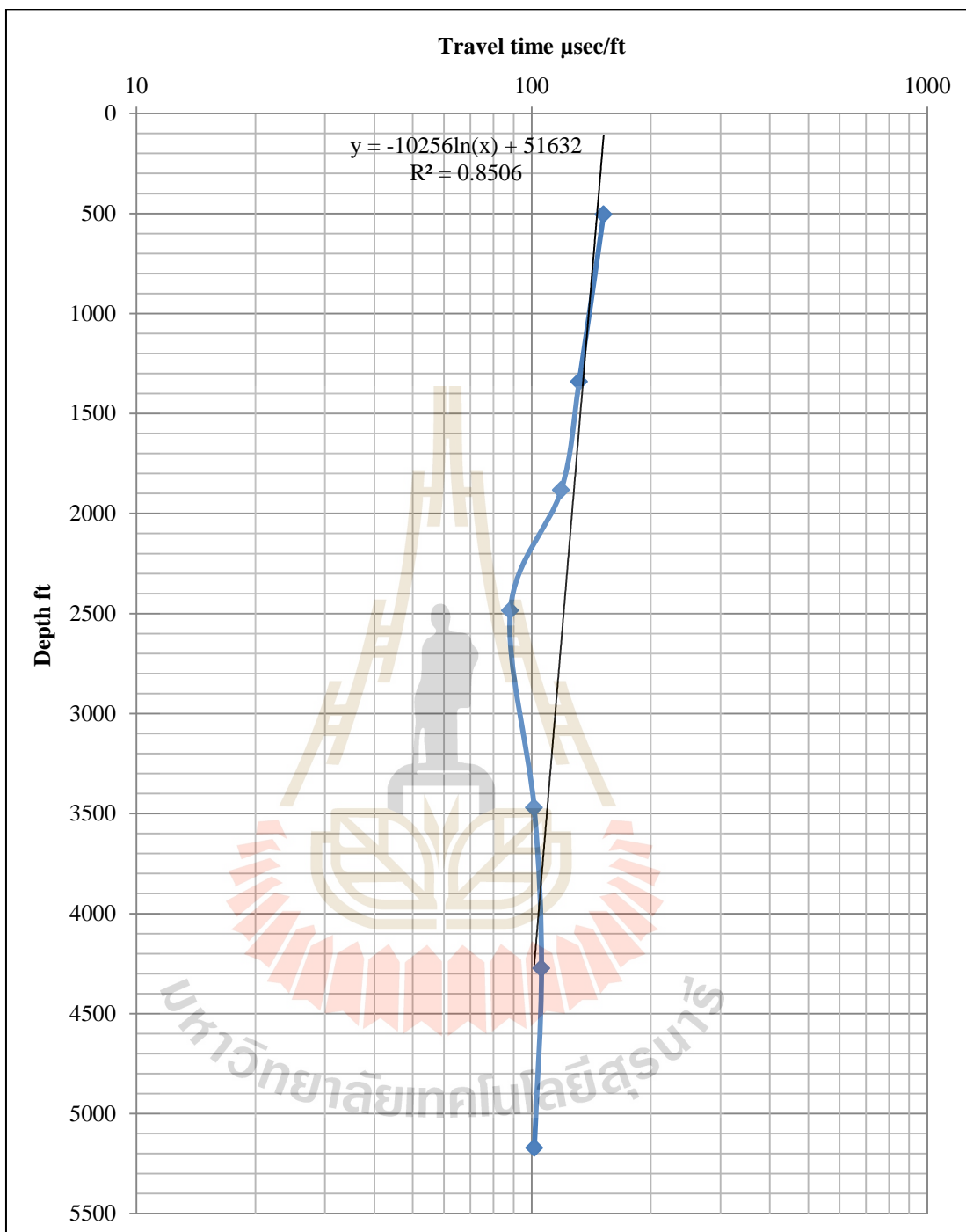
Figure 4.10 Normal compaction trend line with its corresponding linear equation

generated from seismic line S-3 shot point number 1440 data
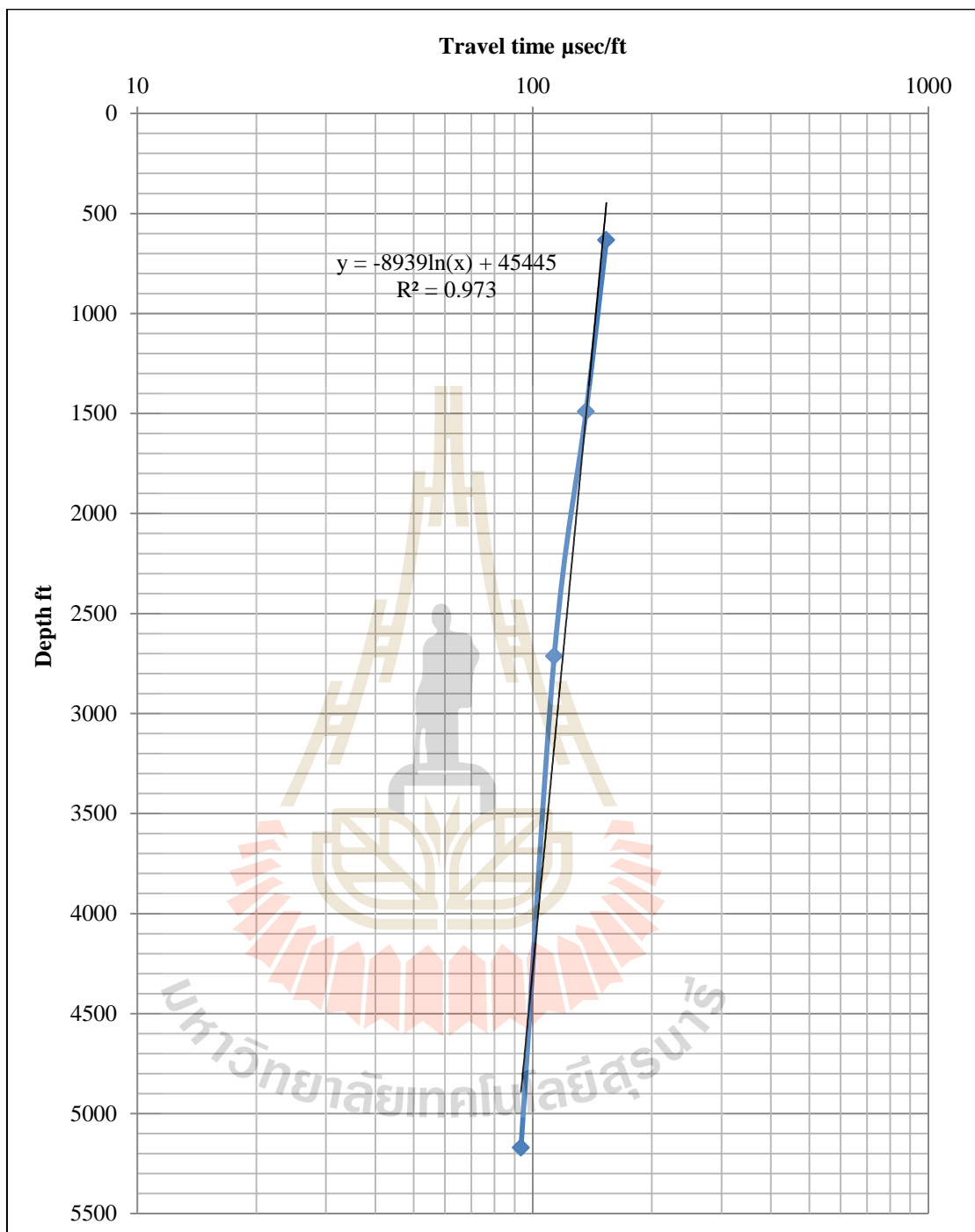
Figure 4.11 Normal compaction trend line with its corresponding linear equation

generated from seismic line F-89-031 shot point number 1189 data

The chart shows Travel time μsec/ft on the x-axis (logarithmic scale from 10 to 1000) and Depth ft on the y-axis (0 to 7000).

y = -10094ln(x) + 51173
R² = 0.9801
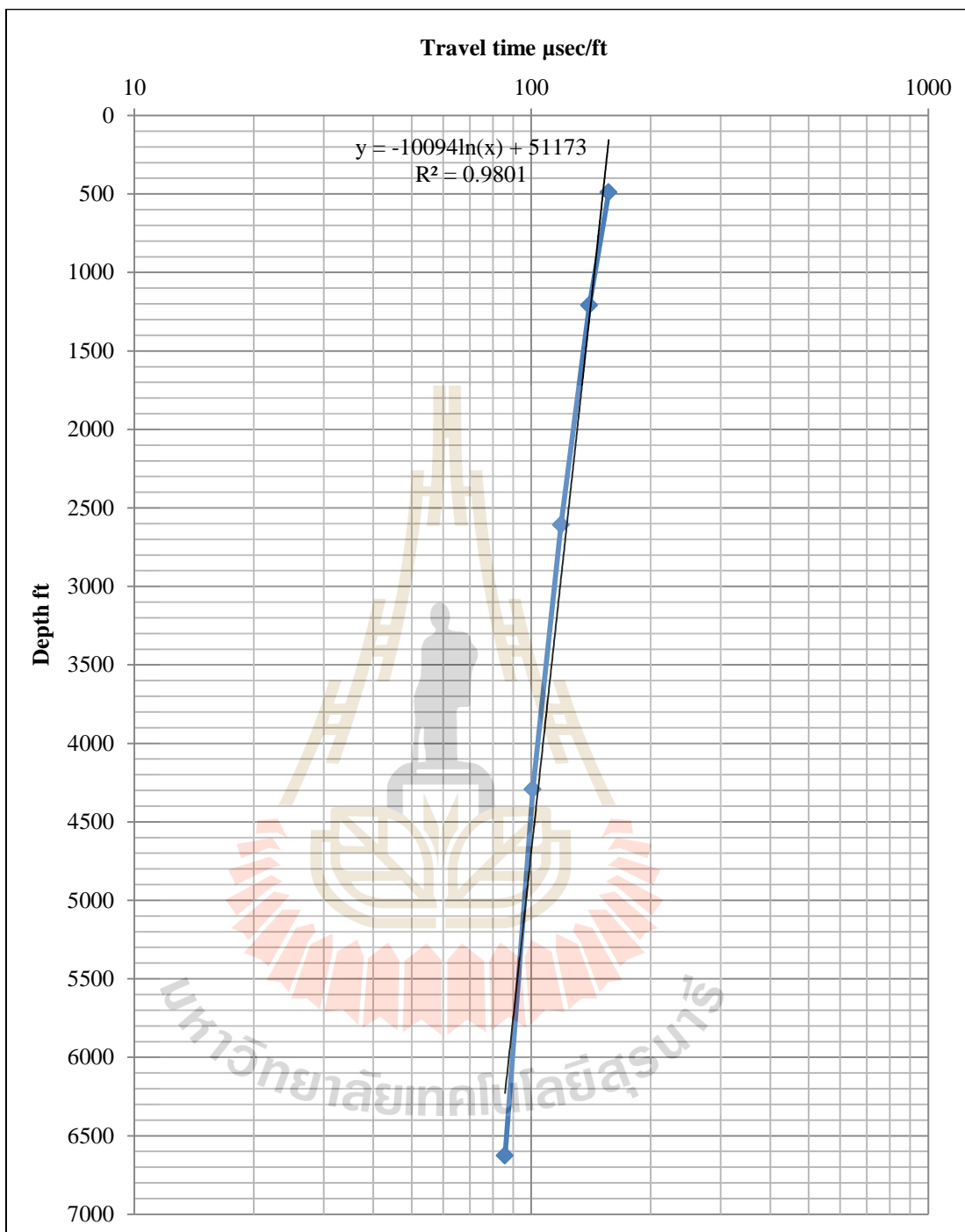
Figure 4.12 Normal compaction trend line with its corresponding linear equation

generated from seismic line F-1 shot point number 1174 data
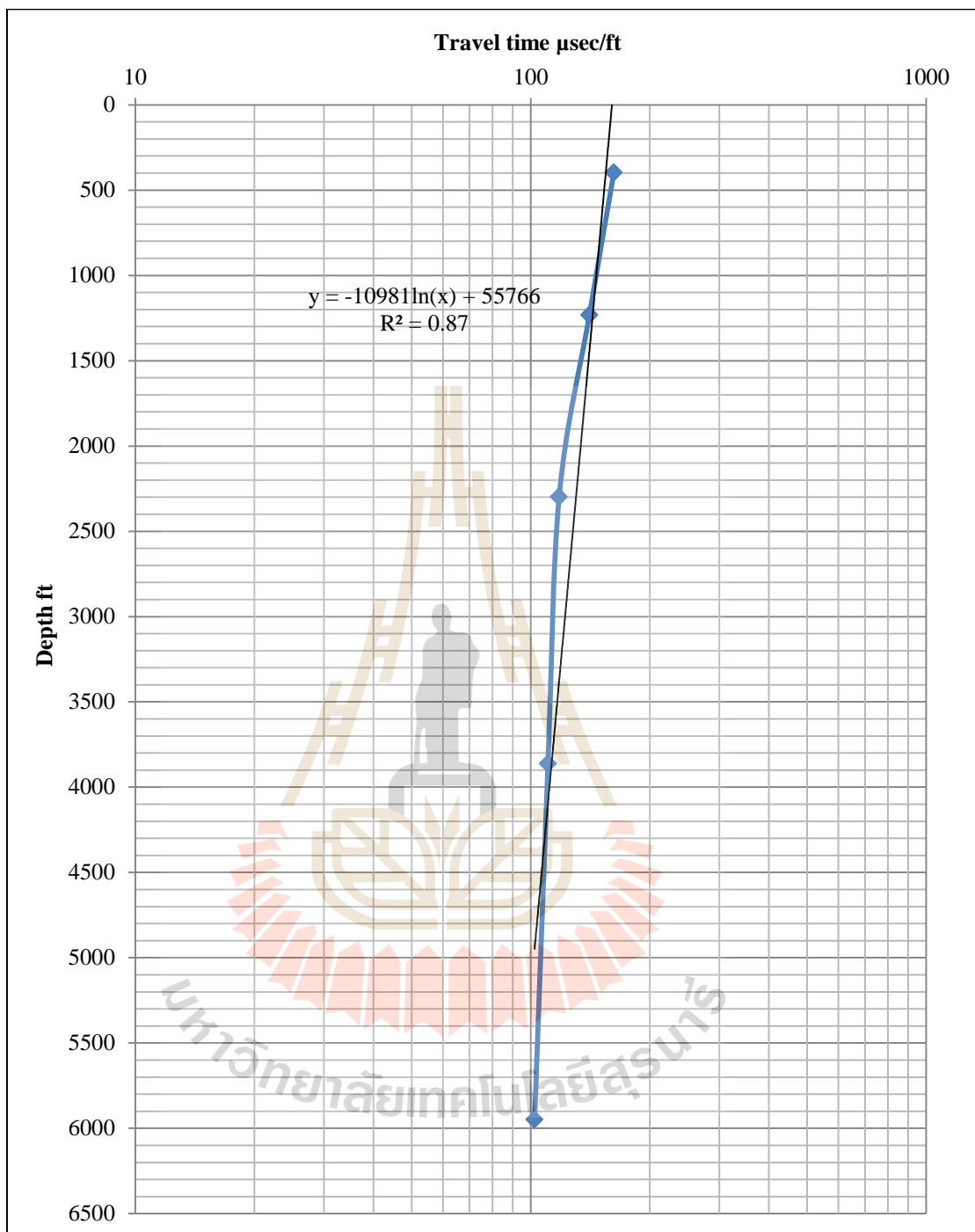
Figure 4.13 Normal compaction trend line with its corresponding linear equation

generated from seismic line F-2 shot point number 1192 data
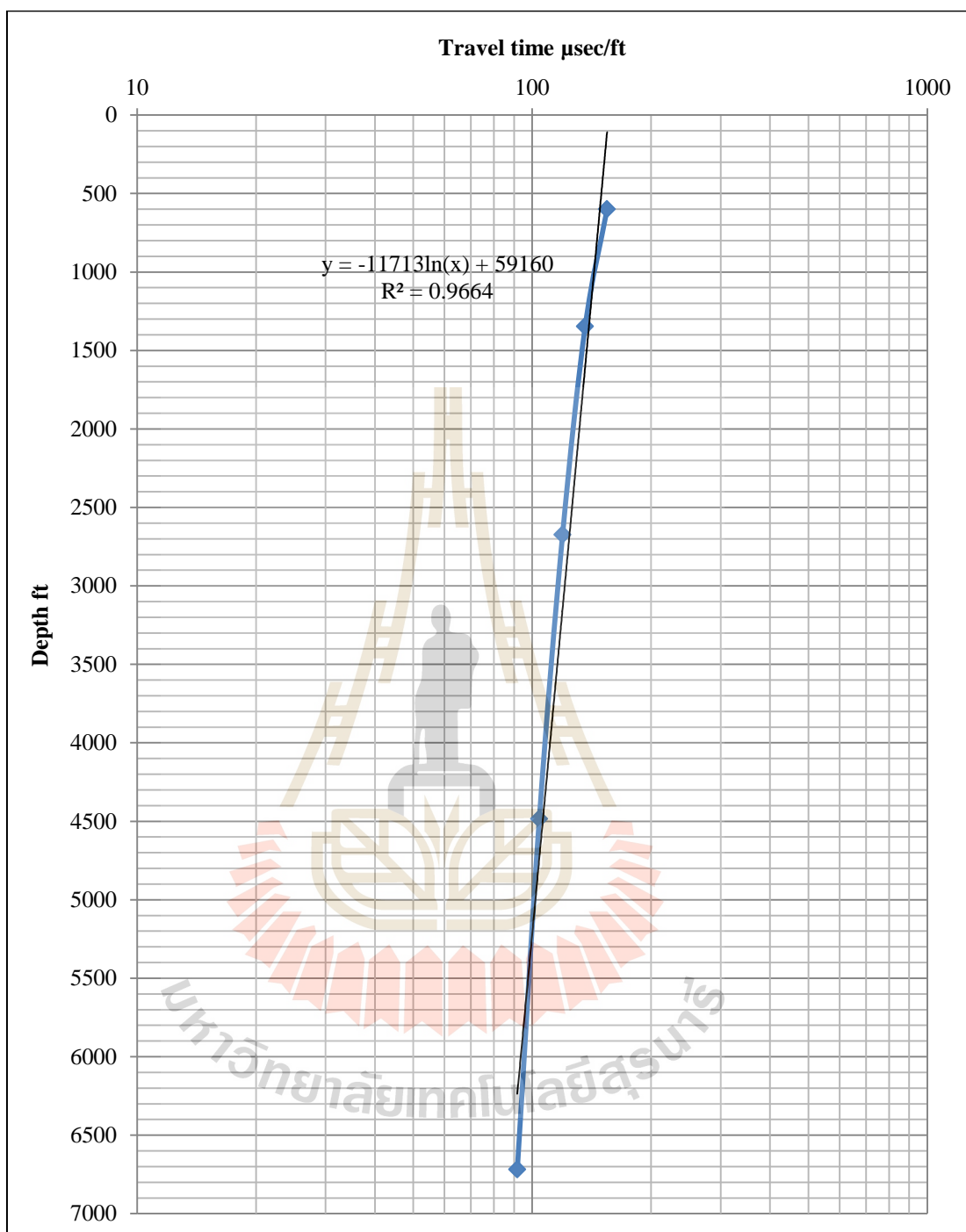
Figure 4.14 Normal compaction trend line with its corresponding linear equation

generated from seismic line F-3 shot point number 1228 data
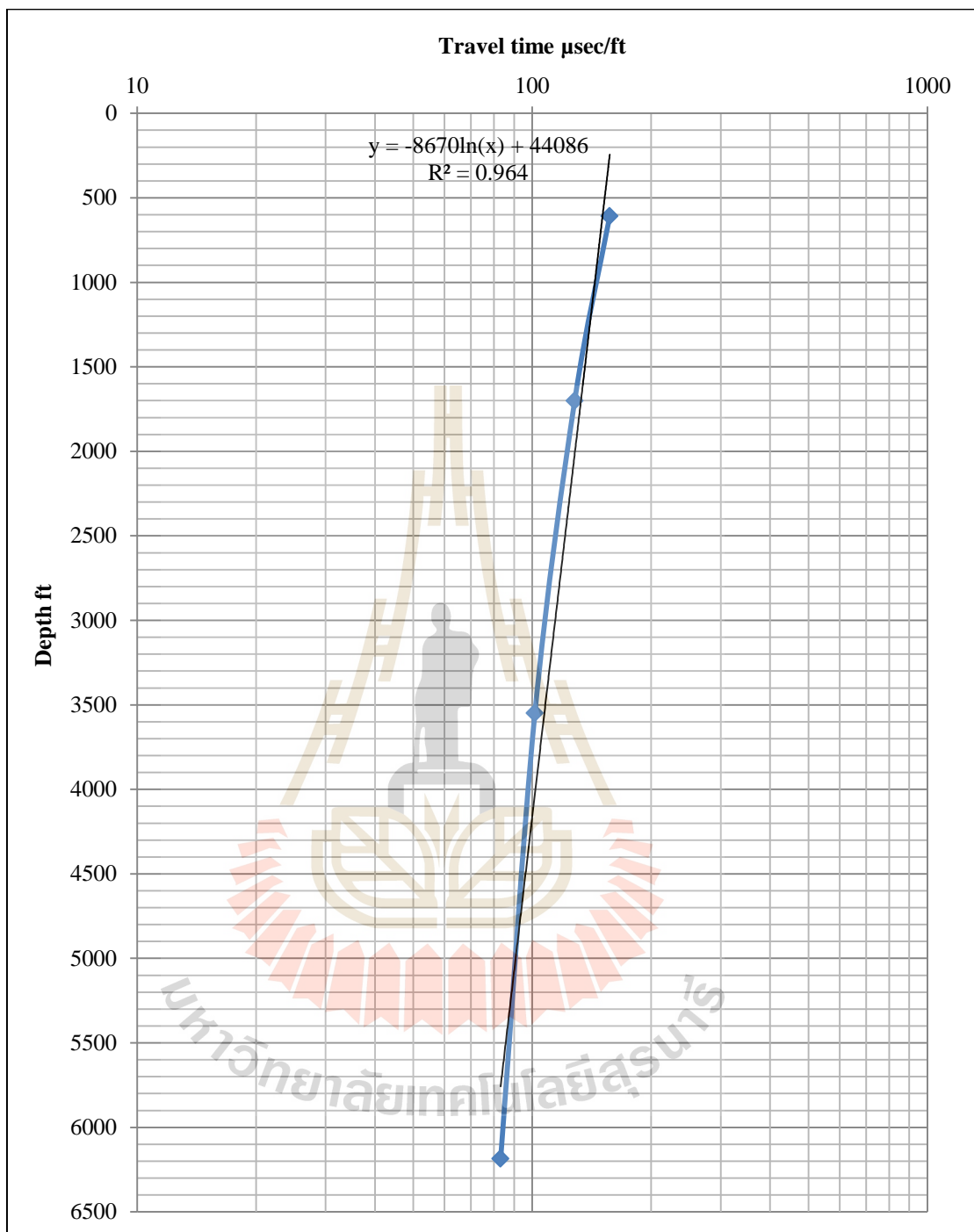
Figure 4.15 Normal compaction trend line with its corresponding linear equation

generated from seismic line F-89-038 shot point number 1079 data
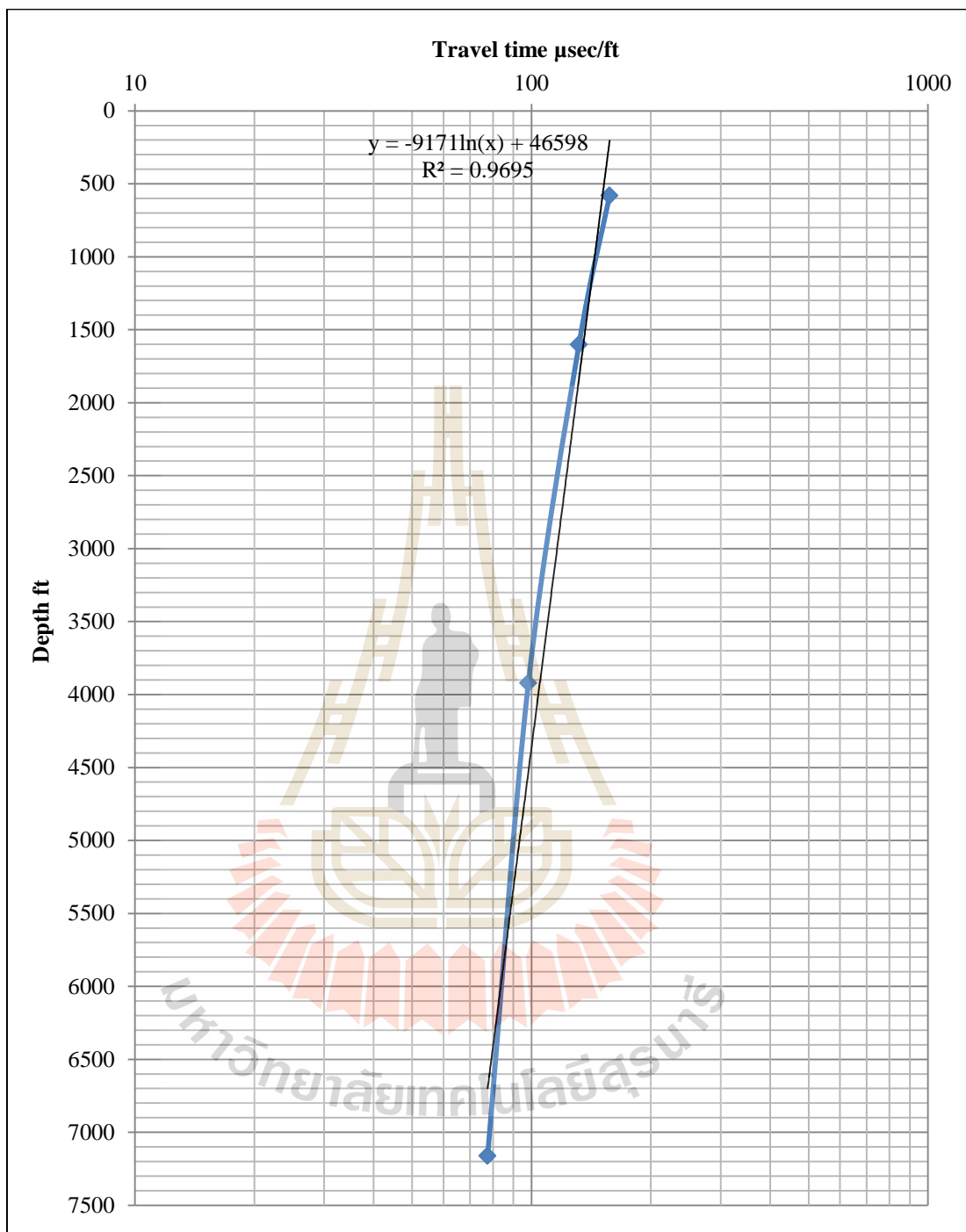
Figure 4.16 Normal compaction trend line with its corresponding linear equation

generated from seismic line F-89-040 shot point number 1085 data
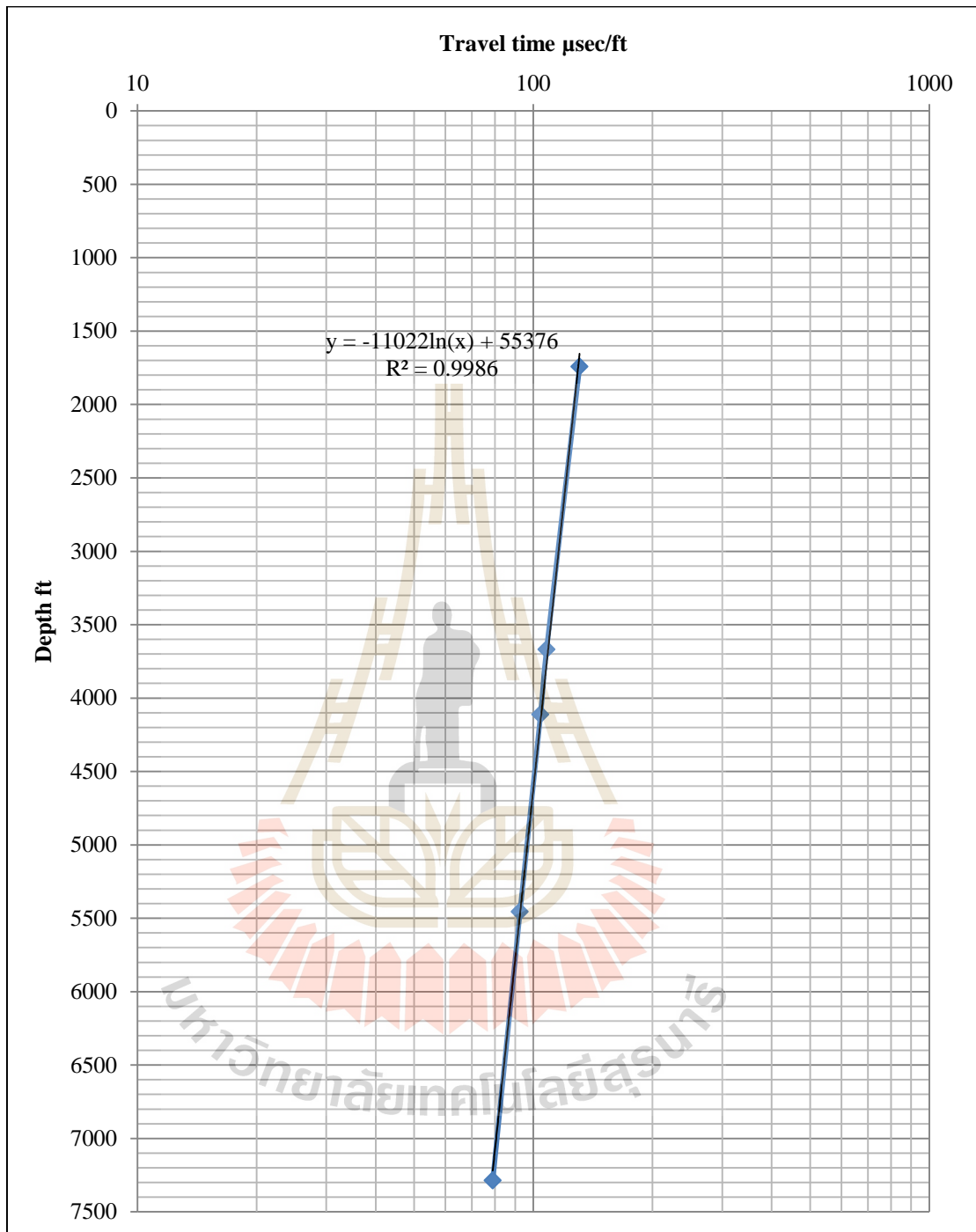
Figure 4.17 Normal compaction trend line with its corresponding linear equation

generated from seismic line S-2 shot point number 1596 data
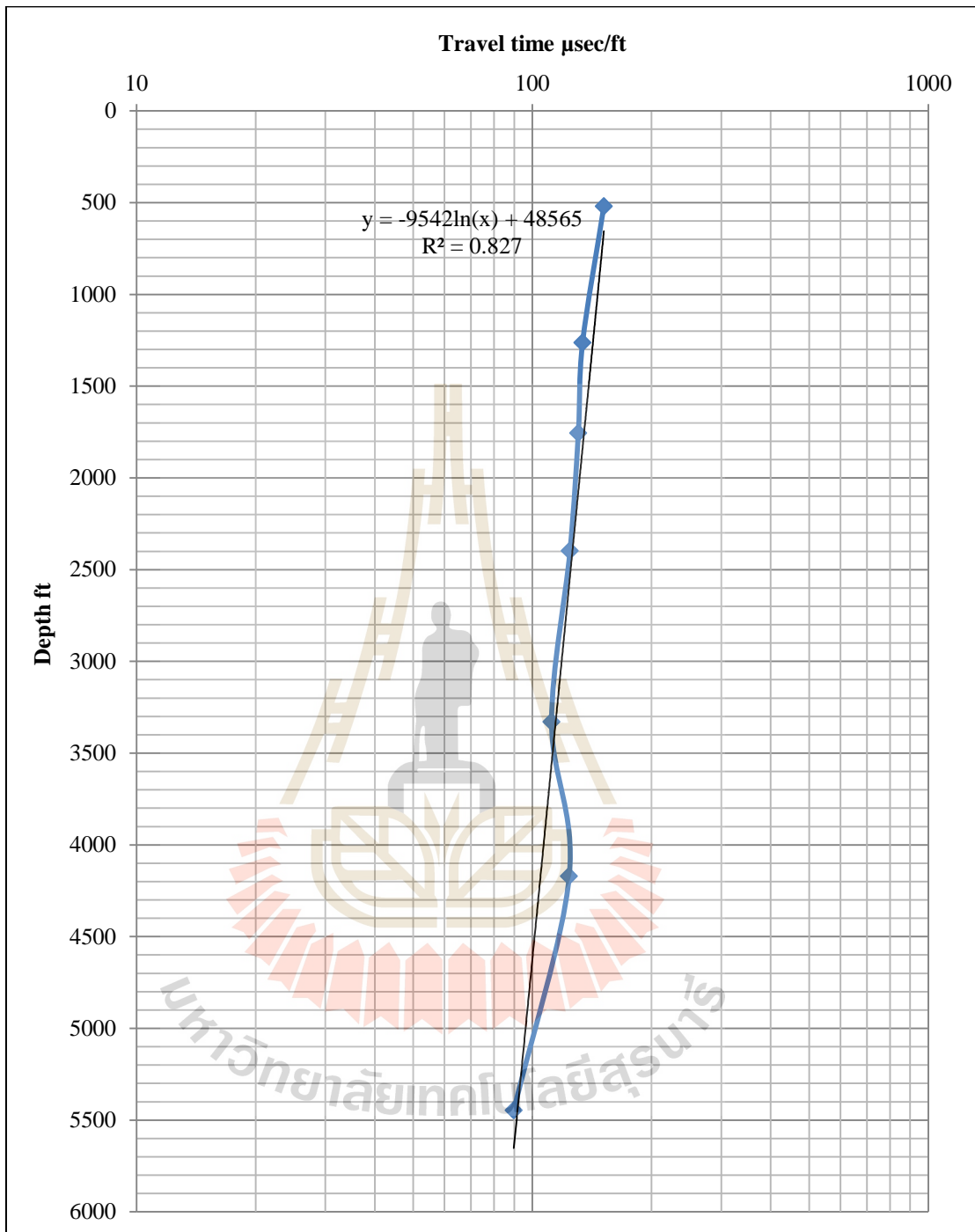
Figure 4.18 Normal compaction trend line with its corresponding linear equation

generated from seismic line S-3 shot point number 1512 data
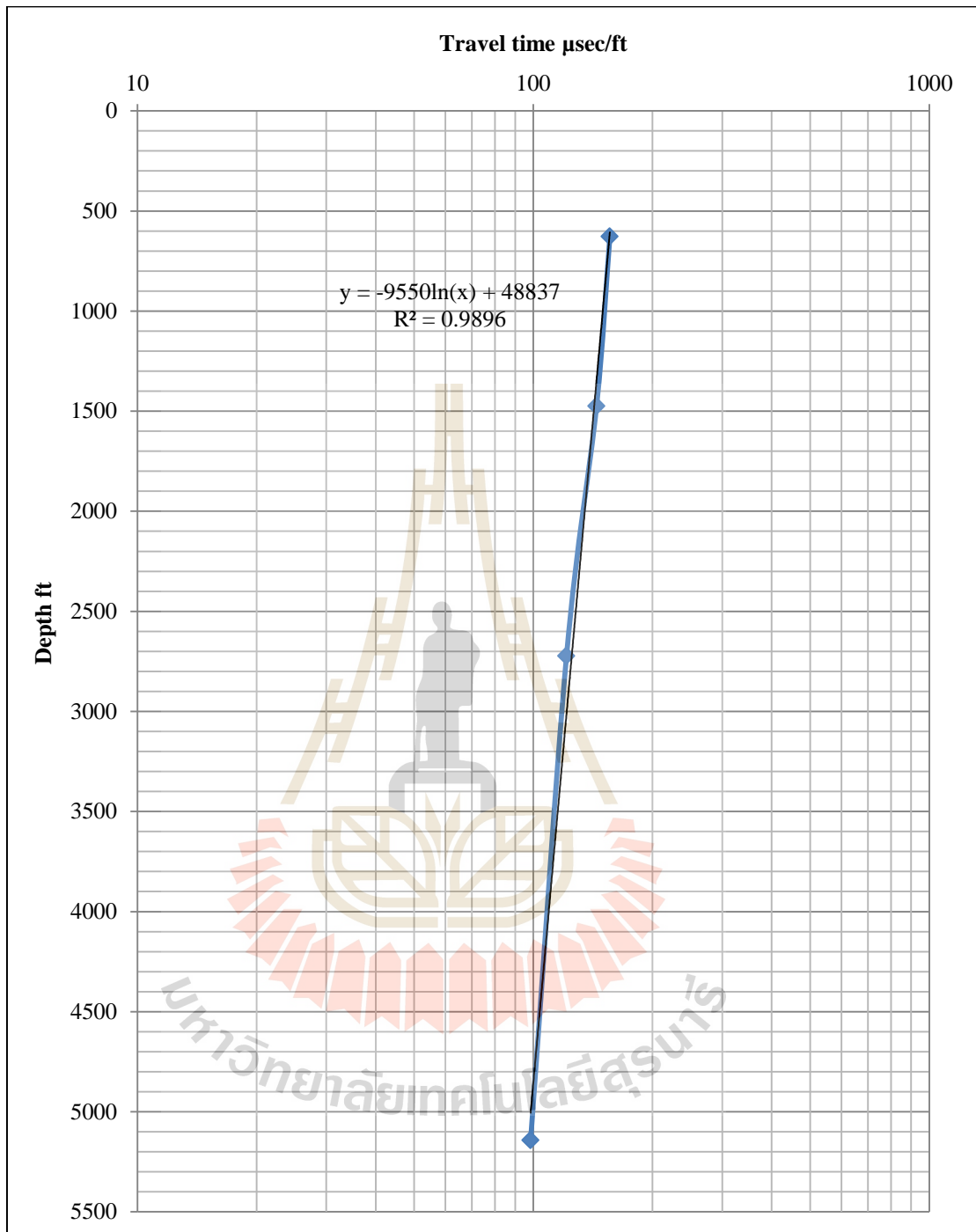
Figure 4.19 Normal compaction trend line with its corresponding linear equation

generated from seismic line F-89-031 shot point number 1313 data
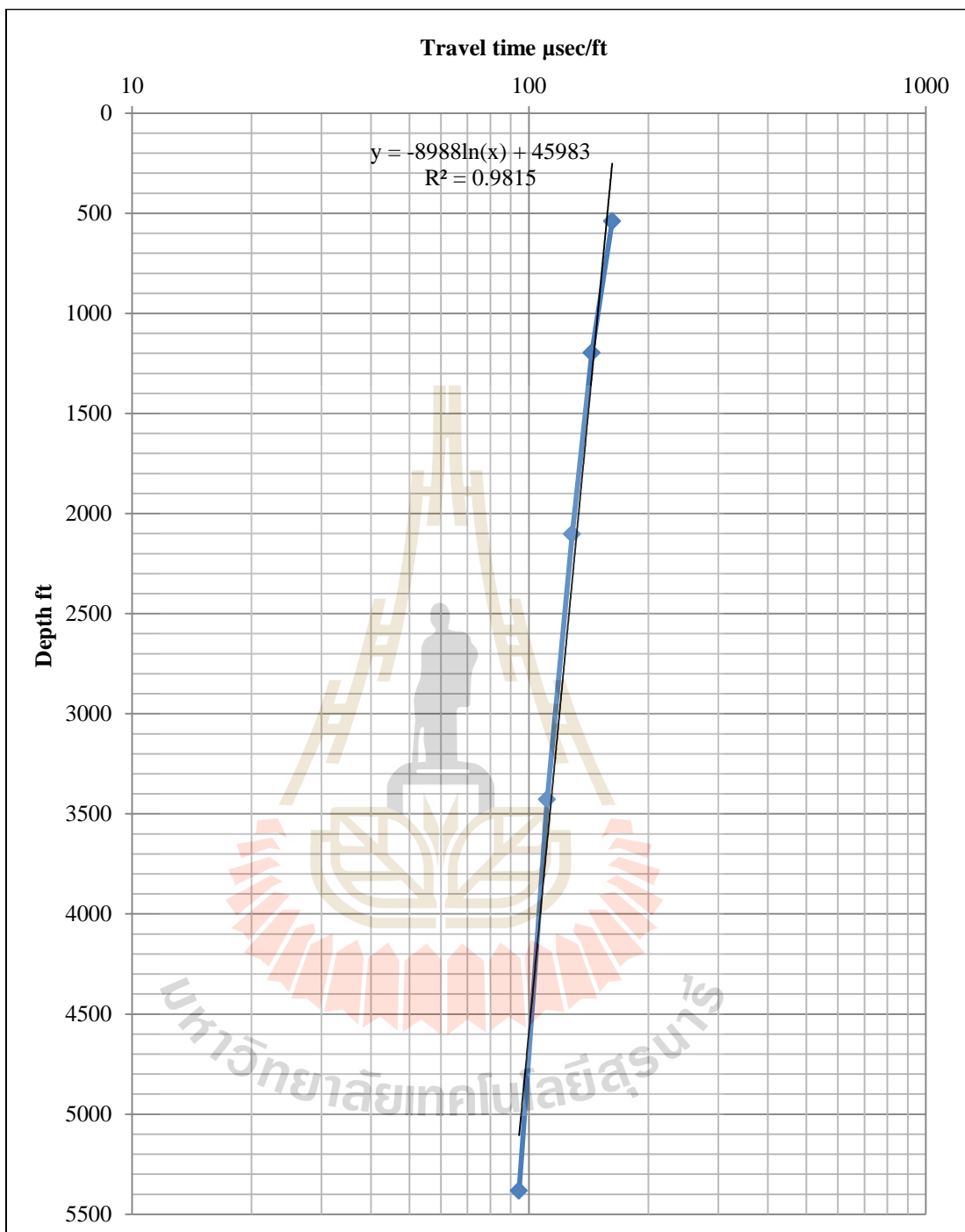
Figure 4.20 Normal compaction trend line with its corresponding linear equation

generated from seismic line F-1 shot point number 1286 data
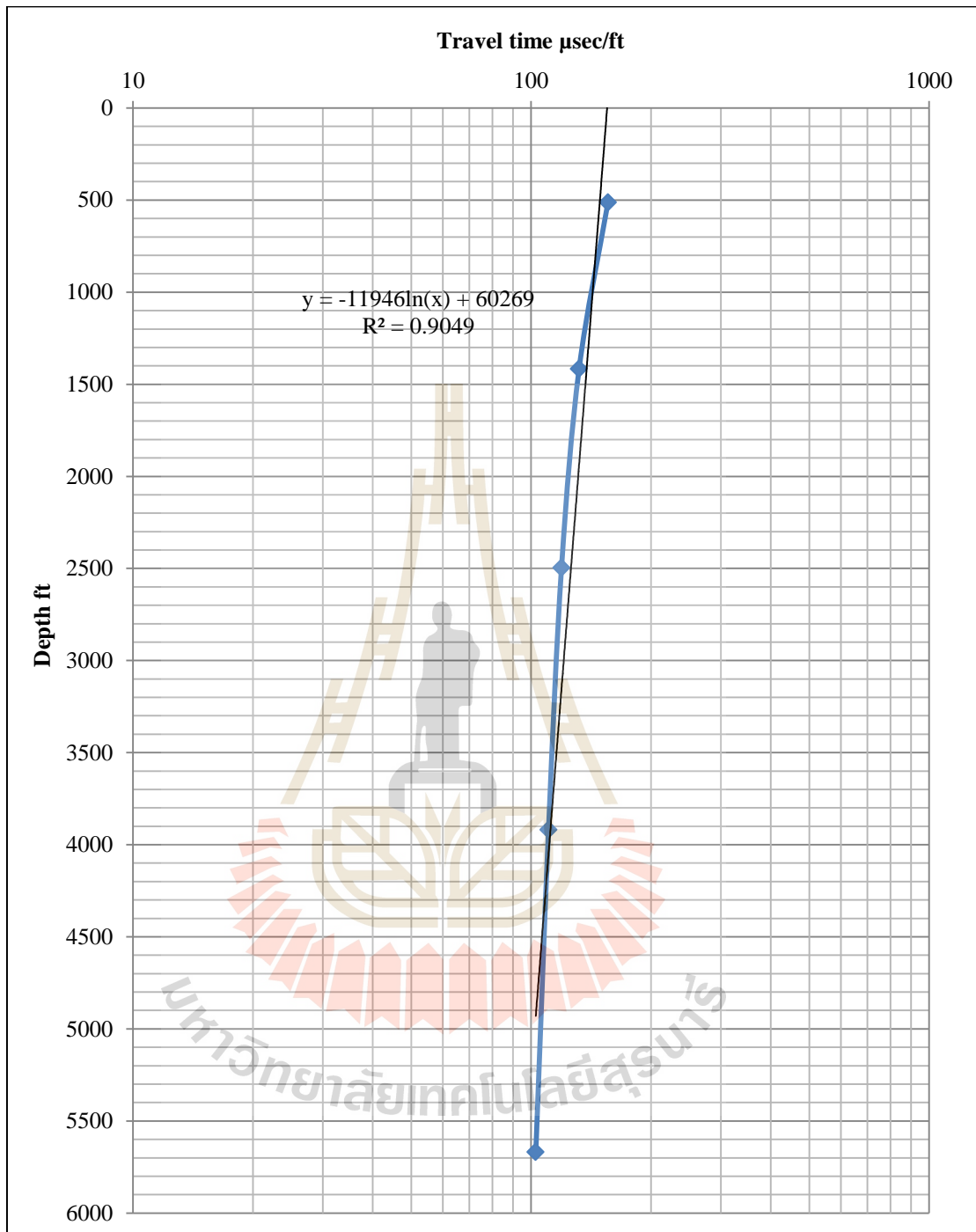
Figure 4.21 Normal compaction trend line with its corresponding linear equation

generated from seismic line F-2 shot point number 1271 data
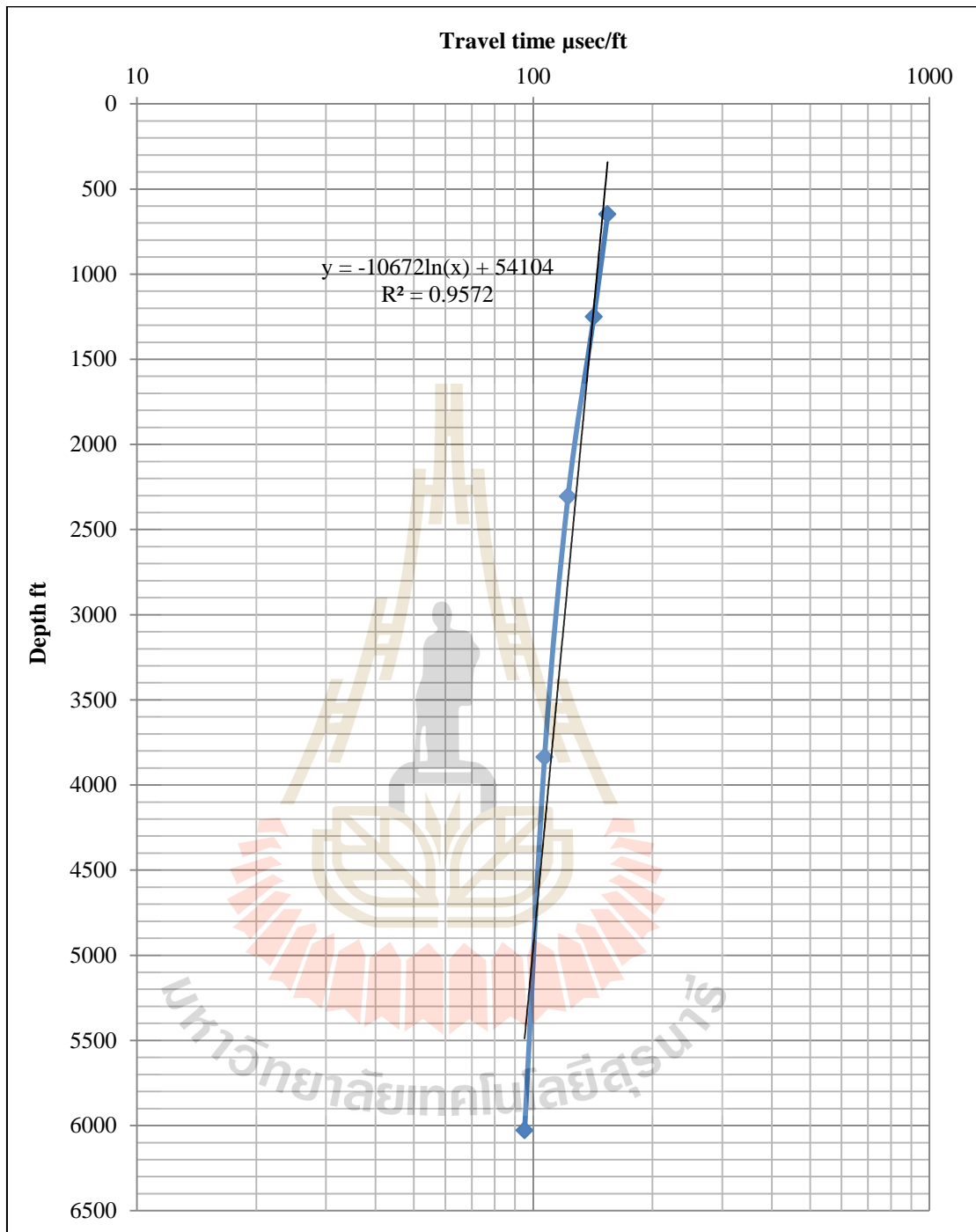
Figure 4.22 Normal compaction trend line with its corresponding linear equation

generated from seismic line F-3 shot point number NULL data

Travel time µsec/ft

$$y = -6908\ln(x) + 35341$$
$$R^2 = 0.9739$$
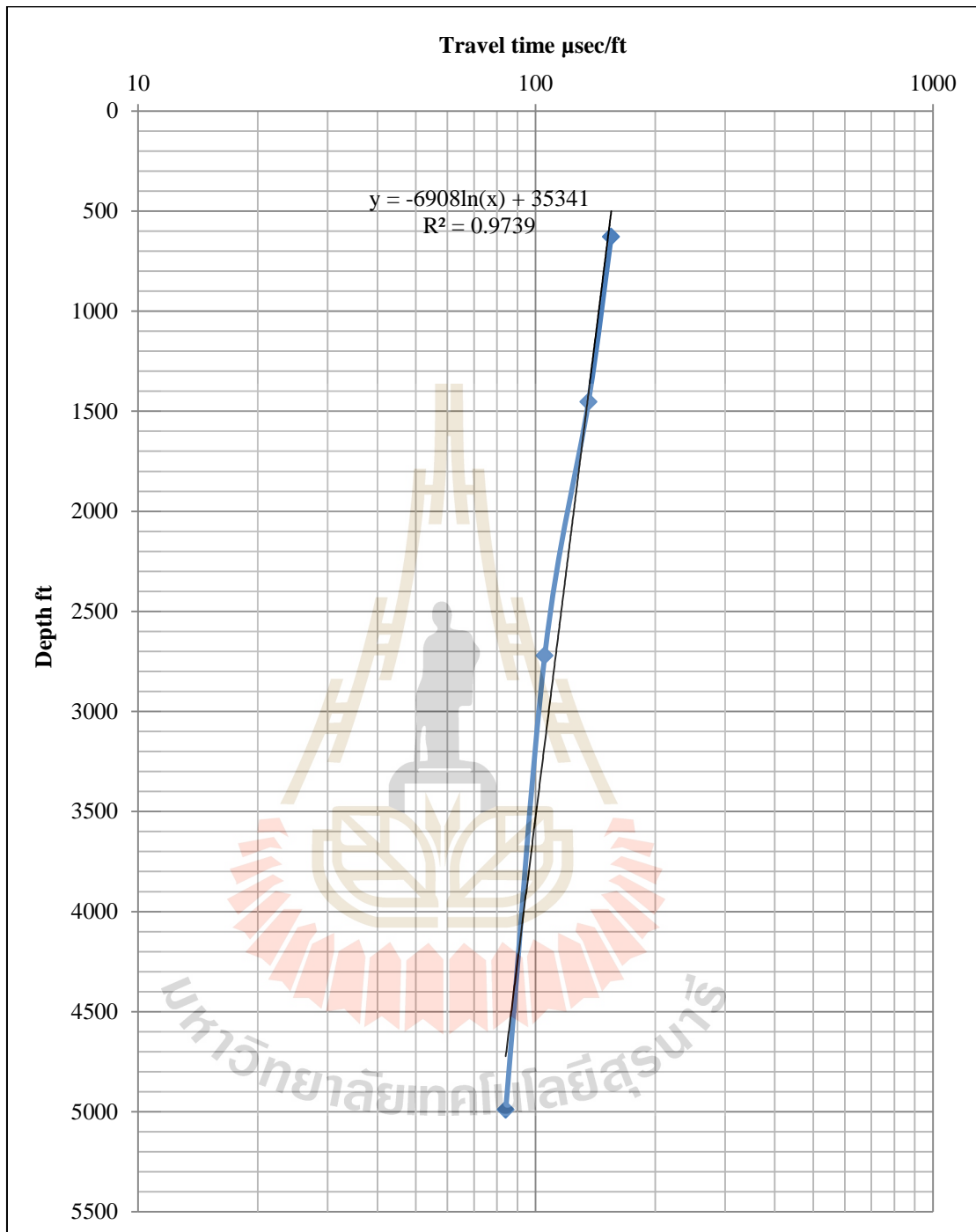
Figure 4.23 Normal compaction trend line with its corresponding linear equation

generated from seismic line F-89-038 shot point number 1192 data
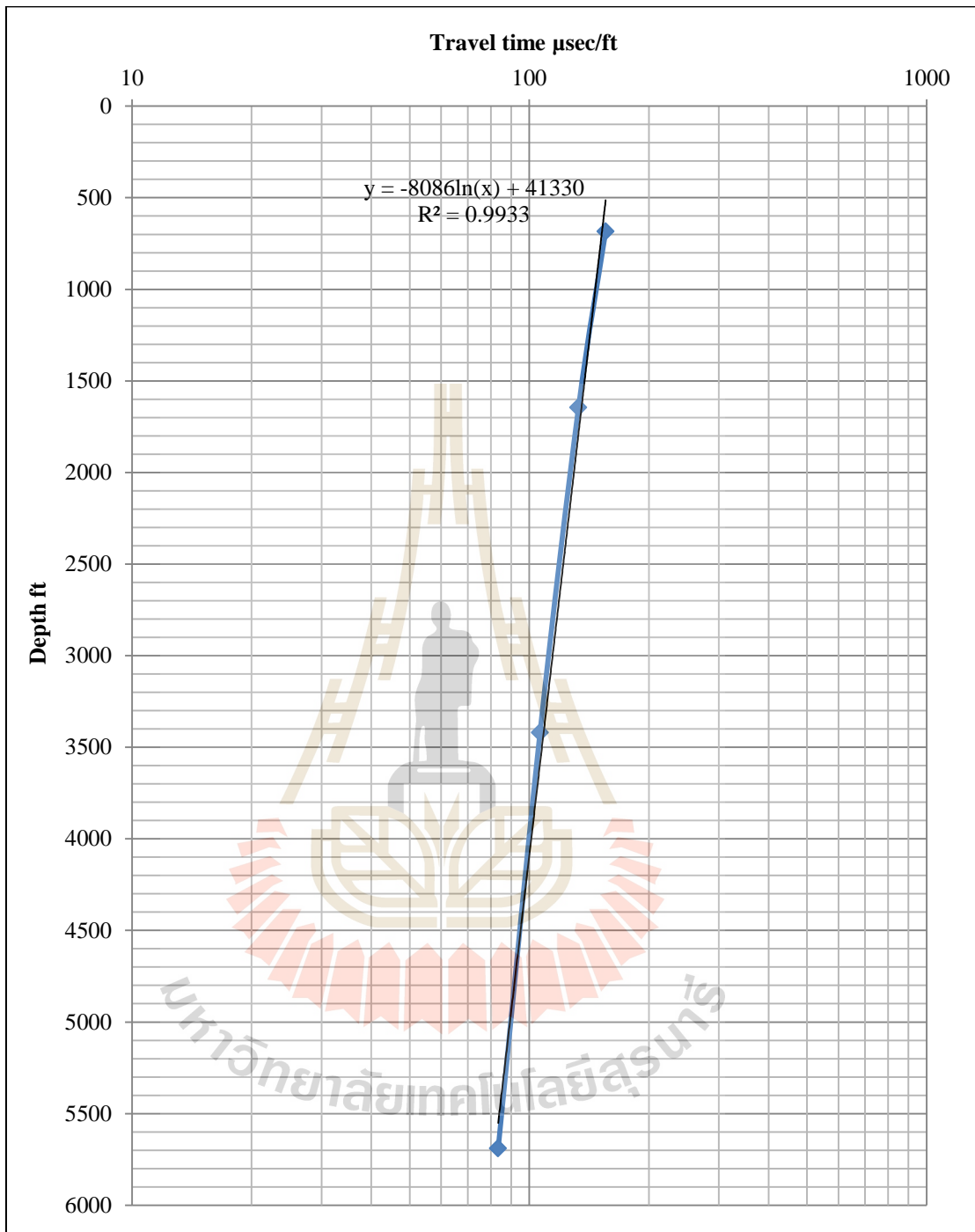
Figure 4.24 Normal compaction trend line with its corresponding linear equation

generated from seismic line F-89-040 shot point number 1167 data

4.2   Pore pressure calculation

Pore pressure were calculated after normal compaction travel time had been calculated and known from the previous section. Microsoft Excel 2010 was then used to calculated pore pressure by using equation 3.3.

Resulted pore pressure of the first data set including Line S-2 SPN 1560, Line S-3 SPN 1476, Line F-89-031 SPN 1257, Line F-1 SPN 1231, Line F-2 SPN 1227, Line F-3 SPN 1266, Line F-89-038 SPN 1127, and Line F-89-040 SPN 1131 compared with pressure data from Repeat Formation Test (RFT) of well FA-SS-37-08 and from the pressure gradient of well FA-SS-37-07 (depth in between 2,238 and 4,625 ft) are showed in Figure 4.25 – Figure 4.32.

Resulted pore pressure of the second data set including Line S-2 SPN 1524, Line S-3 SPN 1440, Line F-89-031 SPN 1189, Line F-1 SPN 1174, Line F-2 SPN 1192, Line F-3 SPN 1228, Line F-89-038 SPN 1079, and Line F-89-040 SPN 1085 compared with RFT pressure data of well FA-SS-37-08 and from the pressure gradient of well FA-SS-37-07 (depth in between 2,238 and 4,625 ft) are showed in Figure 4.33 – Figure 4.40.

Resulted pore pressure of the second data set including Line S-2 SPN 1596, Line S-3 SPN 1512, Line F-89-031 SPN 1313, Line F-1 SPN 1286, Line F-2 SPN 1271, Line F-3 SPN NULL, Line F-89-038 SPN 1192, and Line F-89-040 SPN 1167 compared with RFT pressure data of well FA-SS-37-08 and from the pressure gradient of well FA-SS-37-07 (depth in between 2,238 and 4,625 ft) are showed in Figure 4.41 – Figure 4.48.
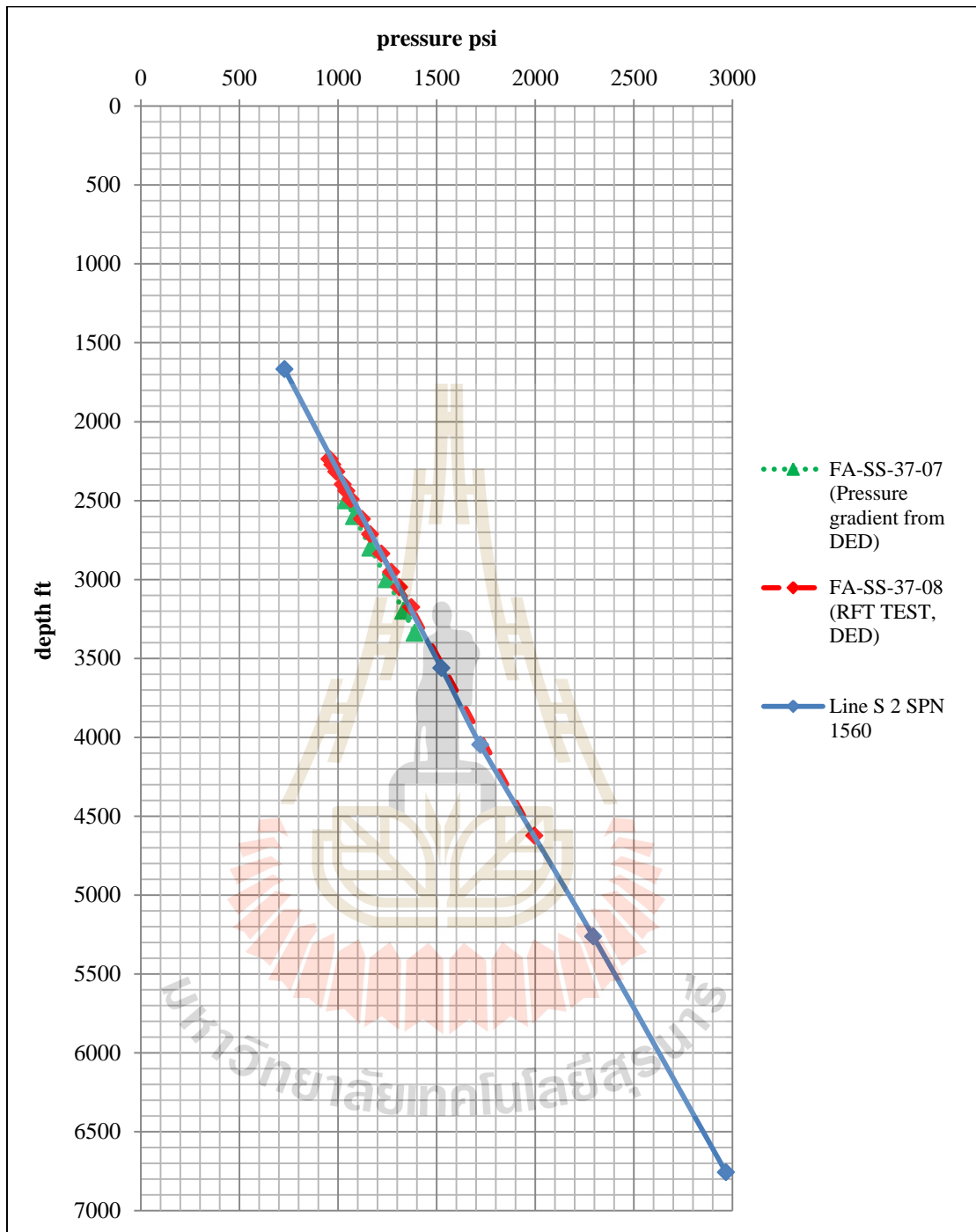
Figure 4.25 Pore pressure calculated from seismic line S-2 shot point number 1560
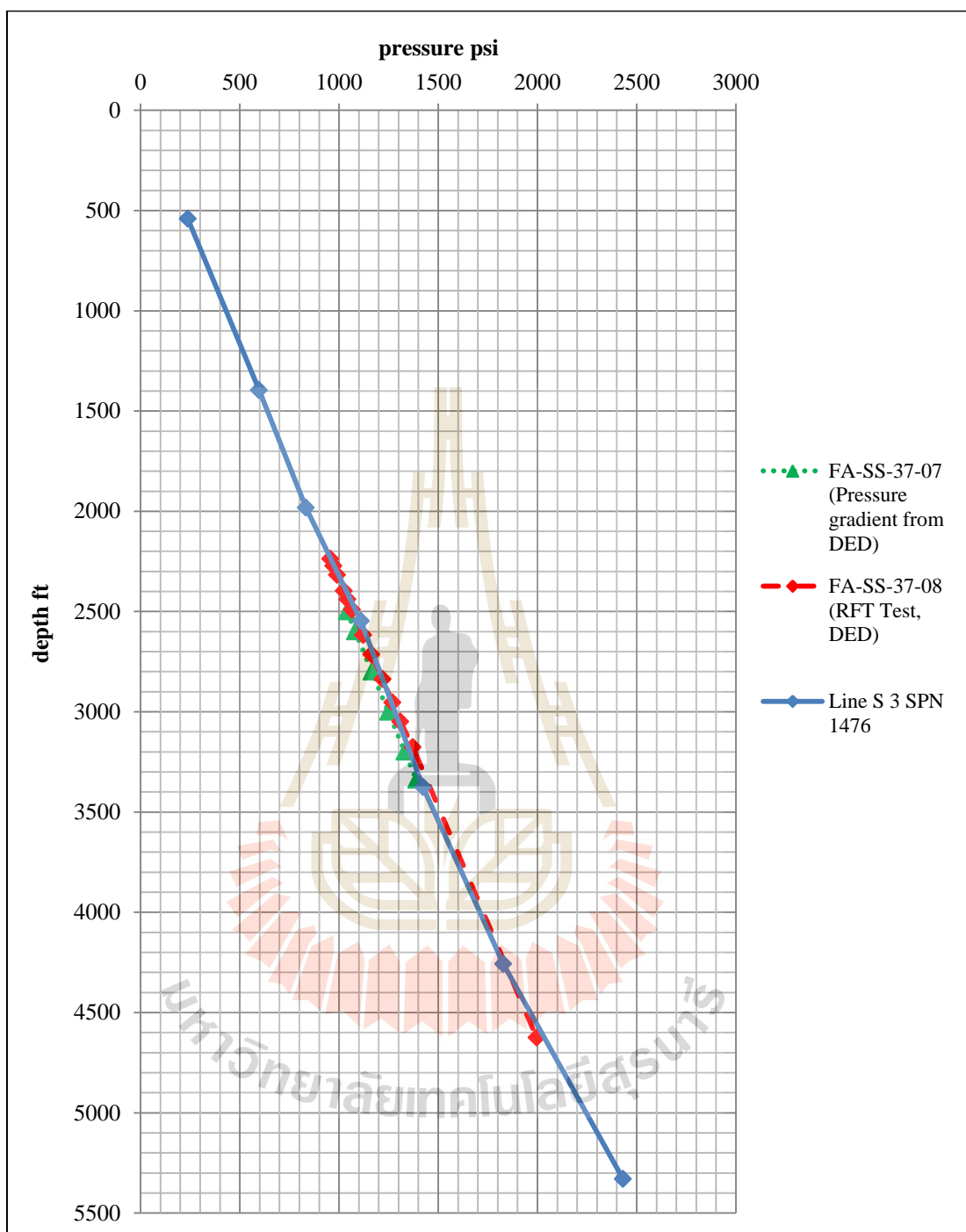
data

Figure 4.26 Pore pressure calculated from seismic line S-3 shot point number 1476
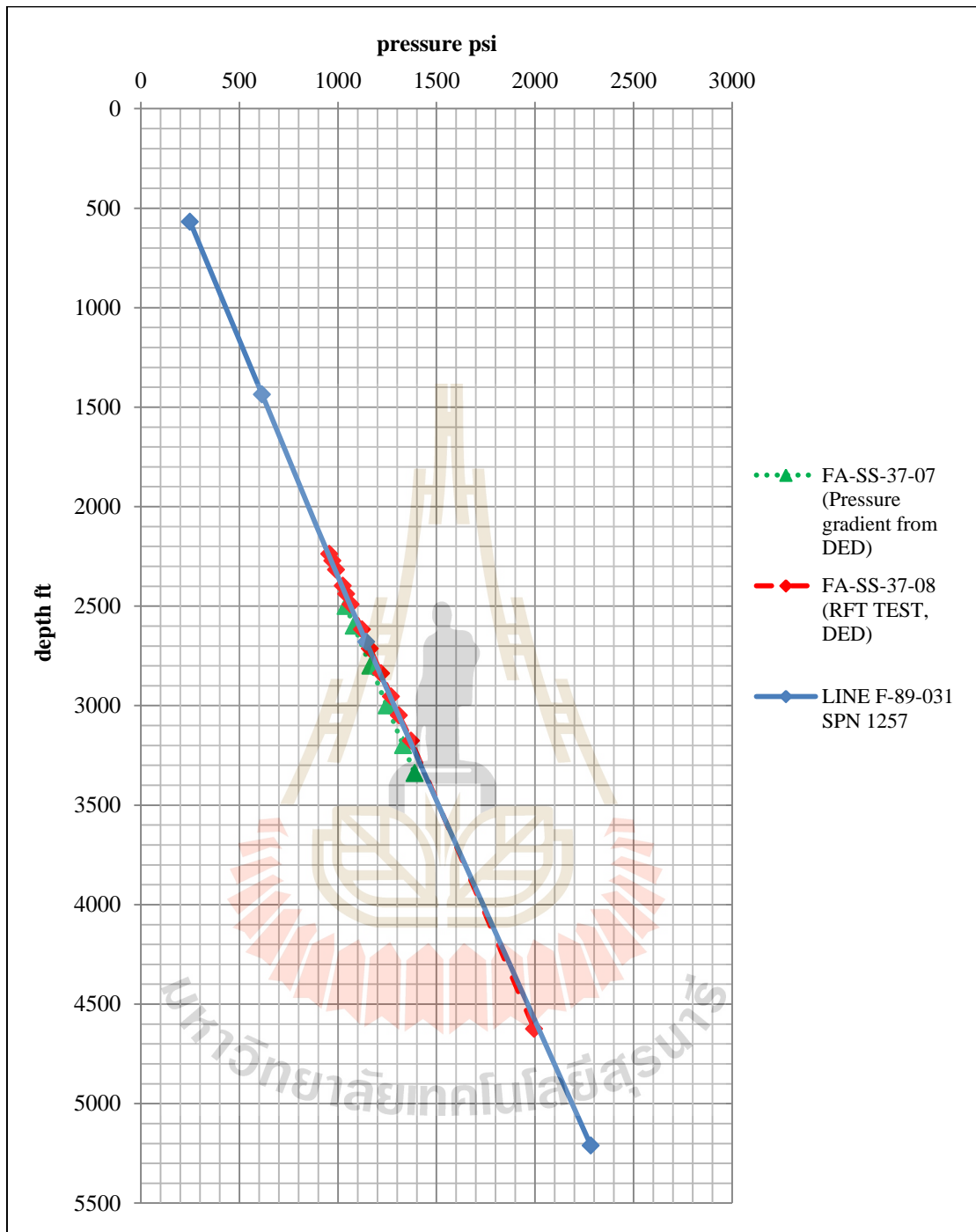
data

Figure 4.27 Pore pressure calculated from seismic line F-89-031 shot point number

1257 data
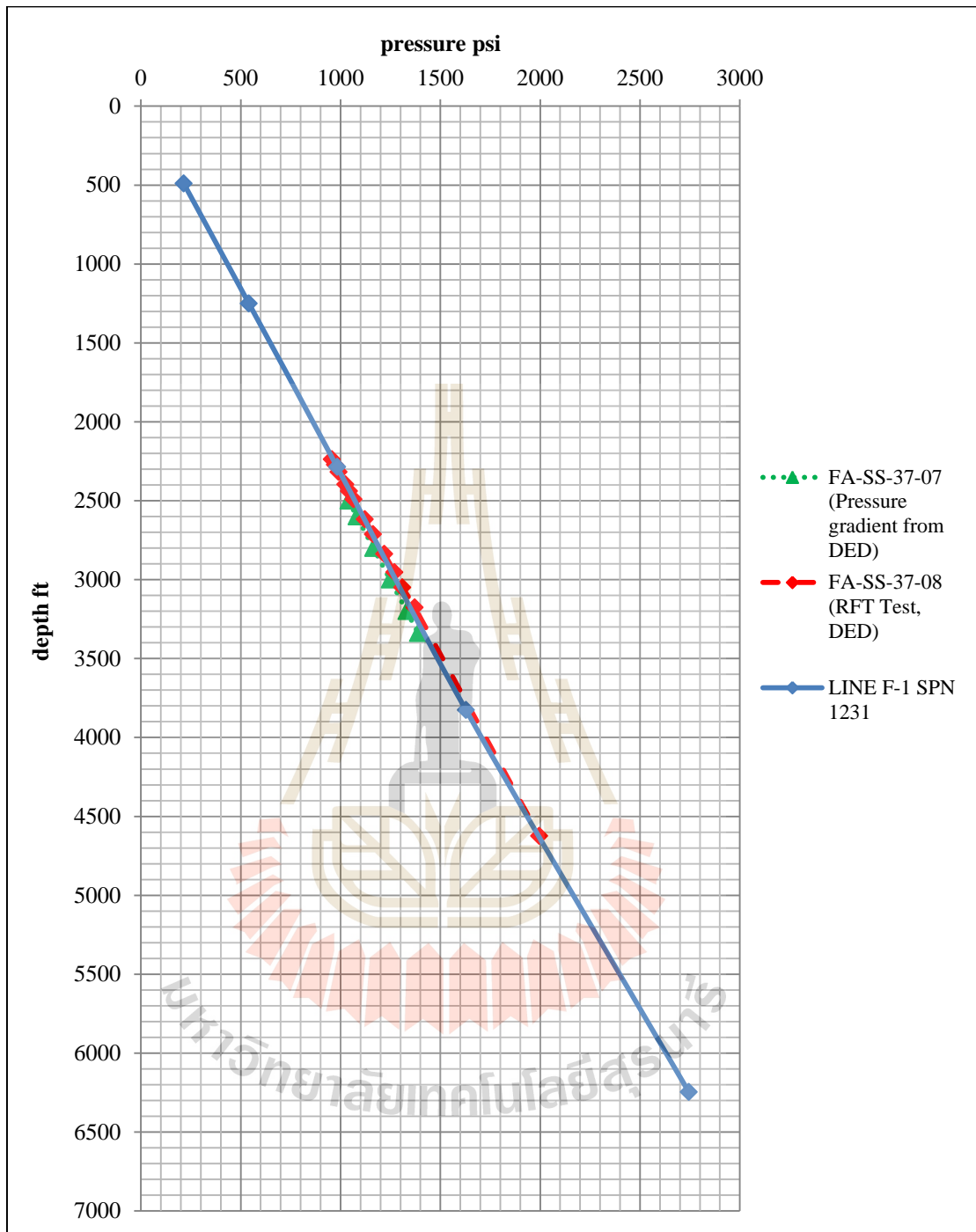
Figure 4.28 Pore pressure calculated from seismic line F-1 shot point number 1231
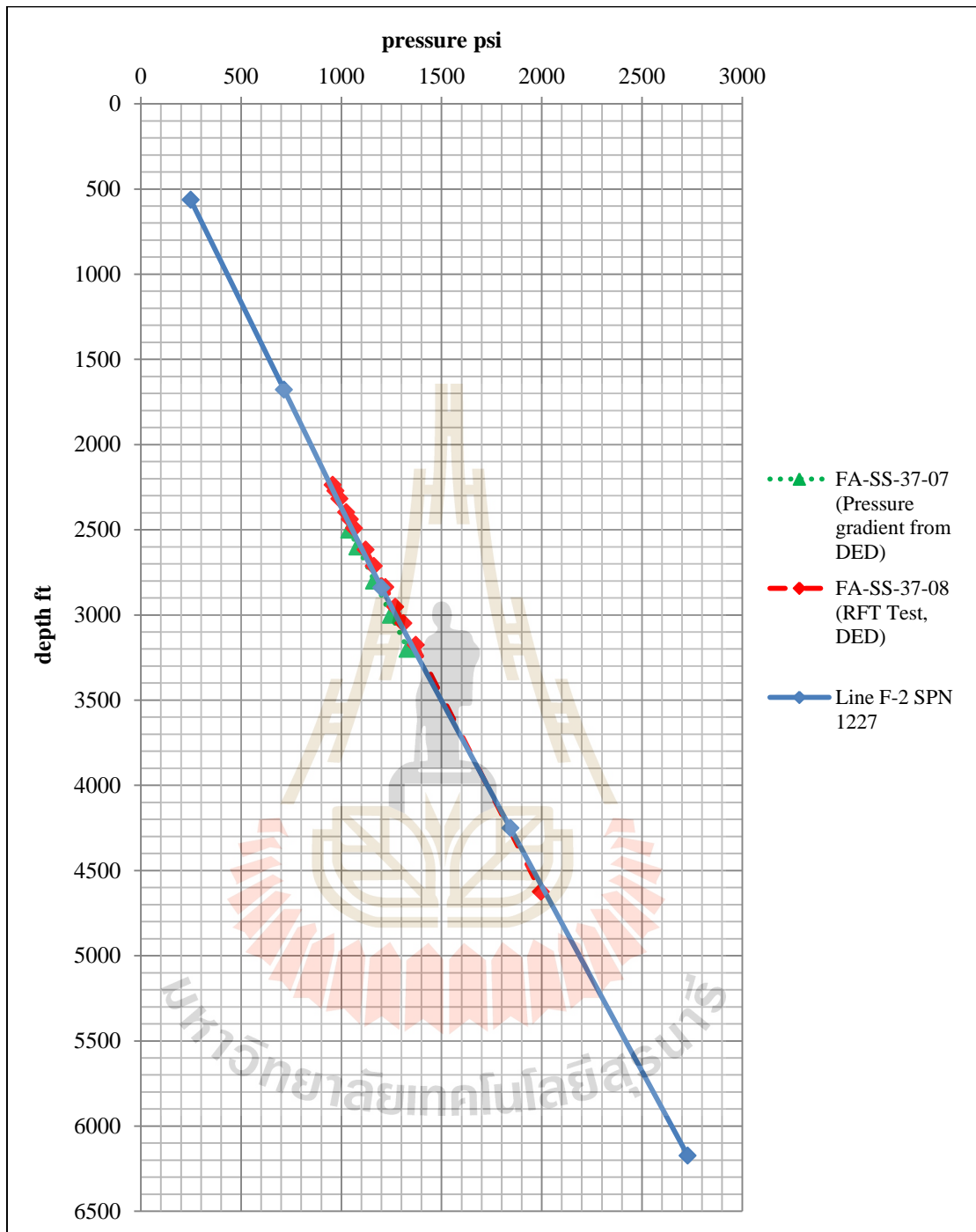
data

Figure 4.29 Pore pressure calculated from seismic line F-2 shot point number 1227
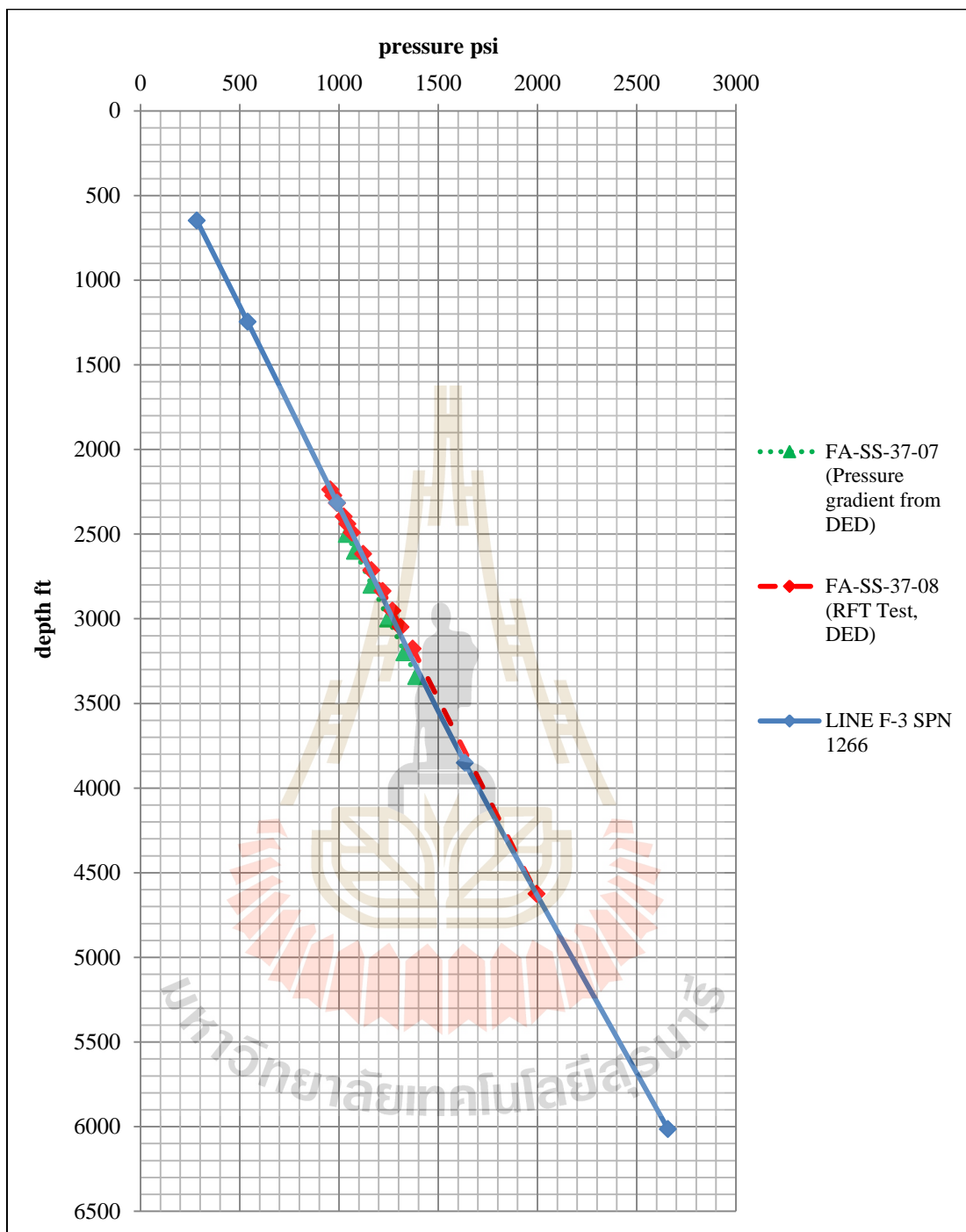
data

Figure 4.30 Pore pressure calculated from seismic line F-3 shot point number 1266
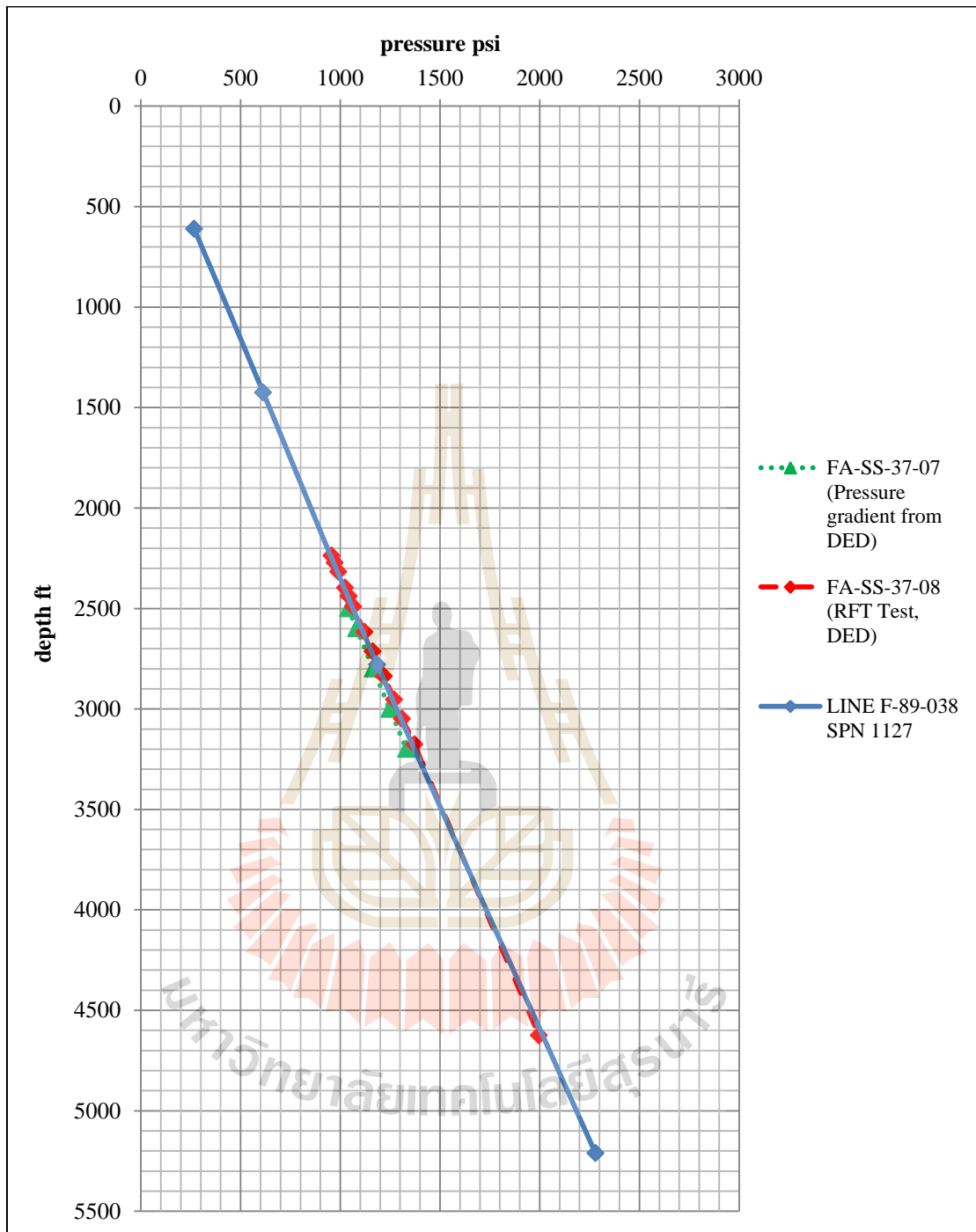
data

Figure 4.31 Pore pressure calculated from seismic line F-89-038 shot point number

1127 data
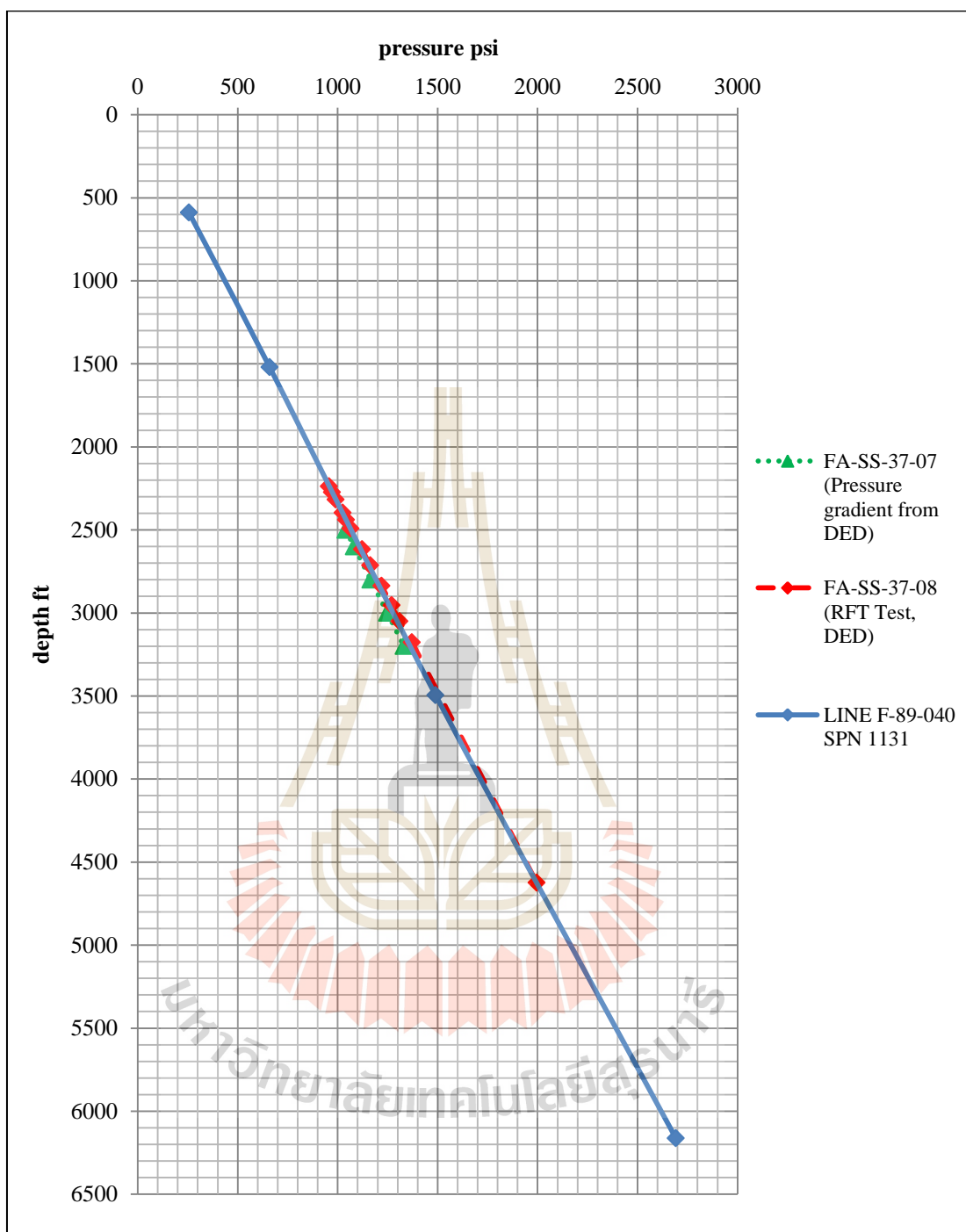
Figure 4.32 Pore pressure calculated from seismic line F-89-040 shot point number

1131 data
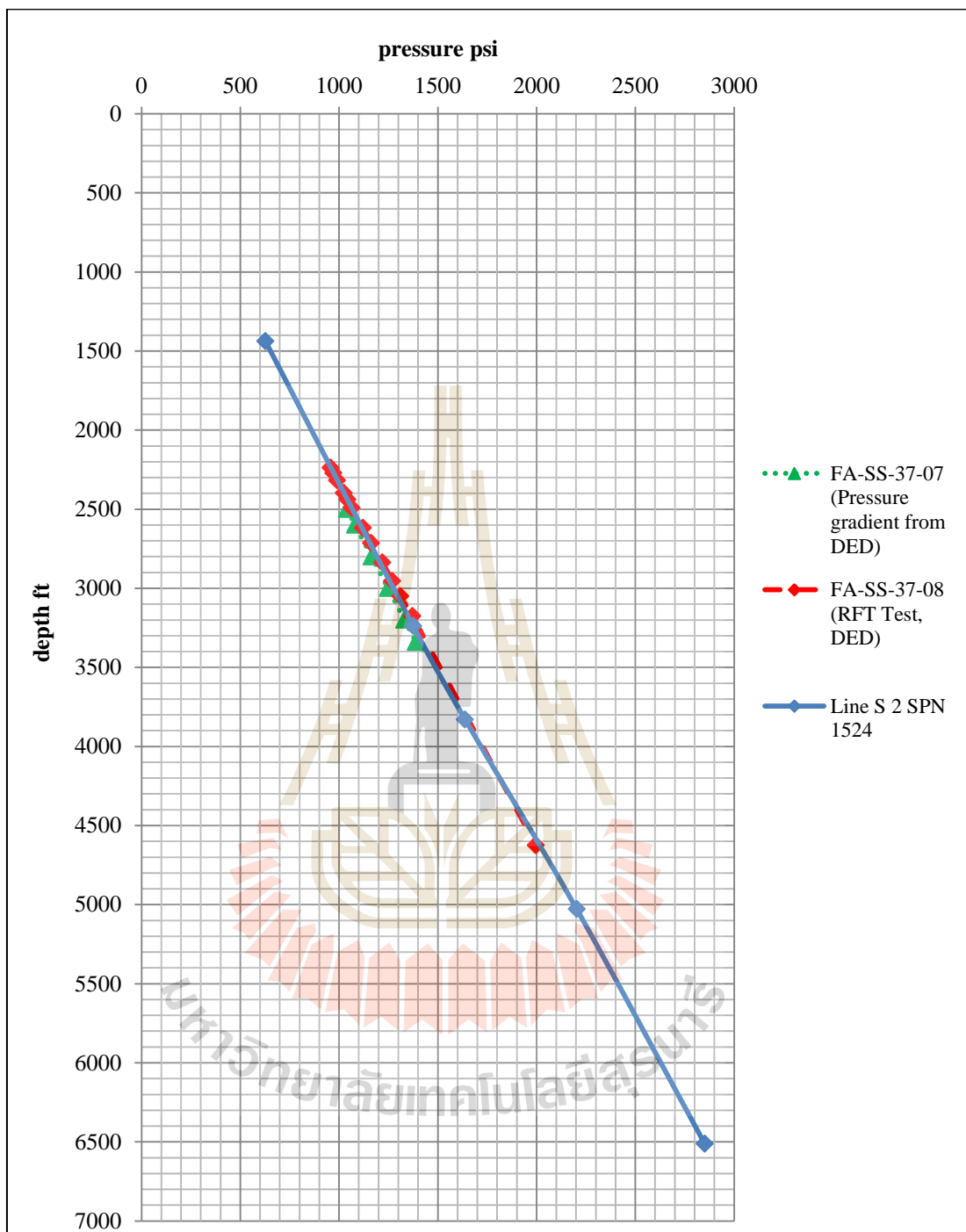
Figure 4.33 Pore pressure calculated from seismic line S-2 shot point number 1524
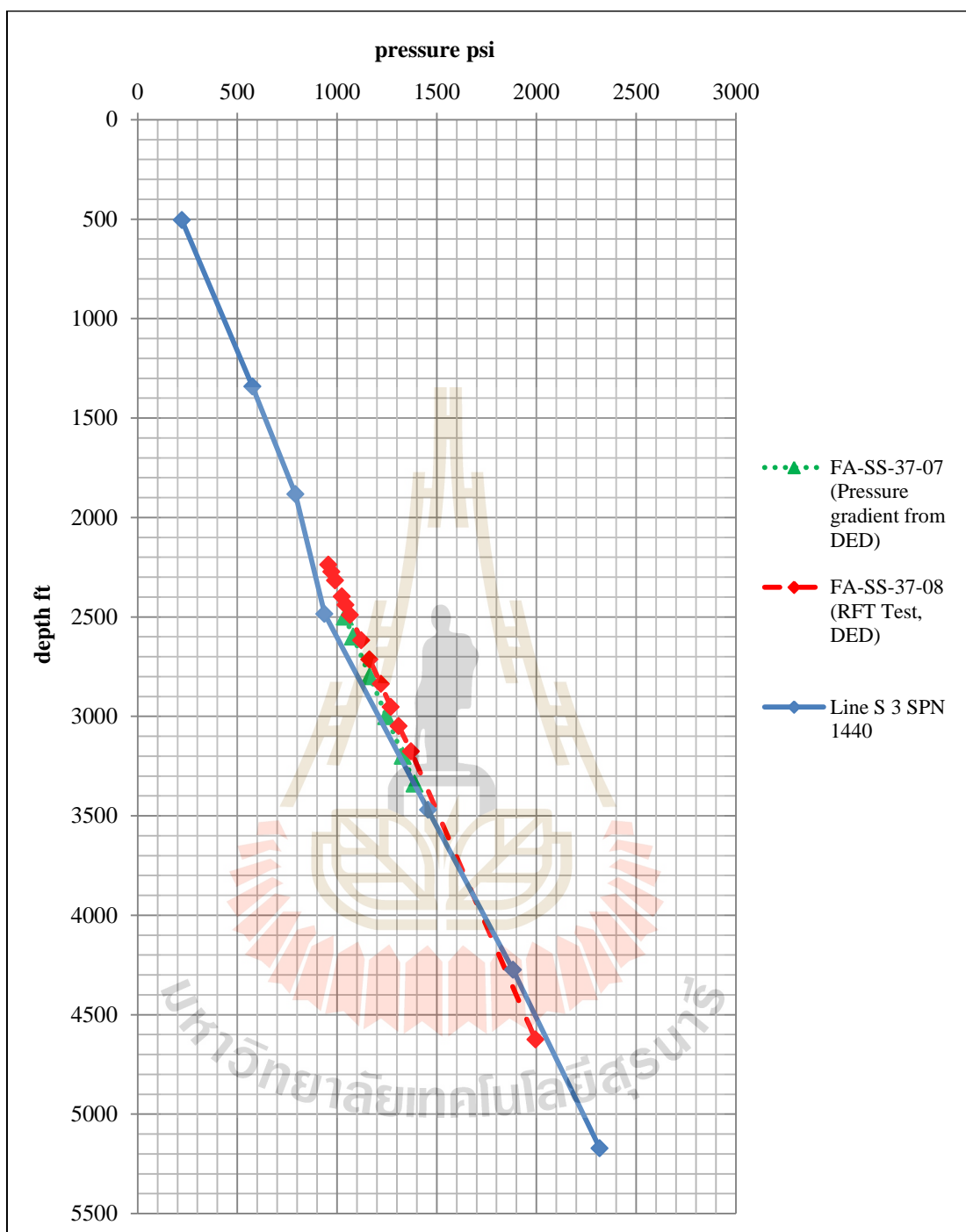
data

Figure 4.34 Pore pressure calculated from seismic line S-3 shot point number 1440
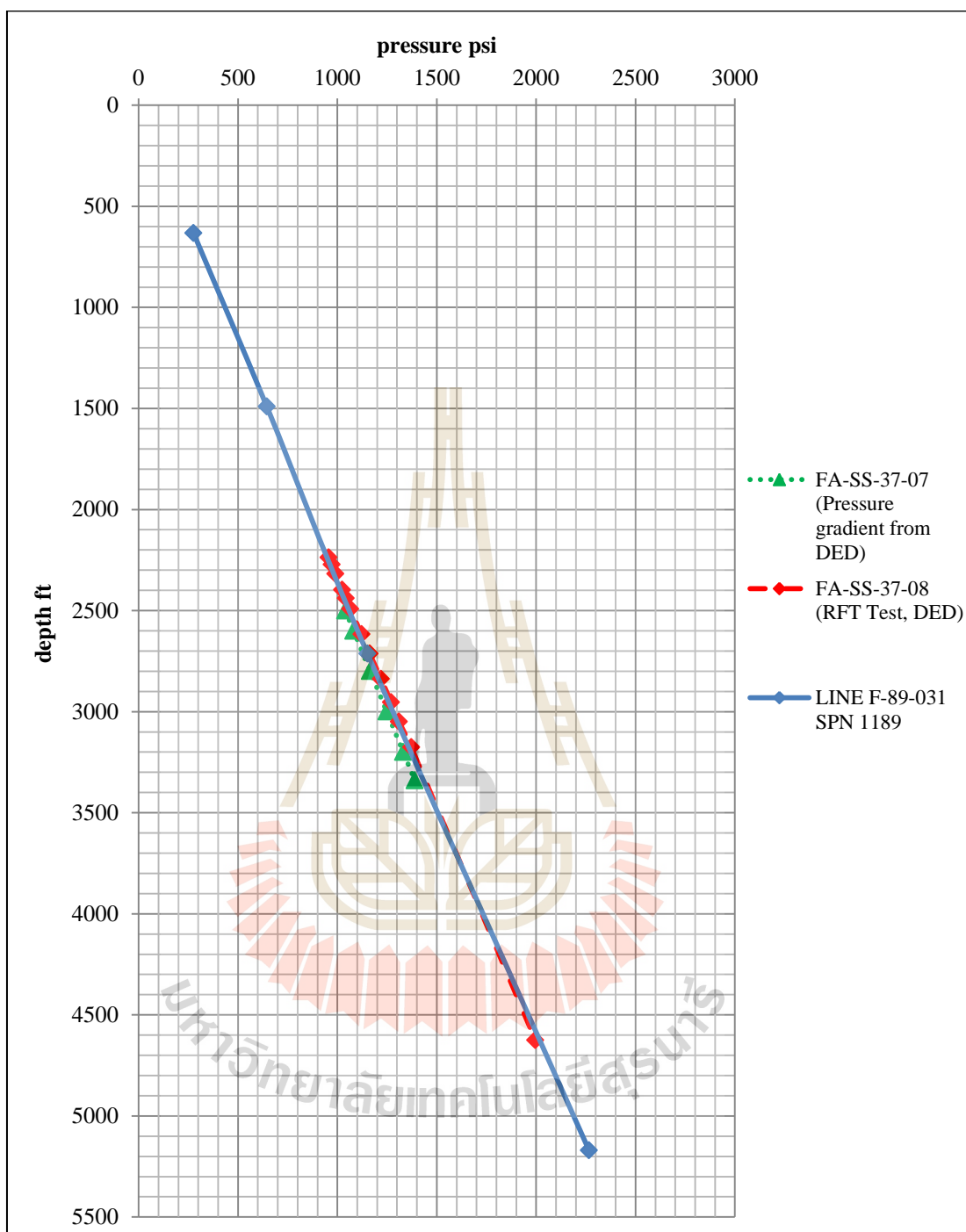
data

Figure 4.35 Pore pressure calculated from seismic line F-89-031 shot point number

1189 data
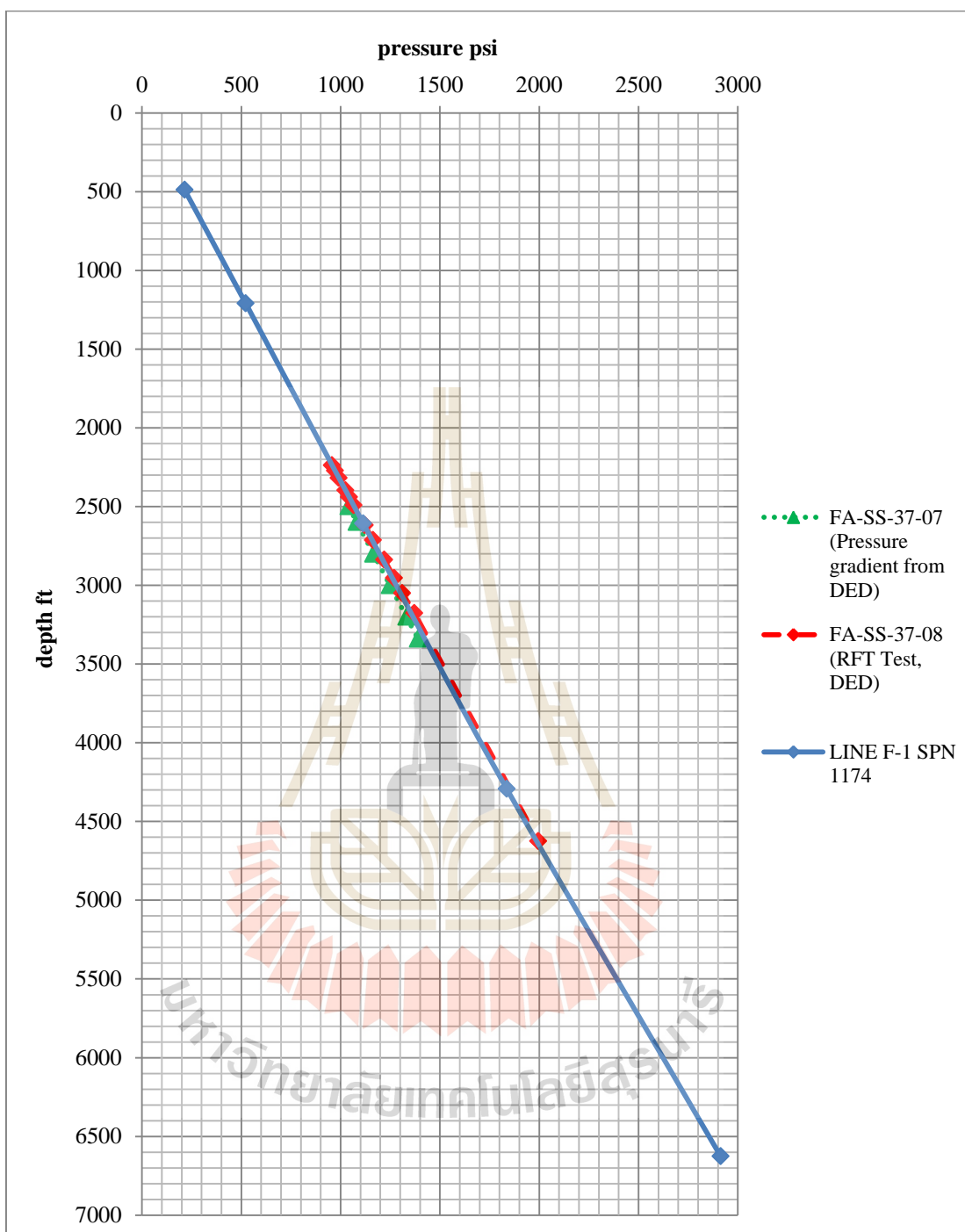
Figure 4.36 Pore pressure calculation of seismic line F-1 shot point number 1174
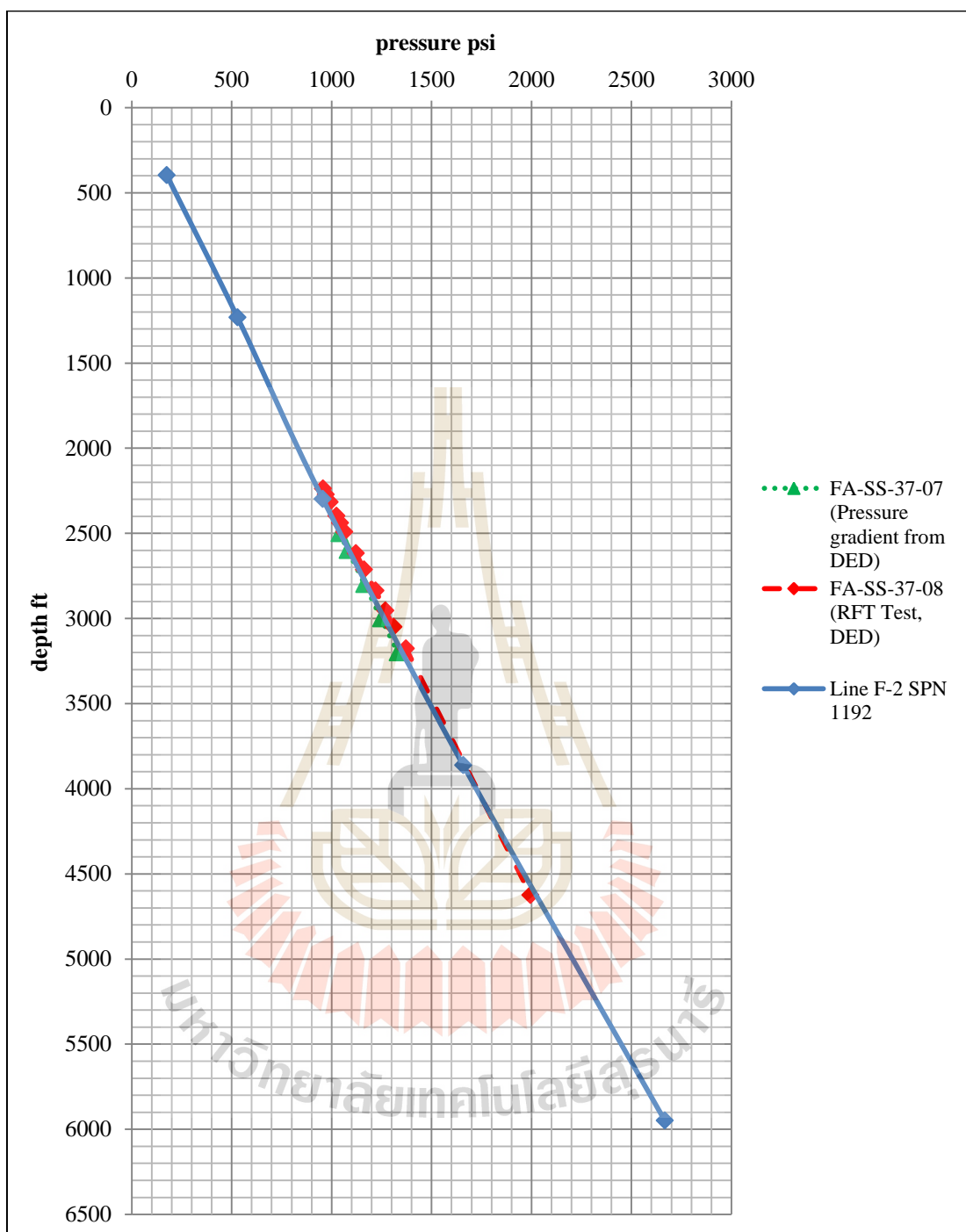
data

Figure 4.37 Pore pressure calculated from seismic line F-2 shot point number 1192
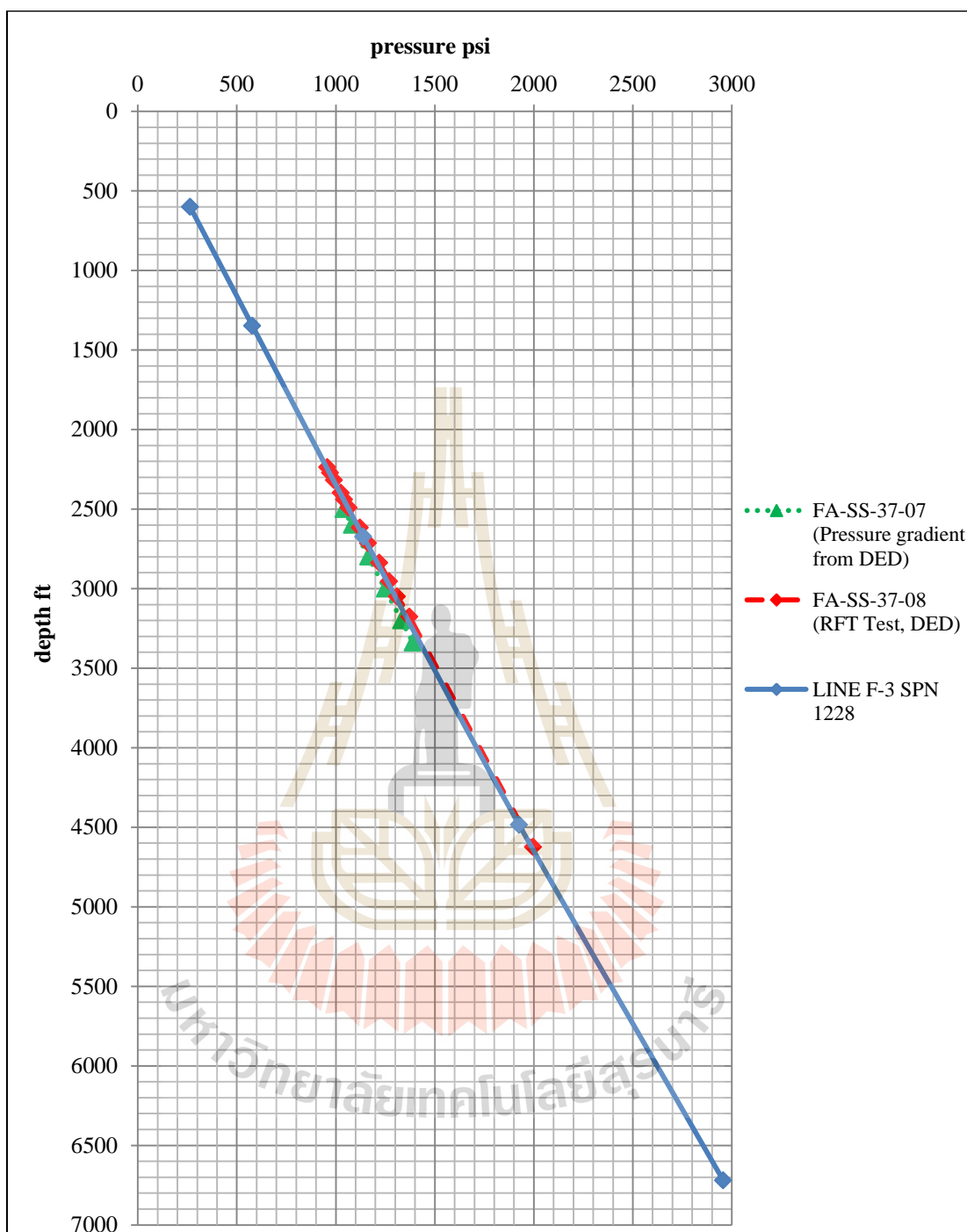
data

Figure 4.38 Pore pressure calculated from seismic line F-3 shot point number 1228
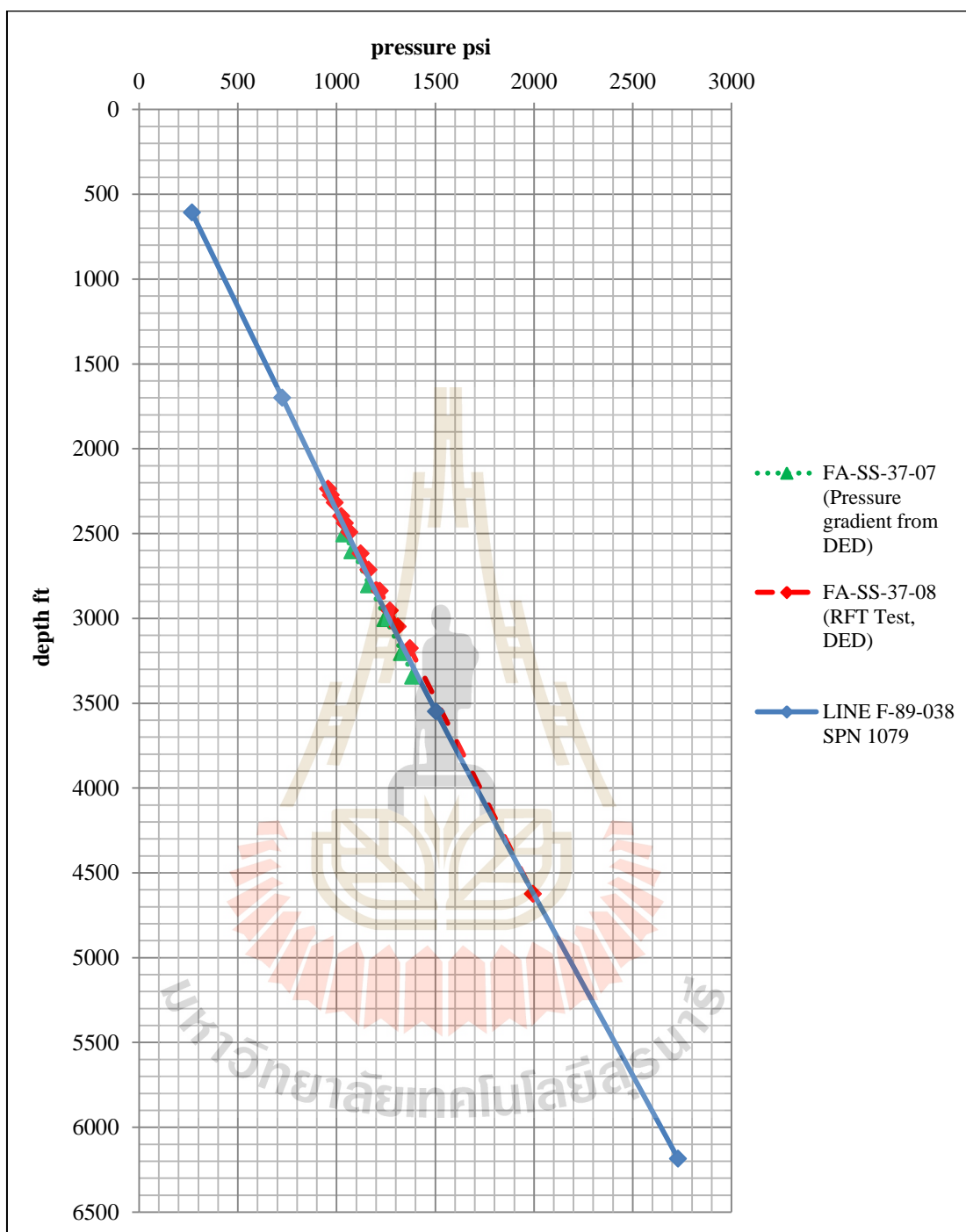
data

Figure 4.39 Pore pressure calculated from seismic line F-89-038 shot point number

1079 data
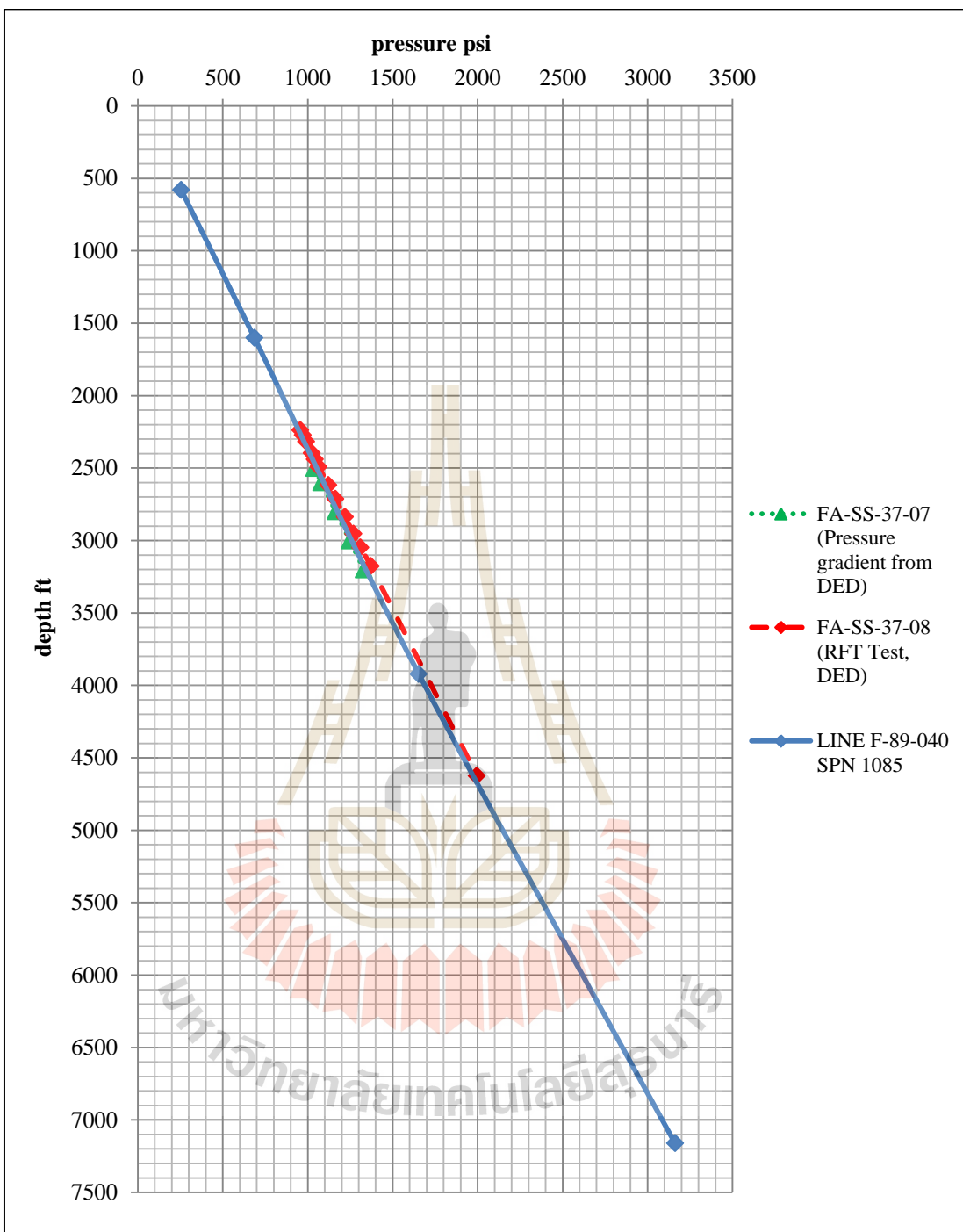
Figure 4.40 Pore pressure calculated from seismic line F-89-040 shot point number

1085
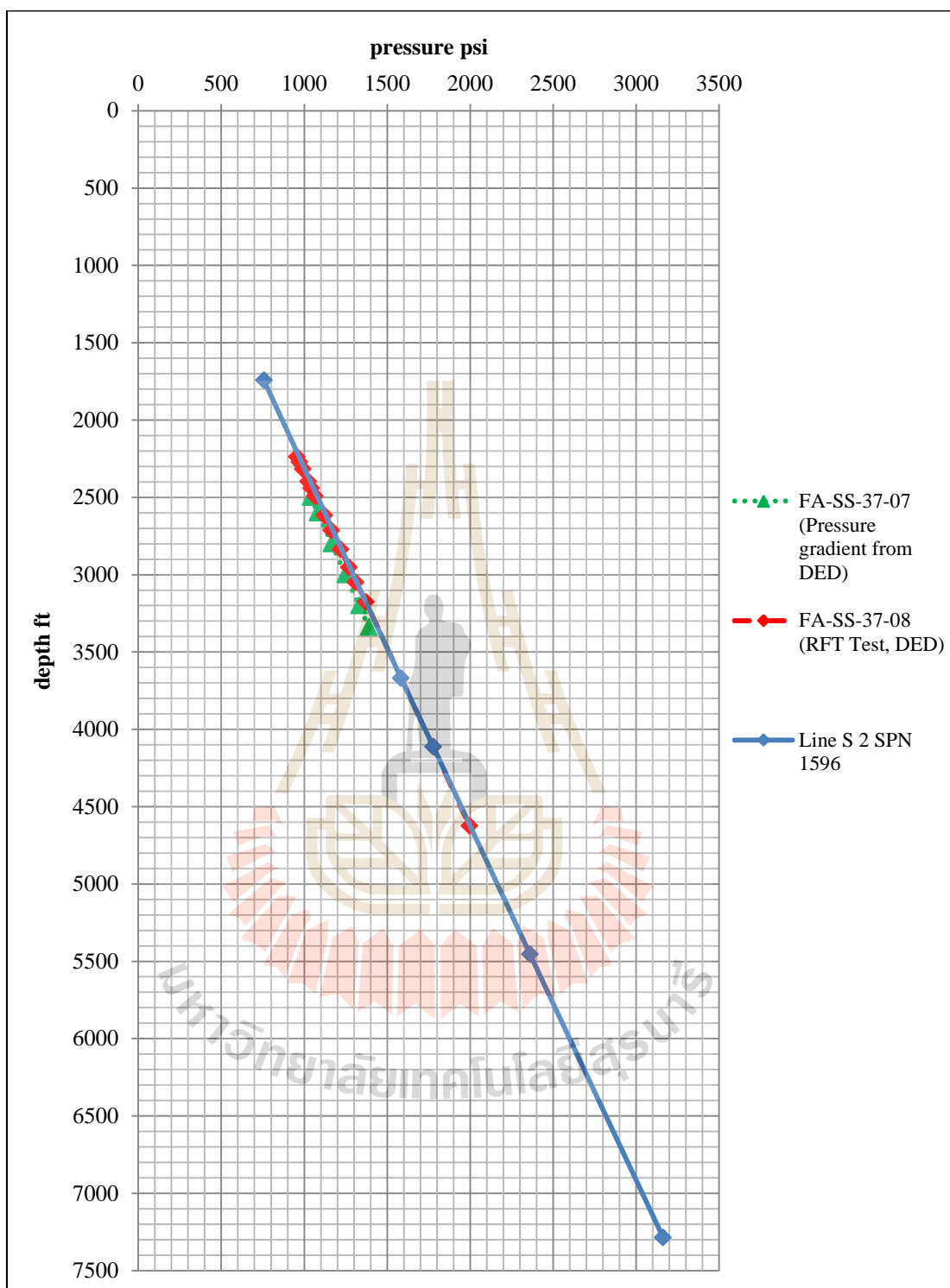
Figure 4.41 Pore pressure calculated from seismic line S-2 shot point number 1596
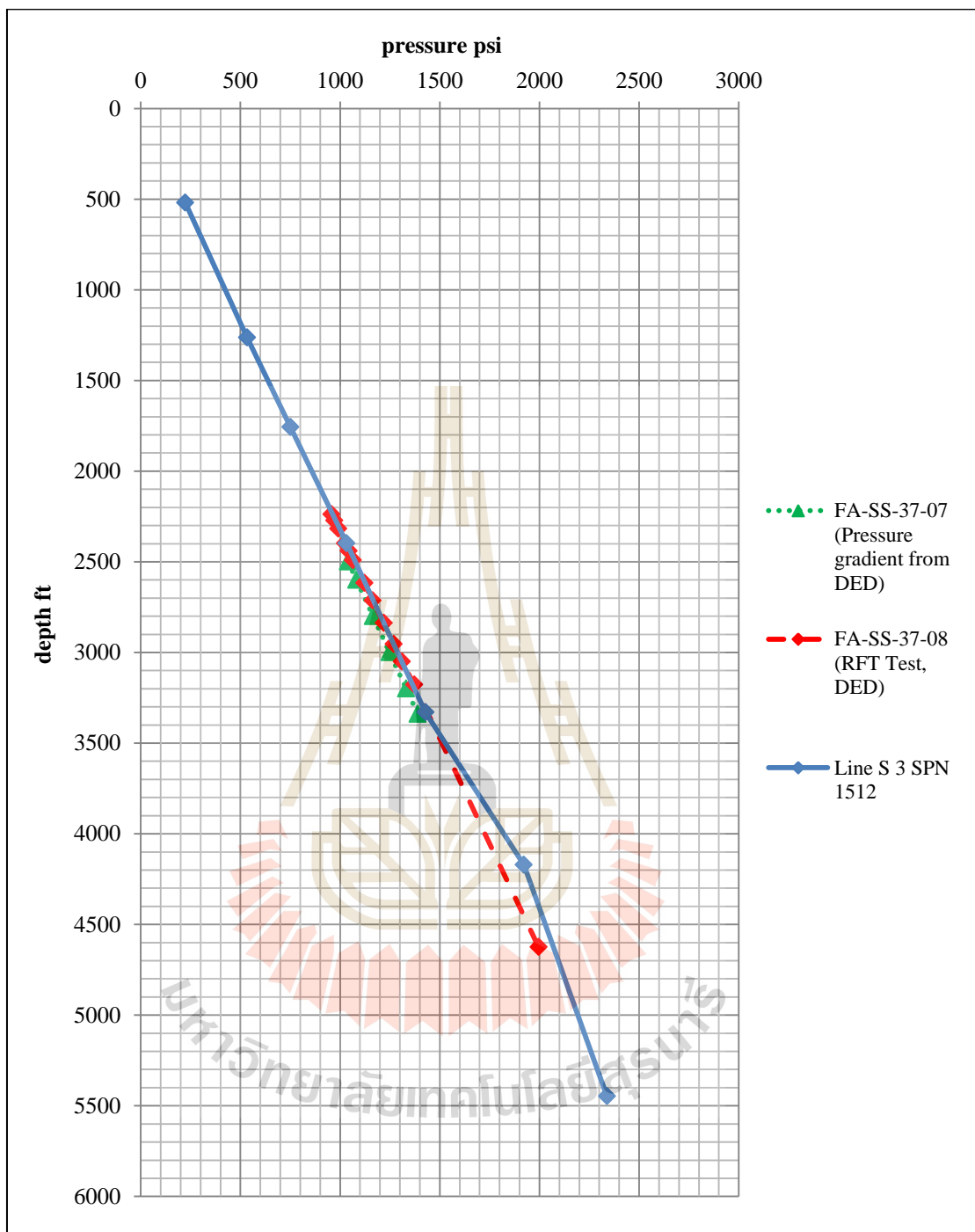
data

Figure 4.42 Pore pressure calculated from seismic line S-3 shot point number 1512
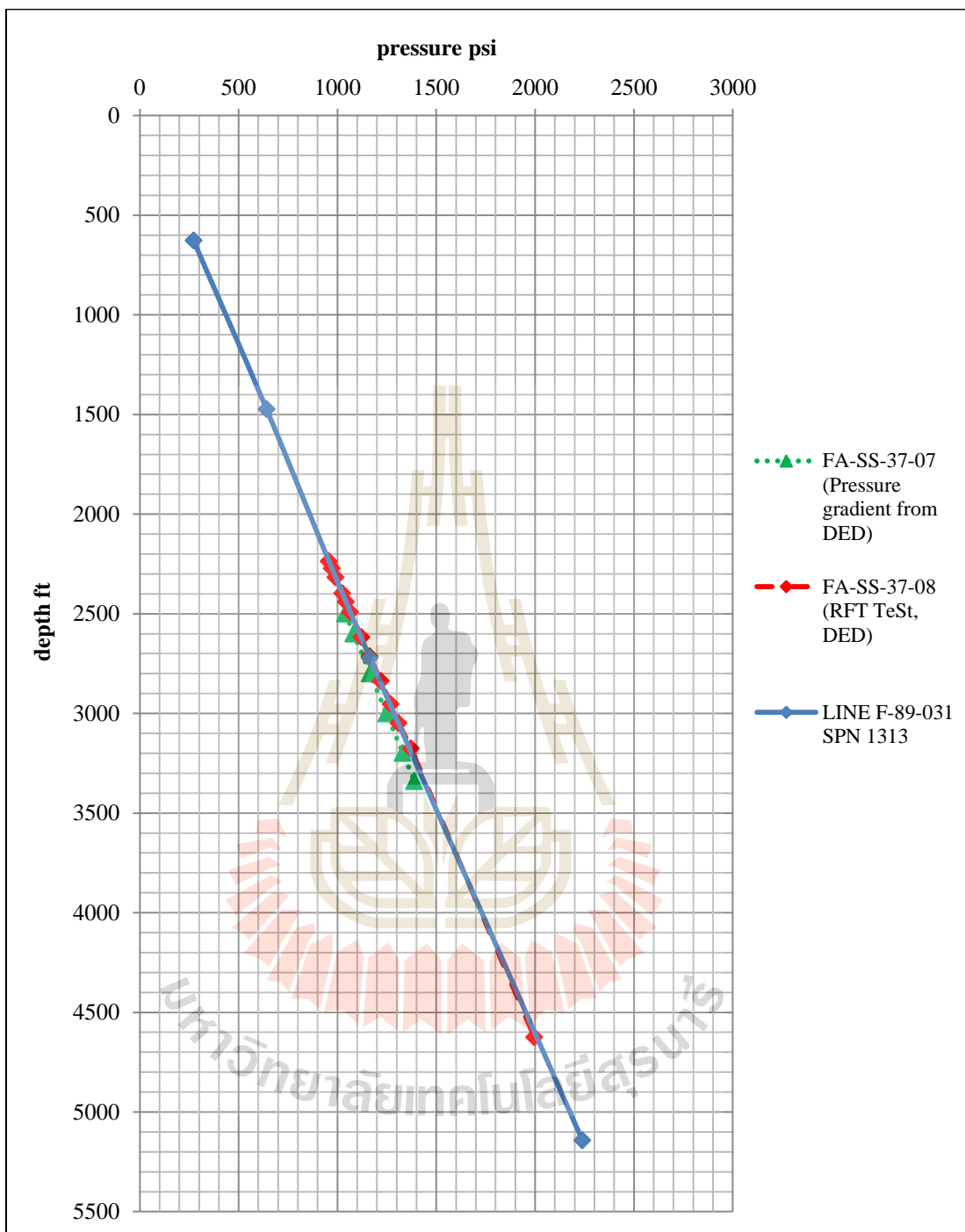
data

Figure 4.43 Pore pressure calculated from seismic line F-89-031 shot point number

1313 data
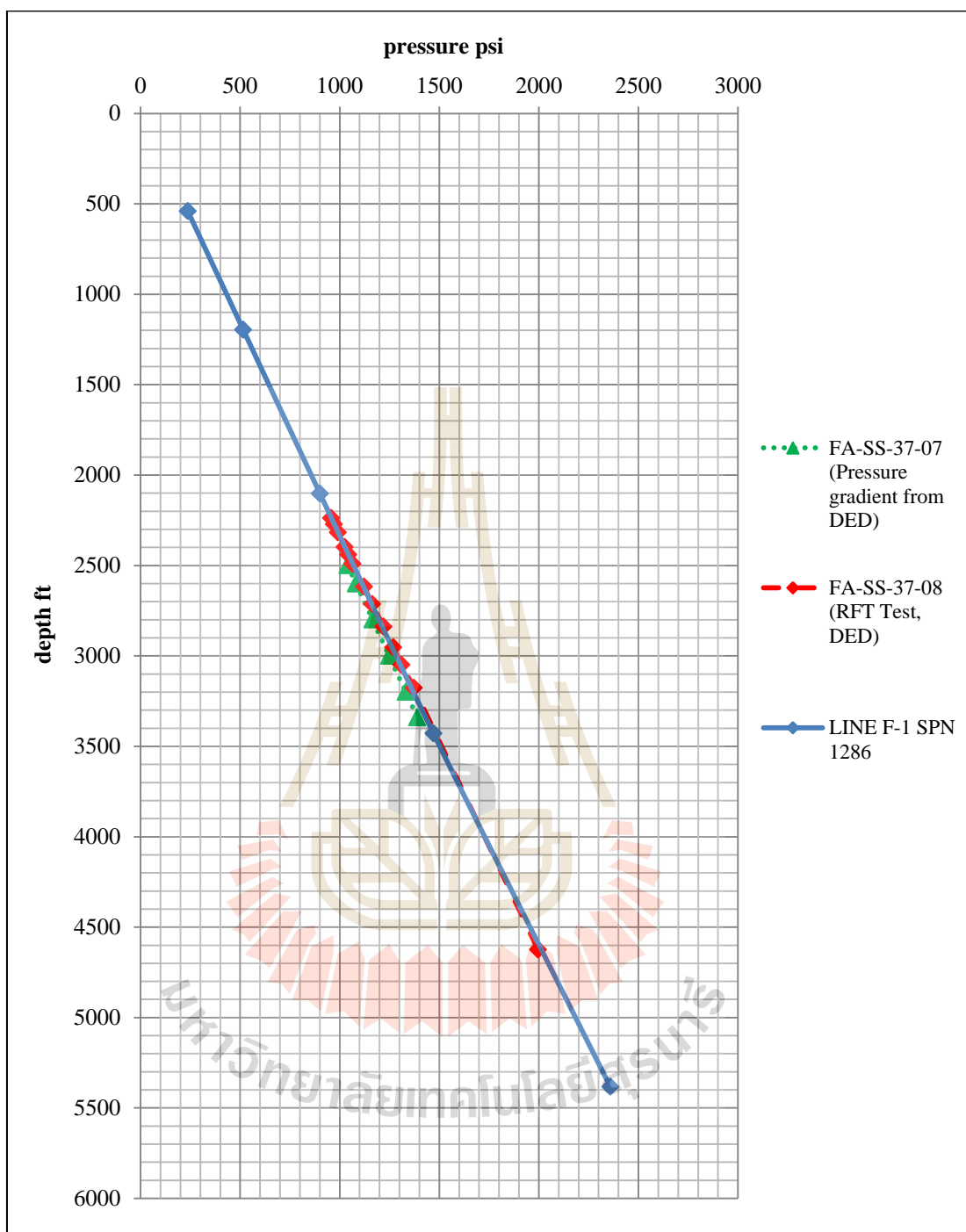
Figure 4.44 Pore pressure calculated from seismic line F-1 shot point number 1286
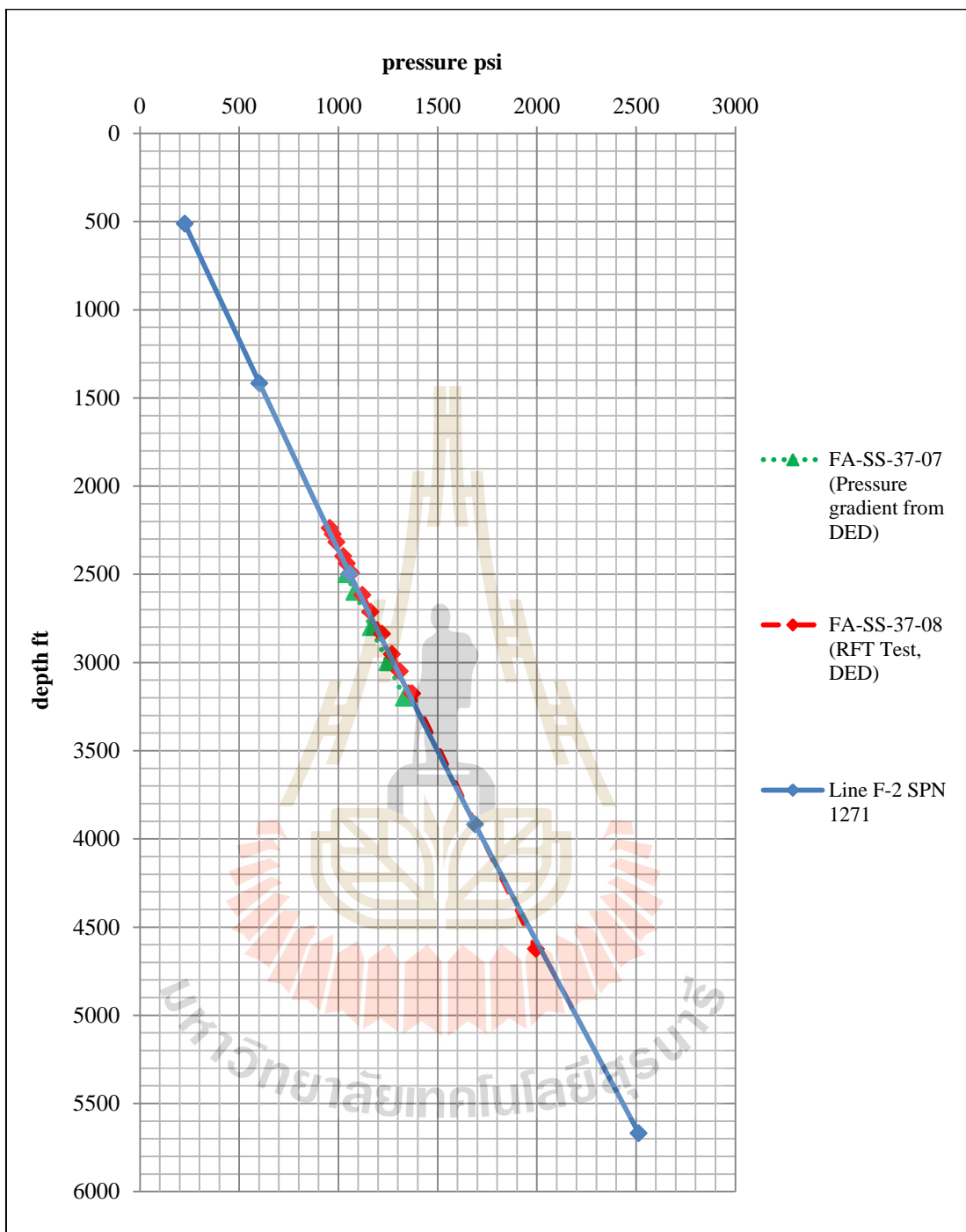
data

Figure 4.45 Pore pressure calculated from seismic line F-2 shot point number 1271
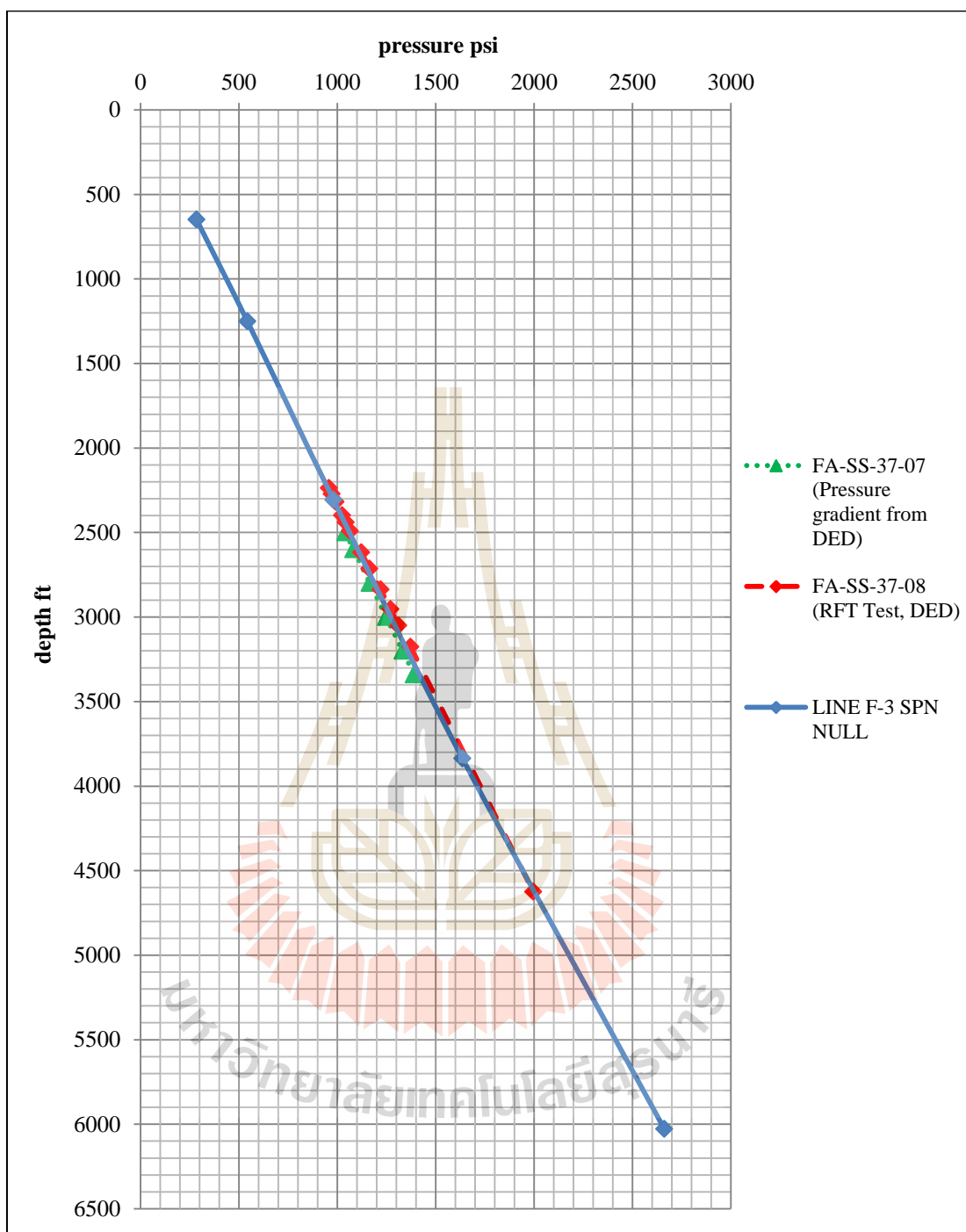
data

Figure 4.46 Pore pressure calculated from seismic line F-3 shot point number

NULL data
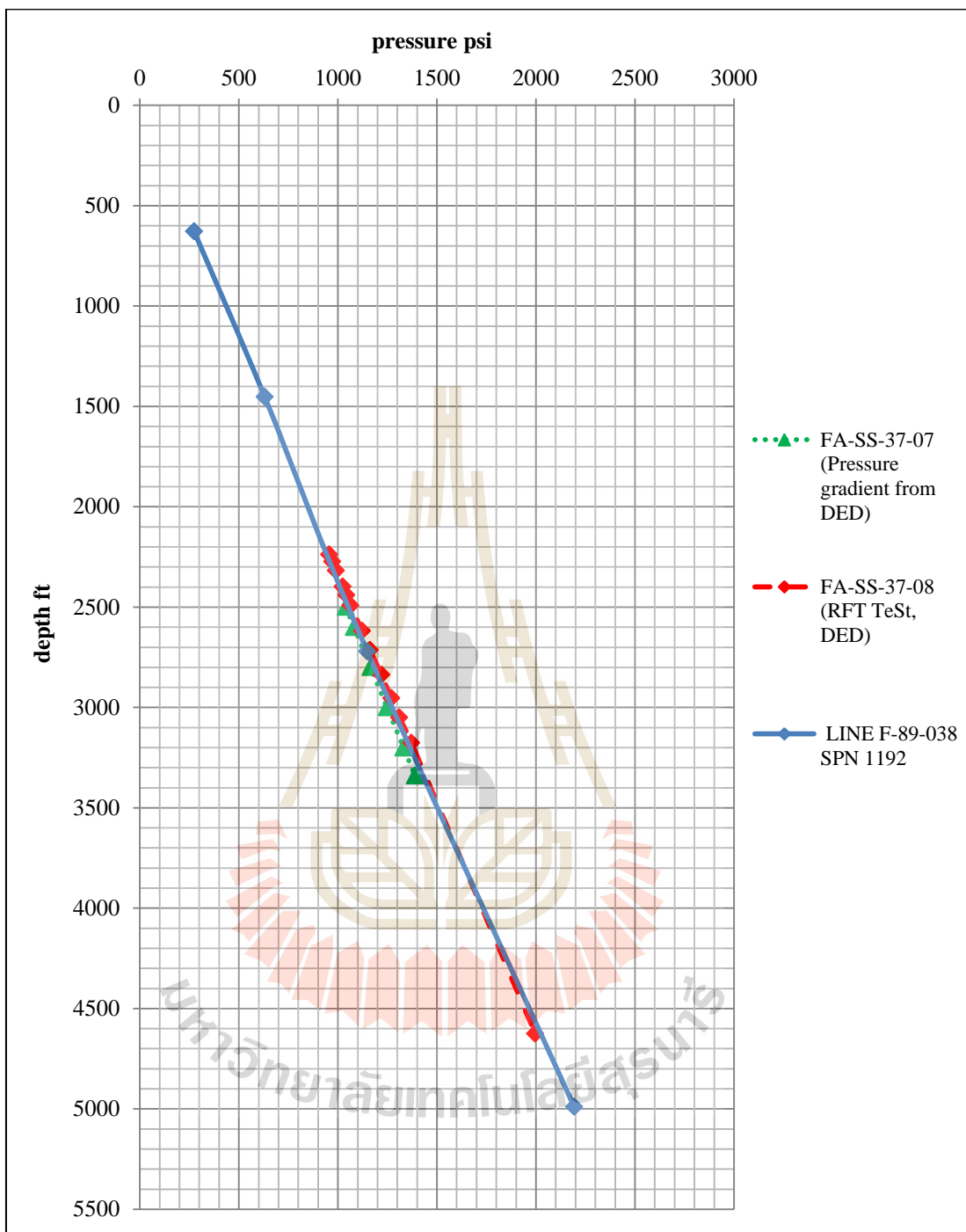
Figure 4.47 Pore pressure calculated from seismic line F-89-038 shot point number

1192 data
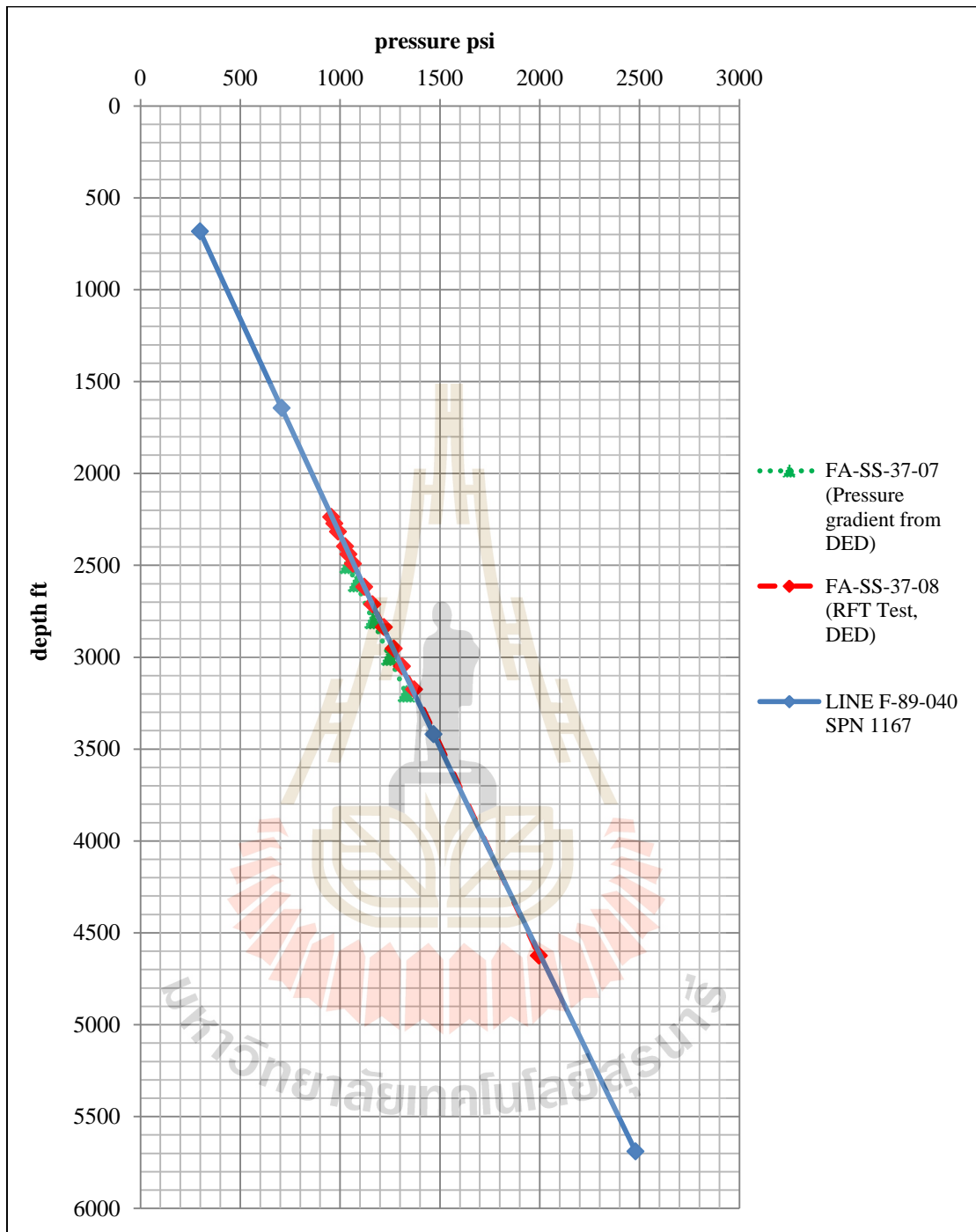
Figure 4.48 Pore pressure calculated from seismic line F-89-040 shot point number

1167 data

According to result of three data sets plotting above, it showed that the pressure trend is coincident with the reference pressure. This may imply that the study area that covered with used shot point numbers in every data set, especially in depth between 2238 and 4625 ft, is in normal pressure zone and its geological characteristic is similar to well FA-SS-37-08 and FA-SS-37-07.

After considering all graphs, some information can be pointed out as follows;

1.) At the beginning of graph, calculated pore pressure tends to high this because that depth is in Mae Fang formation which is semi-consolidated rock. In general, semi-consolidated rock usually has high porosity and high fluid content. This causes P-wave transit time increase and resulted in calculated pore pressure increasing.

2.) Some data of line S-3 are not followed the trend; this probably due to line S-3 may be lain near the fault and some parts of line S-3, especially shot point number 1440 were lain through that fault, this could cause slightly in P-wave velocity and in calculated pore pressure distortion.

4.3 Efficiency testing

In this part, calculated pore pressures derived from this study were tested for check its accuracy by compared with the reference pressure which was recorded from RFT data of well FA-SS-37-08 and by converted from pressure gradient of well FA-SS-37-07.

The reference pressure was re-scale by extrapolated it in to calculated pressure scale then erroneous percentage was calculated from following equation:

$$\left(\frac{P_c - P_r}{P_r}\right) \times 100 \qquad (4.1)$$

where P_c is calculated pore pressure (psi) and P_r is reference pressure (psi)

The following figures and tables show the comparison of calculated pressure and reference pressure of the first data set, including Line S-2 SPN 1560, Line S-3 SPN 1476, Line F-89-031 SPN 1257, Line F-1 SPN 1231, Line F-2 SPN 1227, Line F-3 SPN 1266, Line F-89-038 SPN 1127, and Line F-89-040 SPN 1131, respectively.
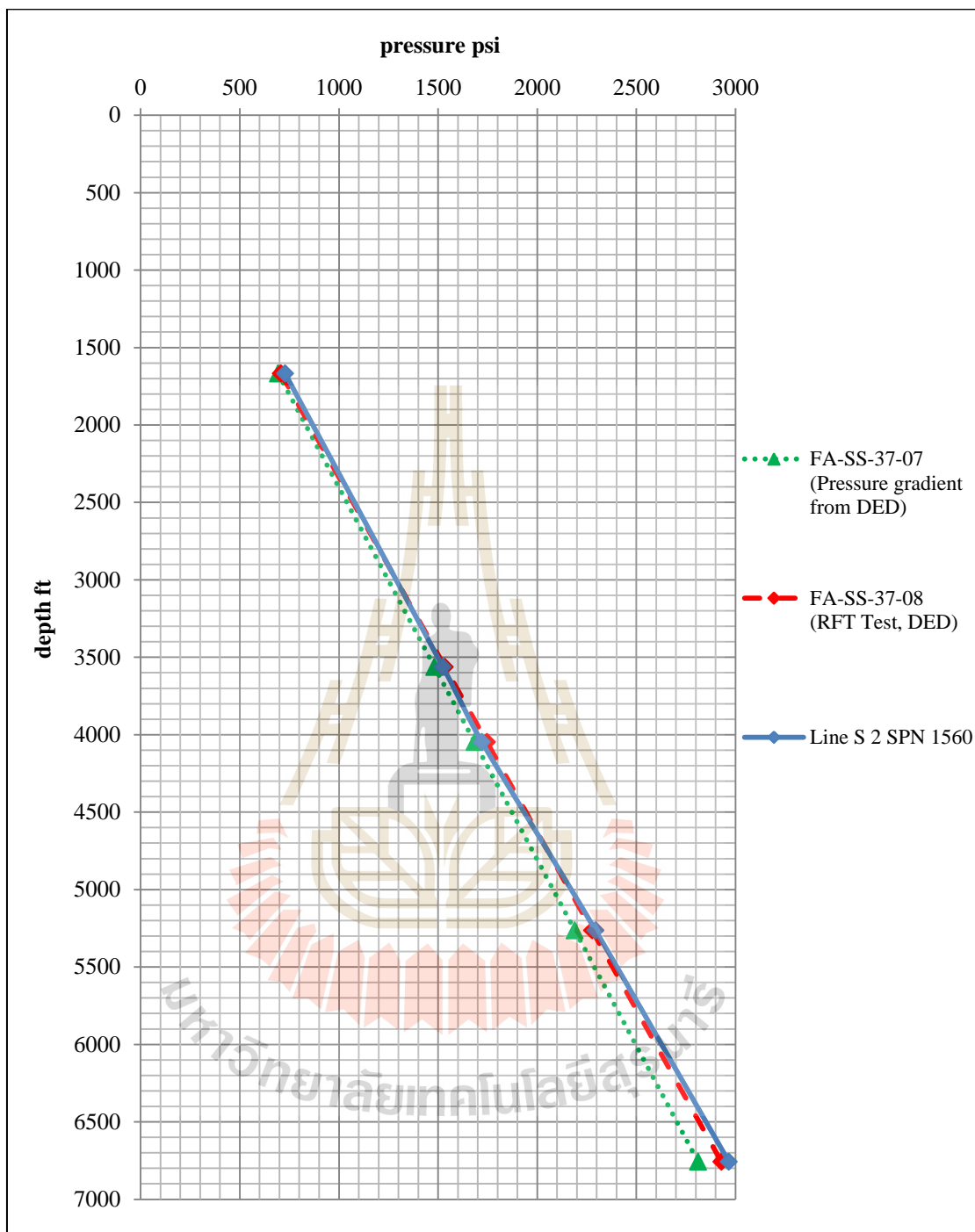
Figure 4.49 Comparison between reference pressure and calculated pressure of line

S-2 shot point number 1560

Table 4.1 Pore pressure calculated from Line S-2 shot point number 1560 compared

with reference pressure

Depth point (ft)	Pressure psi		
	FA-SS-37-08	**FA-SS-37-07**	**S-2 SPN 1560**
1668	708	694	729
3563	1535	1482	1525
4049	1747	1684	1722
5264	2277	2190	2294
6759	2929	2812	2967

Table 4.2 Erroneous percentage of pore pressure calculated from Line S-2 shot point

number 1560 compared with reference pressure

Error From (%)	FA-SS-37-08	FA-SS-37-07
1668	2.95	4.99
3563	0.65	2.86
4049	1.42	2.23
5264	0.77	4.78
6759	1.29	5.53
Average Error (%)	1.42	4.08
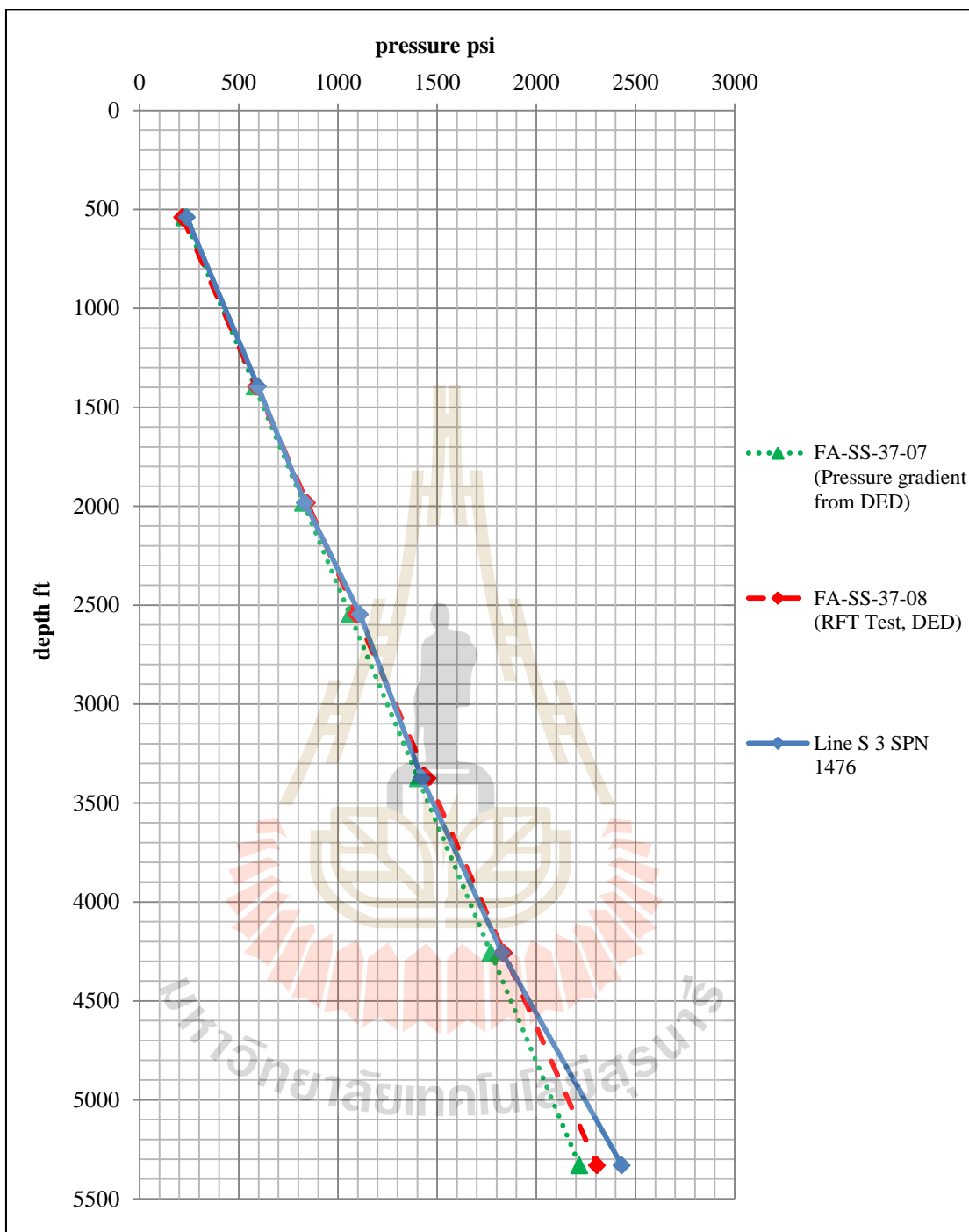
Figure 4.50 Comparison between reference pressure and calculated pressure of line

S-3 shot point number 1476

Table 4.3 Pore pressure calculated from Line S-3 shot point number 1476 compared

with reference pressure

Depth point (ft)	pressure psi		
	FA-SS-37-08	FA-SS-37-07	S-3 SPN 1476
541	216	225	238
1396	589	581	597
1983	845	825	834
2548	1091	1060	1111
3376	1453	1404	1424
4259	1838	1772	1828
5331	2306	2218	2432

Table 4.4 Erroneous percentage of pore pressure calculated from Line S-3 shot point

number 1476 compared with reference pressure

Error From (%)	FA-SS-37-08	FA-SS-37-07
541	10.06	5.53
1396	1.37	2.80
1983	1.38	1.03
2548	1.78	4.83
3376	2.00	1.39
4259	0.56	3.18
5331	5.44	9.65
Average Error (%)	3.23	4.06
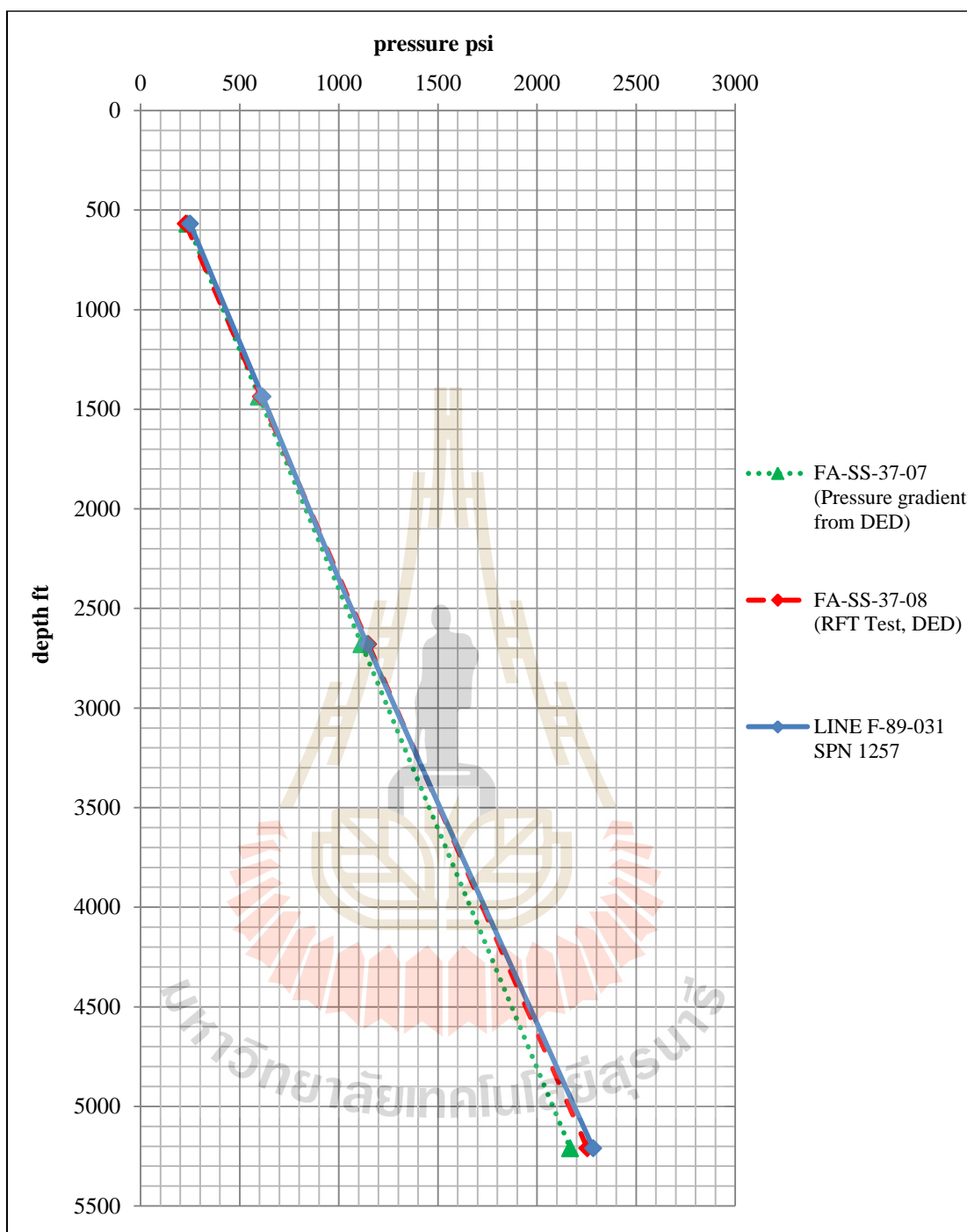
Figure 4.51 Comparison between reference pressure and calculated pressure of line

F-89-031 shot point number 1257

Table 4.5 Pore pressure calculated from Line F-89-031 shot point number

1257compared with reference pressure

Depth point (ft)	pressure psi		
	FA-SS-37-08	FA-SS-37-07	F-89-031 SPN 1257
569	228	237	250
1437	607	598	615
2680	1149	1115	1143
5212	2254	2168	2284

Table 4.6 Erroneous percentage of pore pressure calculated from Line F-89-031 shot

point number 1257 compared with reference pressure

Error From (%)	FA-SS-37-08	FA-SS-37-07
569	9.49	5.47
1437	1.41	2.94
2680	0.53	2.54
5212	1.32	5.35
Average Error (%)	3.19	4.08
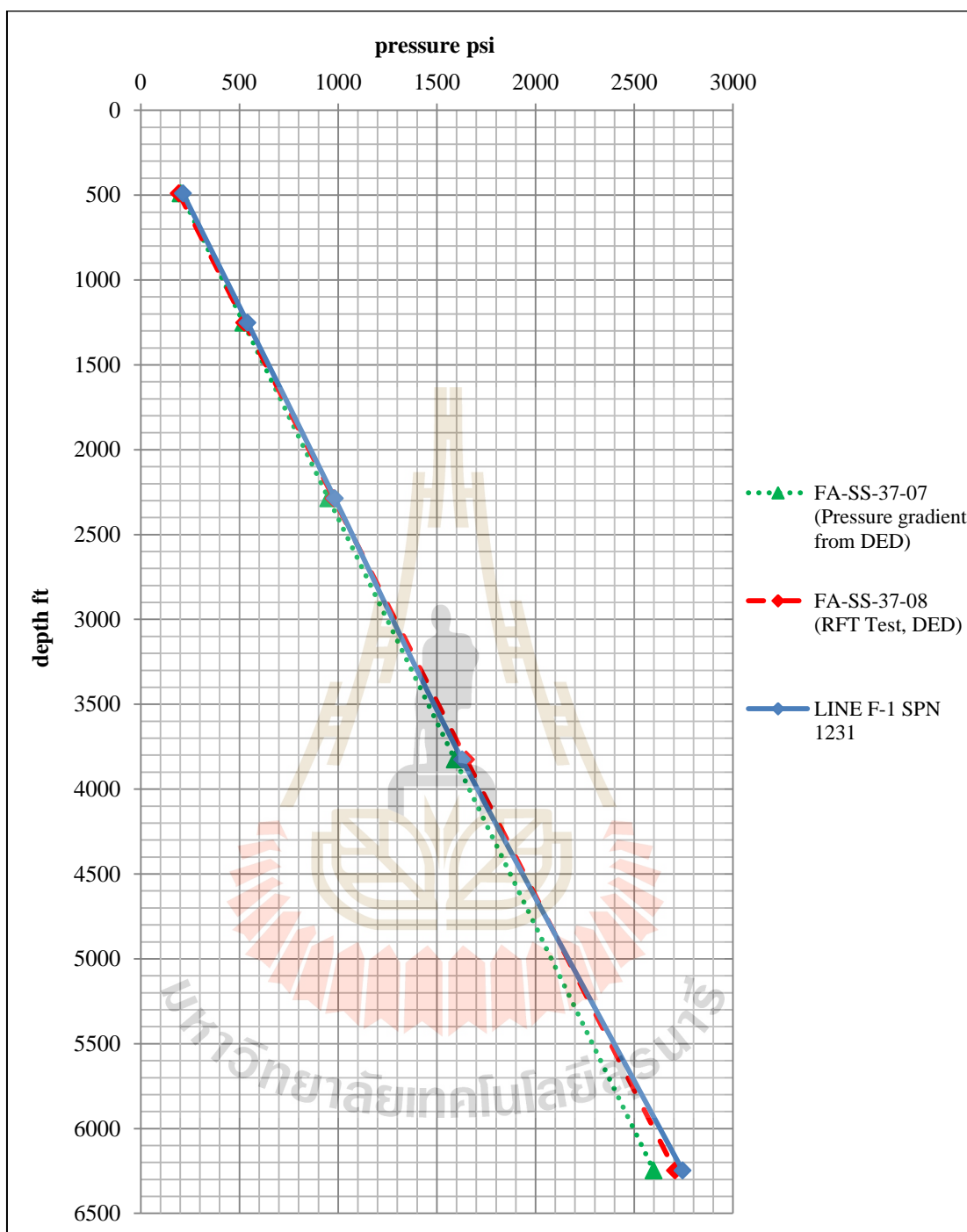
Figure 4.52 Comparison between reference pressure and calculated pressure of line

F-1 shot point number 1231

Table 4.7 Pore pressure calculated from Line F-1 shot point number 1231compared

with reference pressure

Depth point (ft)	pressure psi		
	FA-SS-37-08	FA-SS-37-07	F-1 SPN 1231
491	194	204	215
1252	526	521	541
2287	978	951	983
3826	1650	1592	1628
6248	2706	2599	2745

Table 4.8 Erroneous percentage of pore pressure calculated from Line F-1 shot point

number 1231 compared with reference pressure

Error From (%)	FA-SS-37-08	FA-SS-37-07
491	10.73	5.15
1252	2.92	3.96
2287	0.55	3.34
3826	1.29	2.30
6248	1.44	5.62
Average Error (%)	3.39	4.08
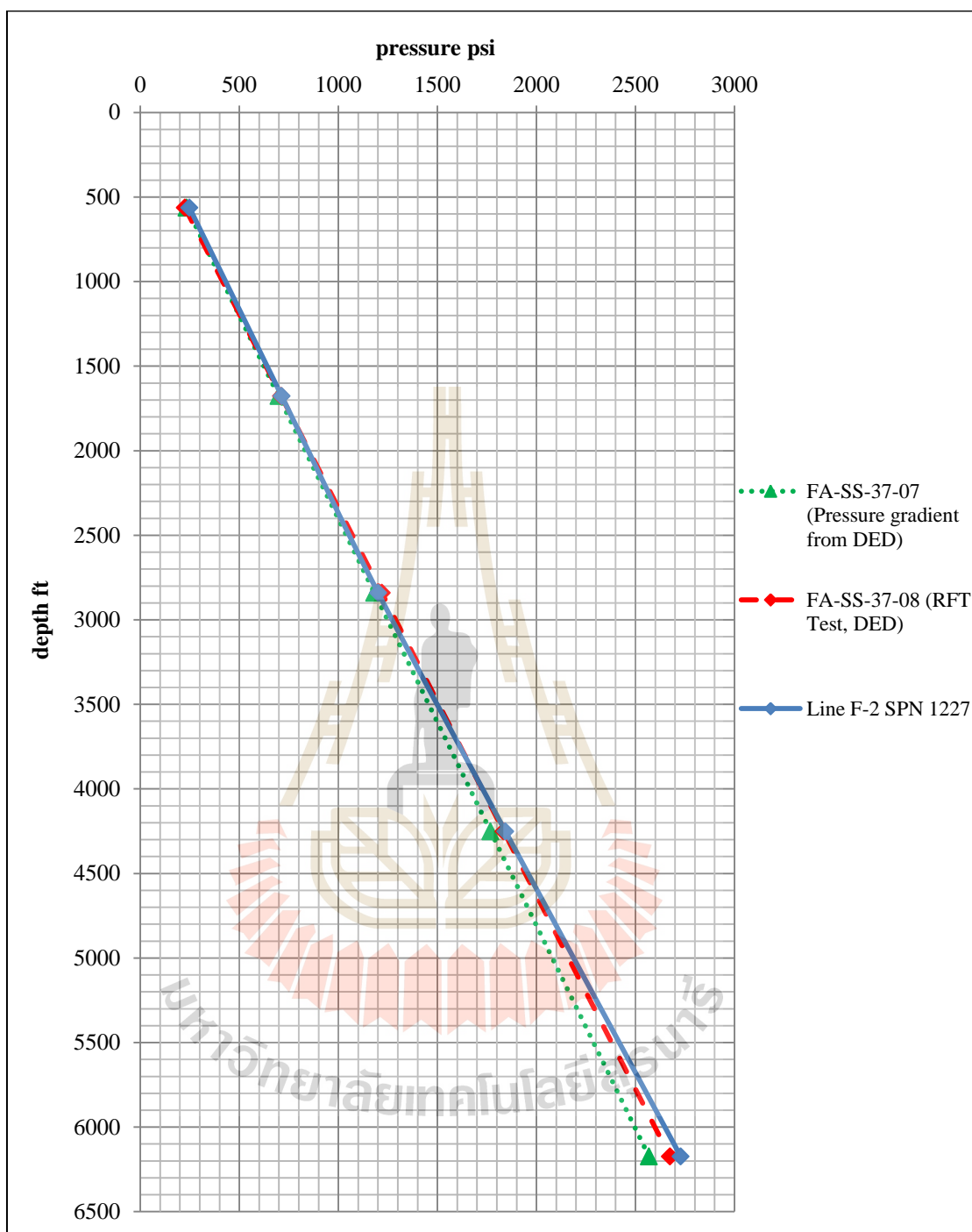
Figure 4.53 Comparison between reference pressure and calculated pressure of line

F-2 shot point number 1227

Table 4.9 Pore pressure calculated from Line F-2 shot point number 1227 compared

with reference pressure

Depth point (ft)	pressure psi		
	FA-SS-37-08	FA-SS-37-07	F-2 SPN 1227
564	226	235	249
1678	712	698	714
2841	1220	1182	1201
4252	1835	1769	1844
6175	2674	2569	2729

Table 4.10 Erroneous percentage of pore pressure calculated from Line F-2 shot

point number 1227 compared with reference pressure

Error From (%)	FA-SS-37-08	FA-SS-37-07
564	10.00	5.89
1678	0.34	2.35
2841	1.52	1.62
4252	0.47	4.25
6175	2.04	6.25
Average Error (%)	2.88	4.07
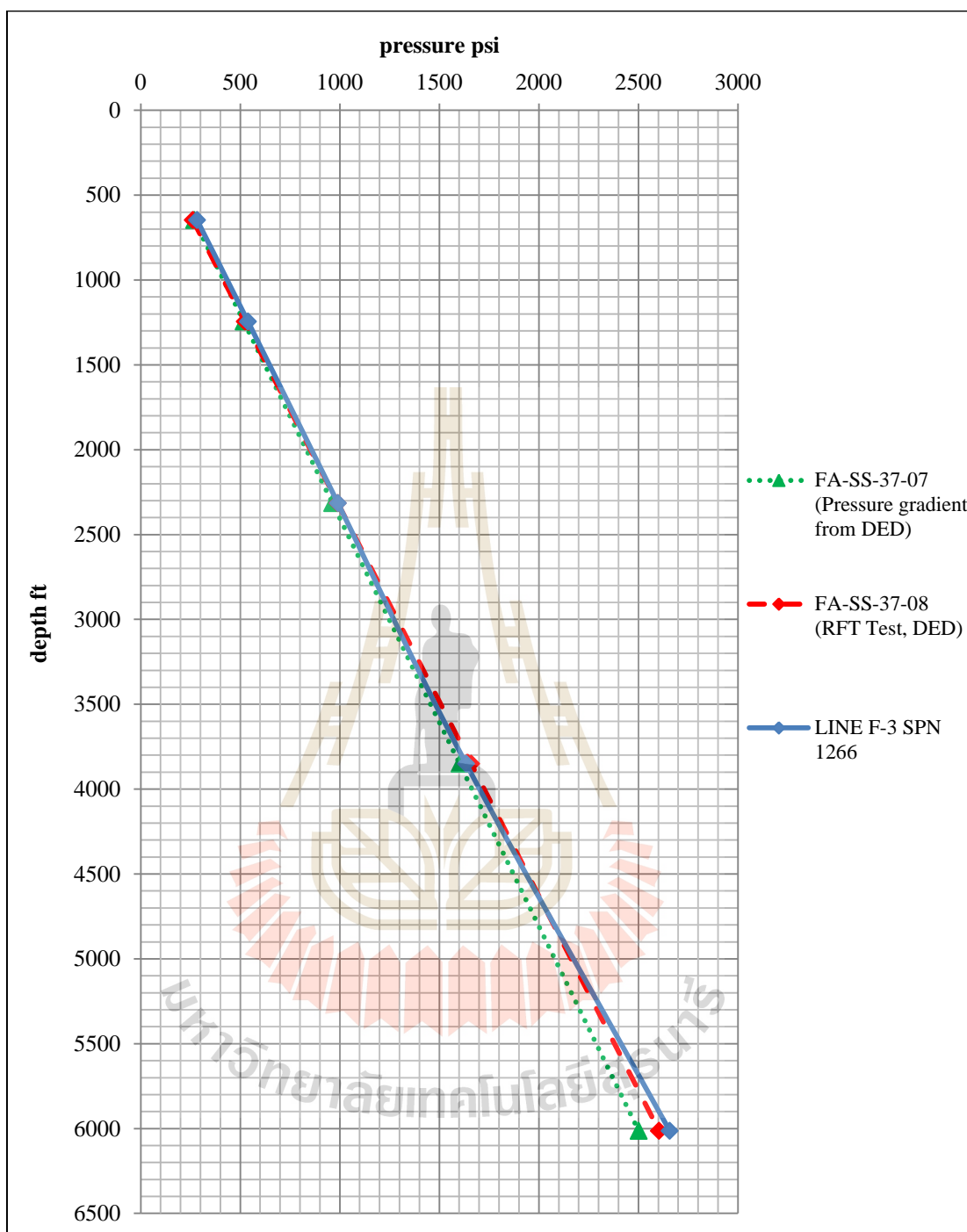
Figure 4.54 Comparison between reference pressure and calculated pressure of line

F-3 shot point number 1266

Table 4.11 Pore pressure calculated from Line F-3 shot point number 1266

compared with reference pressure

Depth point (ft)	pressure psi		
	FA-SS-37-08	**FA-SS-37-07**	**F-3 SPN 1266**
648	262	270	284
1246	524	518	540
2315	990	963	991
3852	1661	1603	1635
6015	2605	2502	2658

Table 4.12 Erroneous percentage of pore pressure calculated from Line F-3 shot

point number 1266 compared with reference pressure

Error From (%)	FA-SS-37-08	FA-SS-37-07
648	8.02	5.18
1246	3.04	4.07
2315	0.08	2.88
3852	1.55	2.04
6015	2.05	6.23
Average Error (%)	2.95	4.08
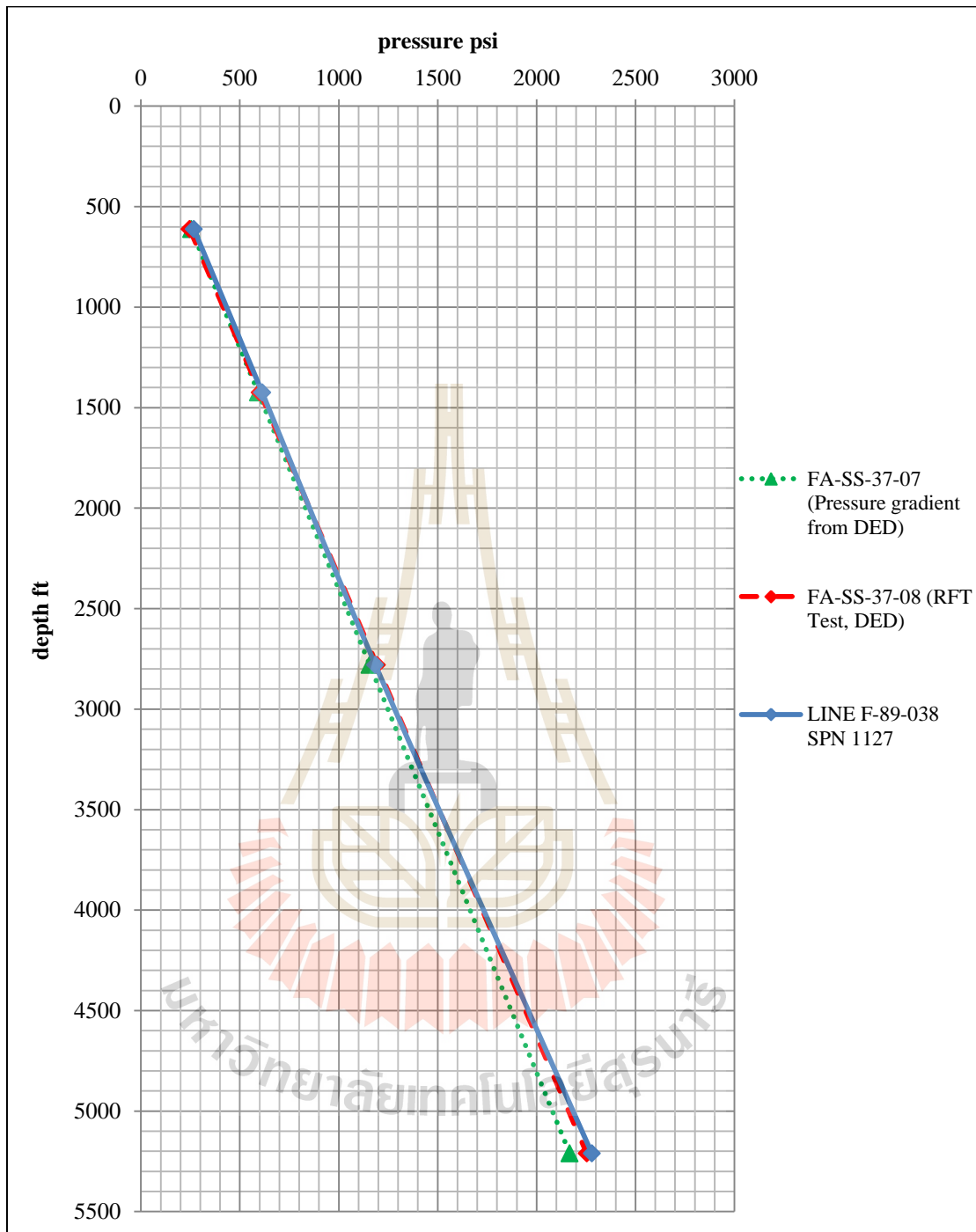
Figure 4.55 Comparison between reference pressure and calculated pressure of line

F-89-038 shot point number 1127

Table 4.13 Pore pressure calculated from Line F-89-038 shot point number 1127

compared with reference pressure

Depth point (ft)	pressure psi		
	FA-SS-37-08	FA-SS-37-07	F-89-038 SPN 1127
612	247	255	268
1426	602	593	613
2781	1193	1157	1185
5212	2254	2168	2280

Table 4.14 Erroneous percentage of pore pressure calculated from Line F-89-038

shot point number 1127 compared with reference pressure

Error From (%)	FA-SS-37-08	FA-SS-37-07
612	8.59	5.26
1426	1.93	3.45
2781	0.64	2.49
5212	1.15	5.16
Average Error (%)	3.08	4.09
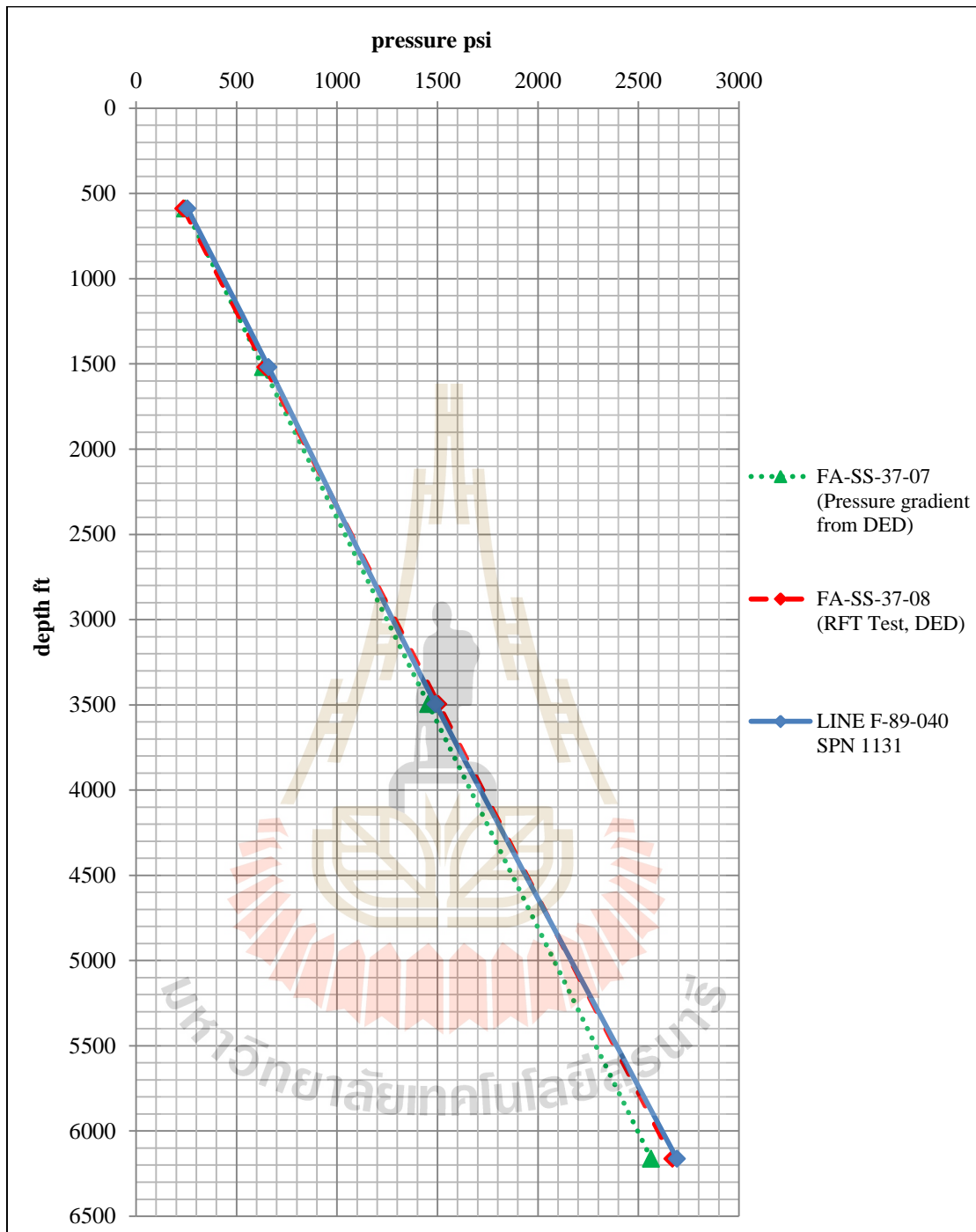
Figure 4.56 Comparison between reference pressure and calculated pressure of line

F-89-040 shot point number 1131

Table 4.15 Pore pressure calculated from Line F-89-040 shot point number 1131

compared with reference pressure

Depth point (ft)	pressure psi		
	FA-SS-37-08	FA-SS-37-07	F-89-040 SPN 1131
589	237	245	256
1521	643	633	660
3496	1505	1454	1490
6163	2669	2564	2692

Table 4.16 Erroneous percentage of pore pressure calculated from Line F-89-040

shot point number 1131 compared with reference pressure

Error From (%)	FA-SS-37-08	FA-SS-37-07
589	8.15	4.50
1521	2.59	4.33
3496	1.00	2.48
6163	0.85	5.00
Average Error (%)	3.15	4.08

Comparison of calculated pressure and reference pressure of the second data
set, including Line S-2 SPN 1524, Line S-3 SPN 1440, Line F-89-031 SPN 1189,
Line F-1 SPN 1174, Line F-2 SPN 1192, Line F-3 SPN 1228, Line F-89-038 SPN
1079, and Line F-89-040 SPN 1085 are showed in Figure 4.57 – 4.64 and in Table
4.17 – 4.32, respectively.
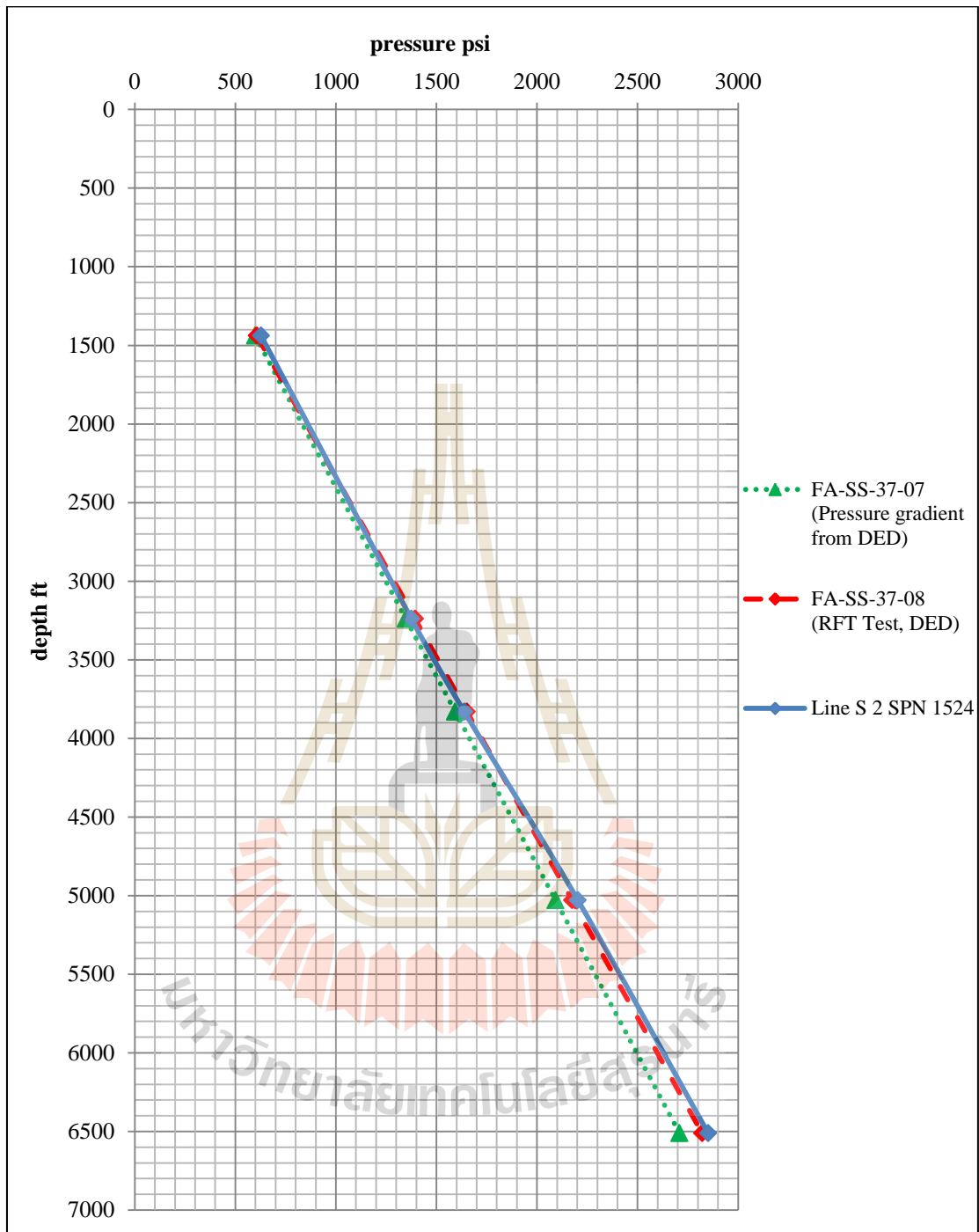
Figure 4.57 Comparison between reference pressure and calculated pressure of line

S-2 shot point number 1524

Table 4.17 Pore pressure calculated from Line S-2 shot point number 1524

compared with reference pressure

Depth point (ft)	Pressure psi		
	FA-SS-37-08	FA-SS-37-07	S-2 SPN 1524
1439	608	598	628
3240	1394	1348	1376
3830	1651	1593	1639
5030	2175	2092	2204
6512	2822	2709	2852

Table 4.18 Erroneous percentage of pore pressure calculated from Line S-2 shot

point number 1524 compared with reference pressure

Error From (%)	FA-SS-37-08	FA-SS-37-07
1439	3.31	4.88
3240	1.27	2.09
3830	0.77	2.83
5030	1.34	5.33
6512	1.05	5.26
Average Error (%)	1.55	4.08
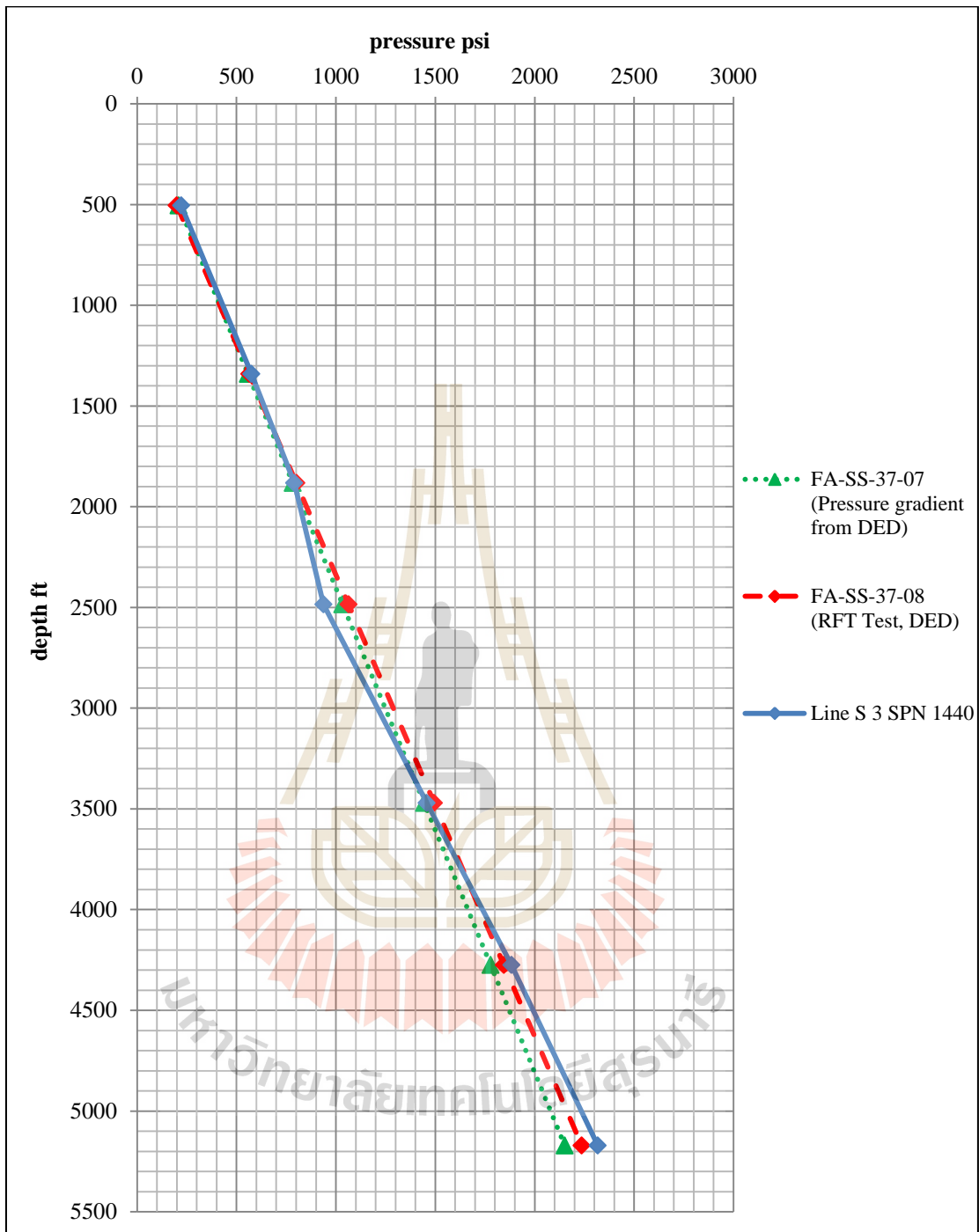
Figure 4.58 Comparison between reference pressure and calculated pressure of line

S-3 shot point number 1440

Table 4.19 Pore pressure calculated from Line S-3 shot point number 1440

compared with reference pressure

Depth point (ft)	pressure psi		
	FA-SS-37-08	FA-SS-37-07	S-3 SPN 1440
505	200	210	222
1342	565	558	576
1883	802	783	791
2485	1064	1034	938
3471	1495	1444	1457
4275	1845	1778	1883
5172	2237	2152	2318

Table 4.20 Erroneous percentage of pore pressure calculated from Line S-3 shot

point number 1440 compared with reference pressure

Error From (%)	FA-SS-37-08	FA-SS-37-07
505	10.92	5.65
1342	1.88	3.17
1883	1.27	1.02
2485	11.88	9.28
3471	2.49	0.92
4275	2.05	5.89
5172	3.61	7.72
Average Error (%)	4.87	4.81
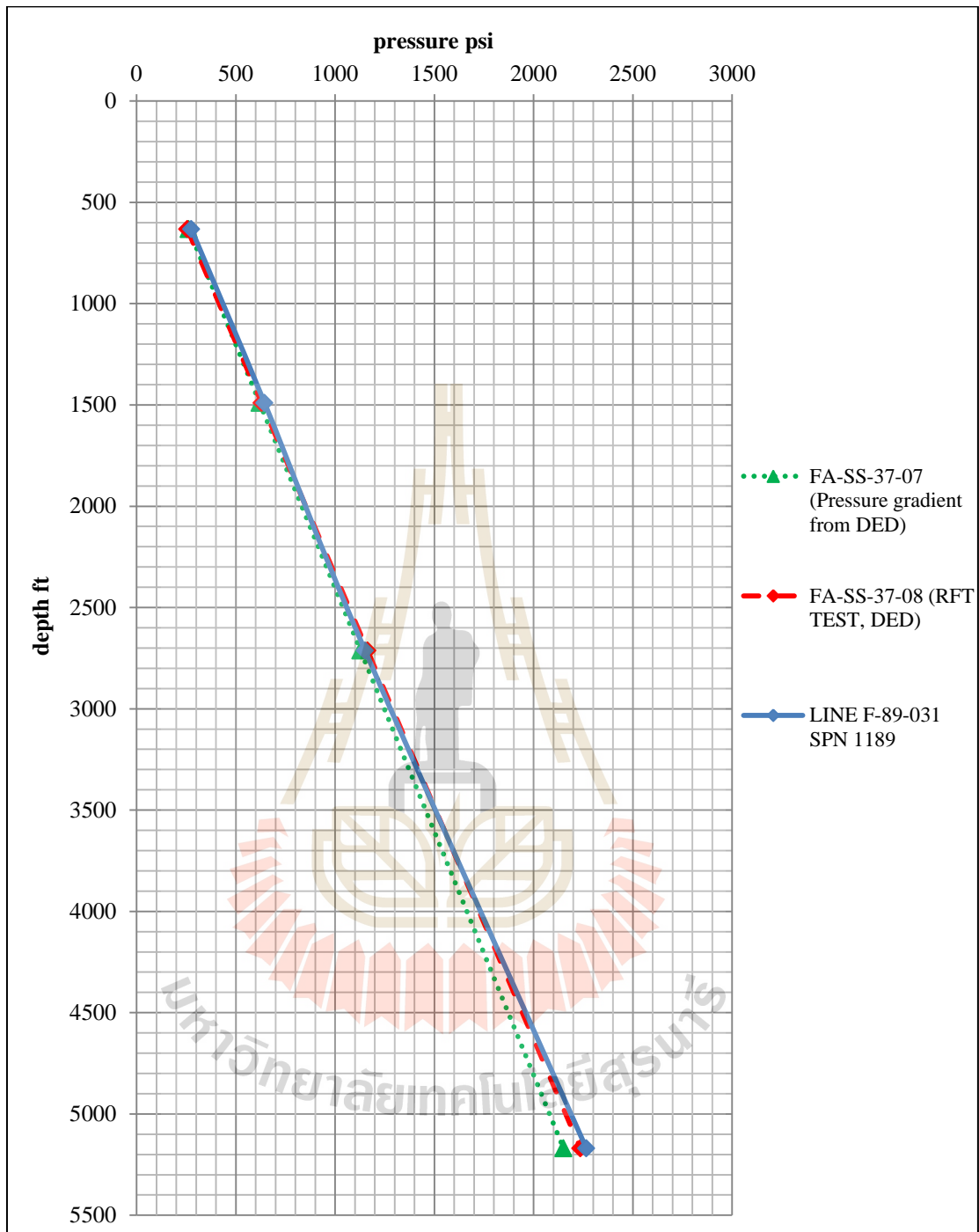
Figure 4.59 Comparison between reference pressure and calculated pressure of line

F-89-031 shot point number 1189

Table 4.21 Pore pressure calculated from Line F-89-031 shot point number

1189compared with reference pressure

Depth point (ft)	pressure psi		
	FA-SS-37-08	FA-SS-37-07	F-89-031 SPN 1189
633	256	263	276
1491	607	620	645
2713	1149	1129	1151
5171	2254	2151	2266

Table 4.22 Erroneous percentage of pore pressure calculated from Line F-89-031

shot point number 1189 compared with reference pressure

Error From (%)	FA-SS-37-08	FA-SS-37-07
633	7.97	4.94
1491	6.33	4.02
2713	0.17	2.02
5171	0.54	5.36
Average Error (%)	3.75	4.08
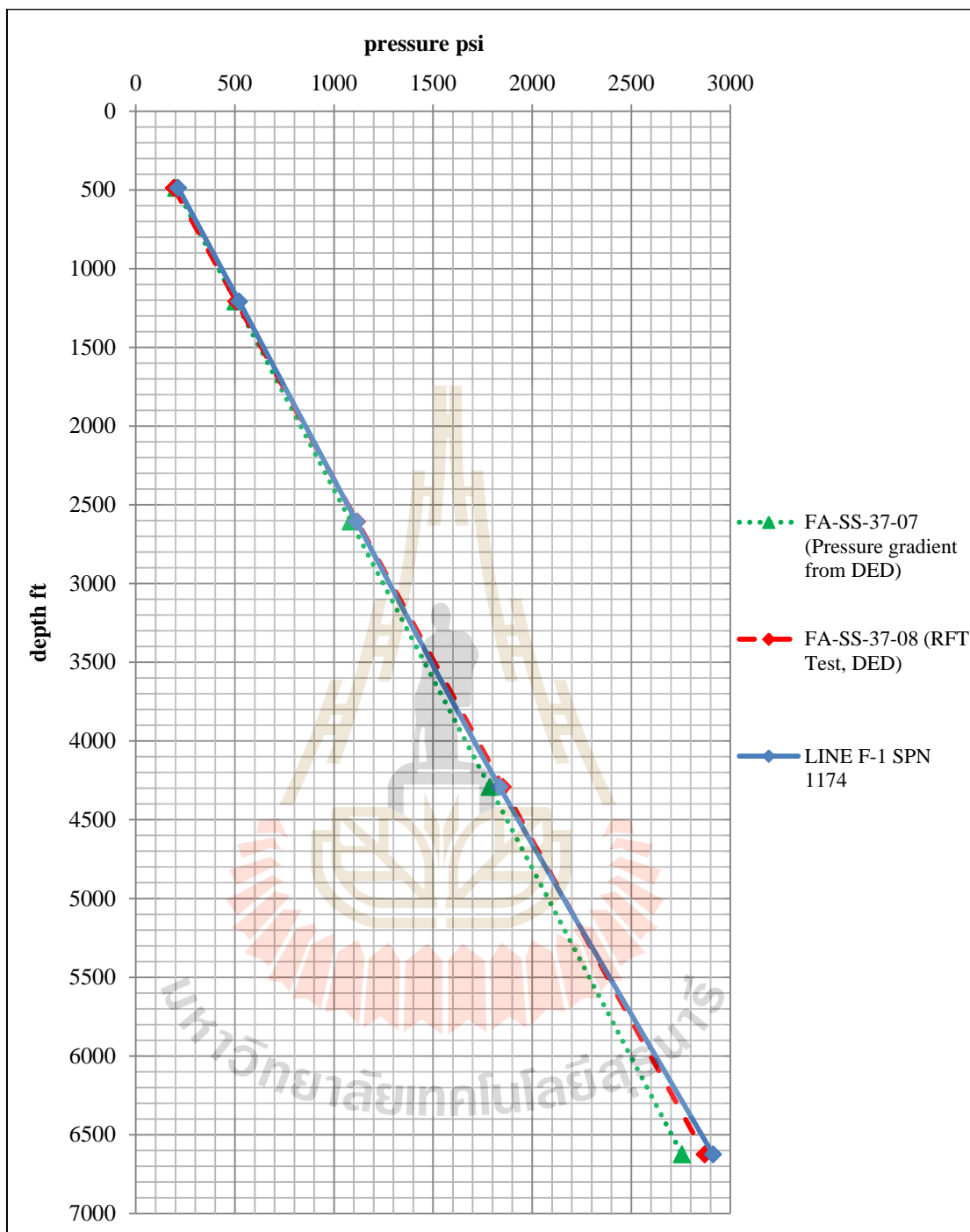
Figure 4.60 Comparison between reference pressure and calculated pressure of line

F-1 shot point number 1174

Table 4.23 Pore pressure calculated from Line F-1 shot point number 1174

compared with reference pressure

Depth point (ft)	pressure psi		
	FA-SS-37-08	FA-SS-37-07	F-1 SPN 1174
489	193	204	215
1210	508	503	522
2608	1118	1085	1114
4293	1853	1786	1836
6627	2872	2757	2914

Table 4.24 Erroneous percentage of pore pressure calculated from Line F-1 shot

point number 1174 compared with reference pressure

Error From (%)	FA-SS-37-08	FA-SS-37-07
489	11.07	5.44
1210	2.86	3.76
2608	0.30	2.72
4293	0.91	2.83
6627	1.46	5.70
Average Error (%)	3.32	4.09
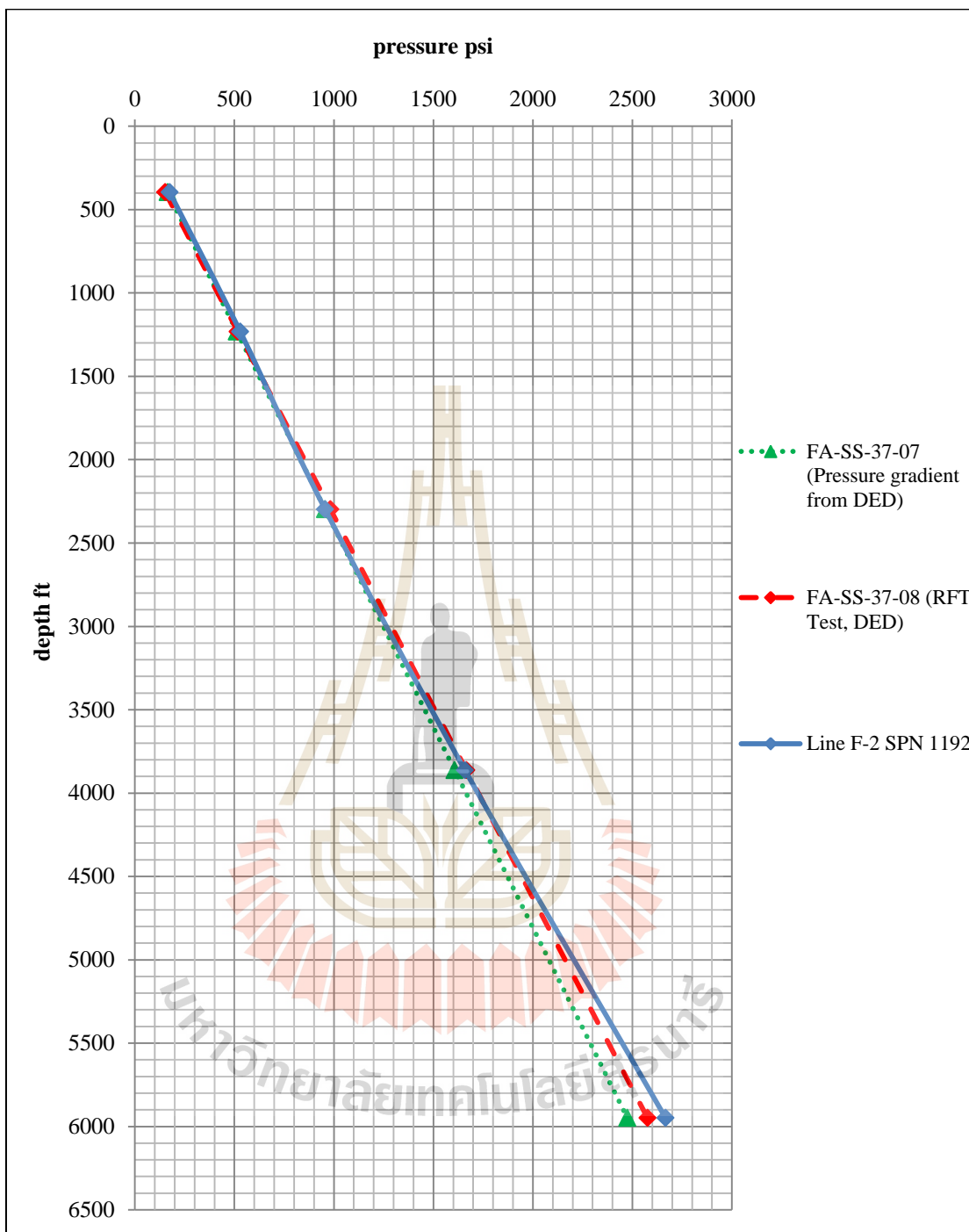
Figure 4.61 Comparison between reference pressure and calculated pressure of line

F-2 shot point number 1192

Table 4.25 Pore pressure calculated from Line F-2 shot point number 1192

compared with reference pressure

Depth point (ft)	pressure psi		
	FA-SS-37-08	FA-SS-37-07	F-2 SPN 1192
397	153	165	175
1232	517	512	529
2298	983	956	956
3863	1666	1607	1659
5950	2576	2475	2667

Table 4.26 Erroneous percentage of pore pressure calculated from Line F-2 shot

point number 1192 compared with reference pressure

Error From (%)	FA-SS-37-08	FA-SS-37-07
397	14.46	6.00
1232	2.32	3.29
2298	2.71	0.00
3863	0.41	3.22
5950	3.53	7.76
Average Error (%)	4.69	4.06
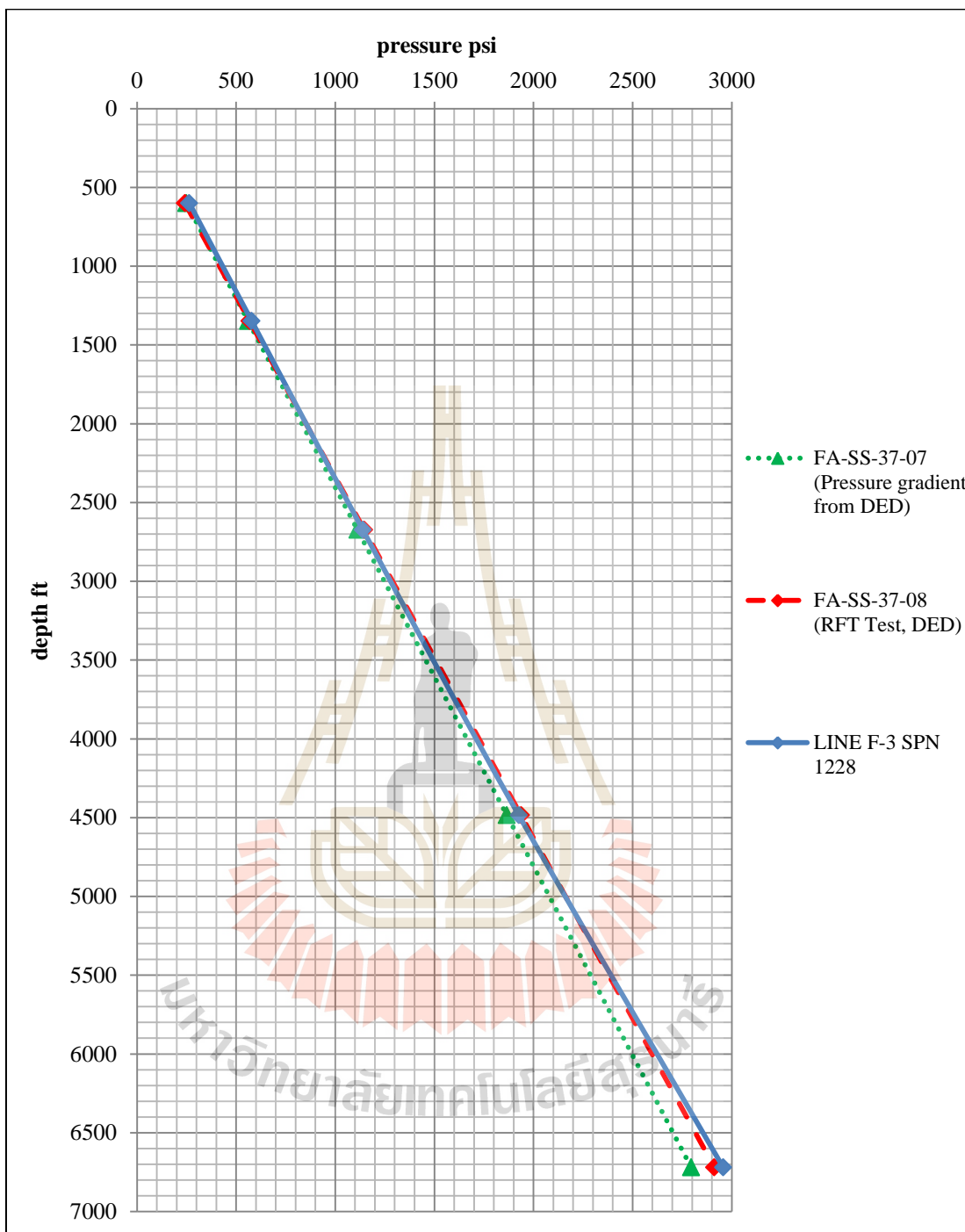
Figure 4.62 Comparison between reference pressure and calculated pressure of line

F-3 shot point number 1228

Table 4.27 Pore pressure calculated from Line F-3 shot point number 1228

compared with reference pressure

Depth point (ft)	pressure psi		
	FA-SS-37-08	**FA-SS-37-07**	**F-3 SPN 1228**
601	242	250	264
1348	568	561	579
2674	1147	1113	1140
4486	1937	1866	1926
6720	2912	2795	2957

Table 4.28 Erroneous percentage of pore pressure calculated from Line F-3 shot

point number 1228 compared with reference pressure

Error From (%)	FA-SS-37-08	FA-SS-37-07
601	9.32	5.80
1348	1.89	3.20
2674	0.63	2.44
4486	0.58	3.22
6720	1.52	5.77
Average Error (%)	2.79	4.08
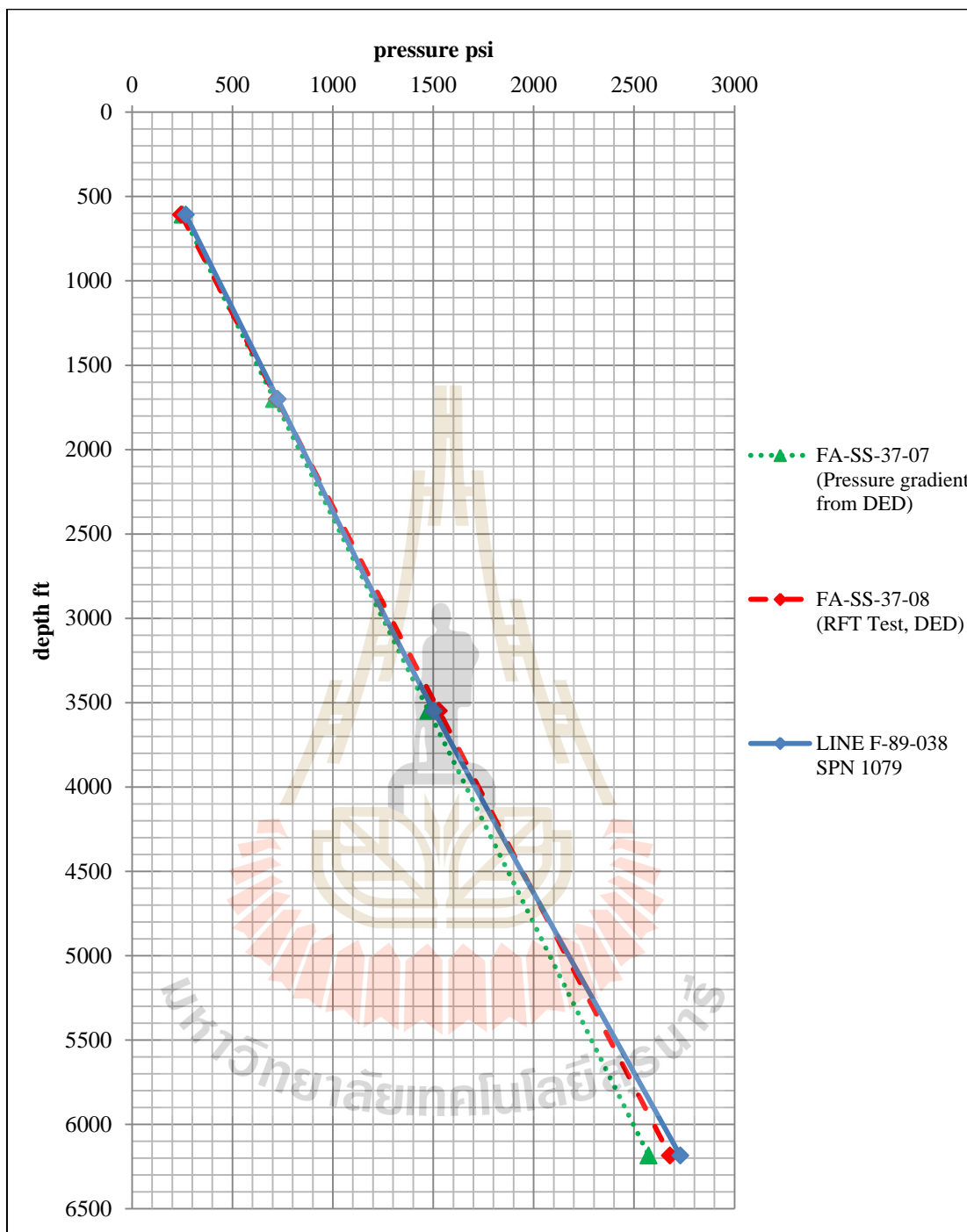
Figure 4.63 Comparison between reference pressure and calculated pressure of line

F-89-038 shot point number 1079

Table 4.29 Pore pressure calculated from Line F-89-038 shot point number 1079

compared with reference pressure

Depth point (ft)	pressure psi		
	FA-SS-37-08	FA-SS-37-07	F-89-038 SPN 1079
609	245	253	268
1701	722	708	726
3550	1529	1477	1504
6186	2679	2573	2730

Table 4.30 Erroneous percentage of pore pressure calculated from Line F-89-038

shot point number 1079 compared with reference pressure

Error From (%)	FA-SS-37-08	FA-SS-37-07
609	9.20	5.80
1701	0.55	2.60
3550	1.64	1.83
6186	1.91	6.10
Average Error (%)	3.33	4.08
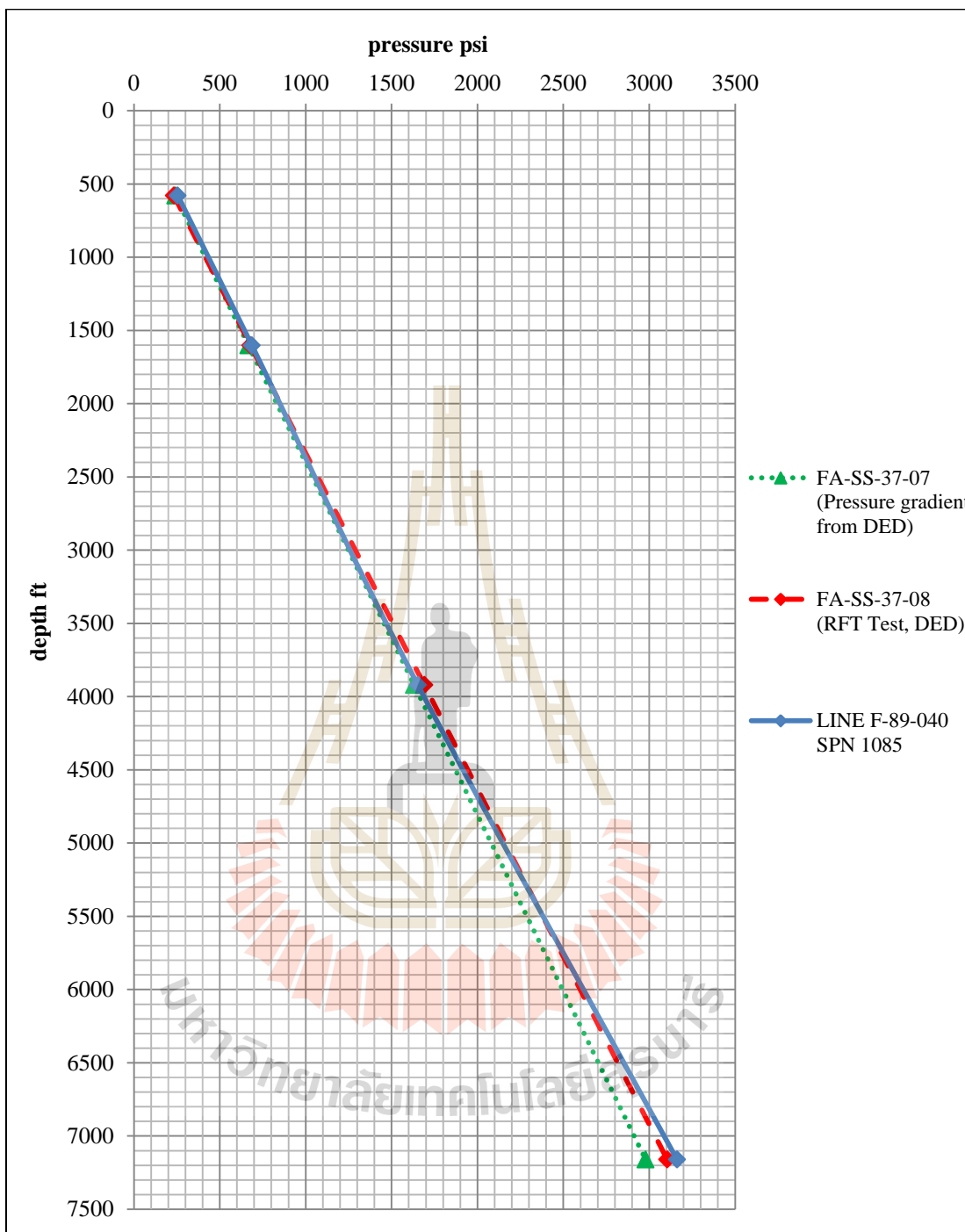
Figure 4.64 Comparison between reference pressure and calculated pressure of line

F-89-040 shot point number 1085

Table 4.31 Pore pressure calculated from Line F-89-040 shot point number 1085

compared with reference pressure

Depth point (ft)	pressure psi		
	FA-SS-37-08	FA-SS-37-07	F-89-040 SPN 1085
581	233	242	256
1603	679	667	687
3922	1691	1632	1654
7162	3105	2979	3162

Table 4.32 Erroneous percentage of pore pressure calculated from Line F-89-040

shot point number 1085 compared with reference pressure

Error From (%)	FA-SS-37-08	FA-SS-37-07
581	9.60	5.77
1603	1.17	3.05
3922	2.22	1.36
7162	1.84	6.14
Average Error (%)	3.71	4.08

Comparison of calculated pressure and reference pressure of the third data set including Line S-2 SPN 1596, Line S-3 SPN 1512, Line F-89-031 SPN 1313, Line F-1 SPN 1286, Line F-2 SPN 1271, Line F-3 SPN NULL, Line F-89-038 SPN 1192, and Line F-89-040 SPN 1167 are showed in Figure 4.65 – 4.72 and in Table 4.33 – 4.48, respectively.
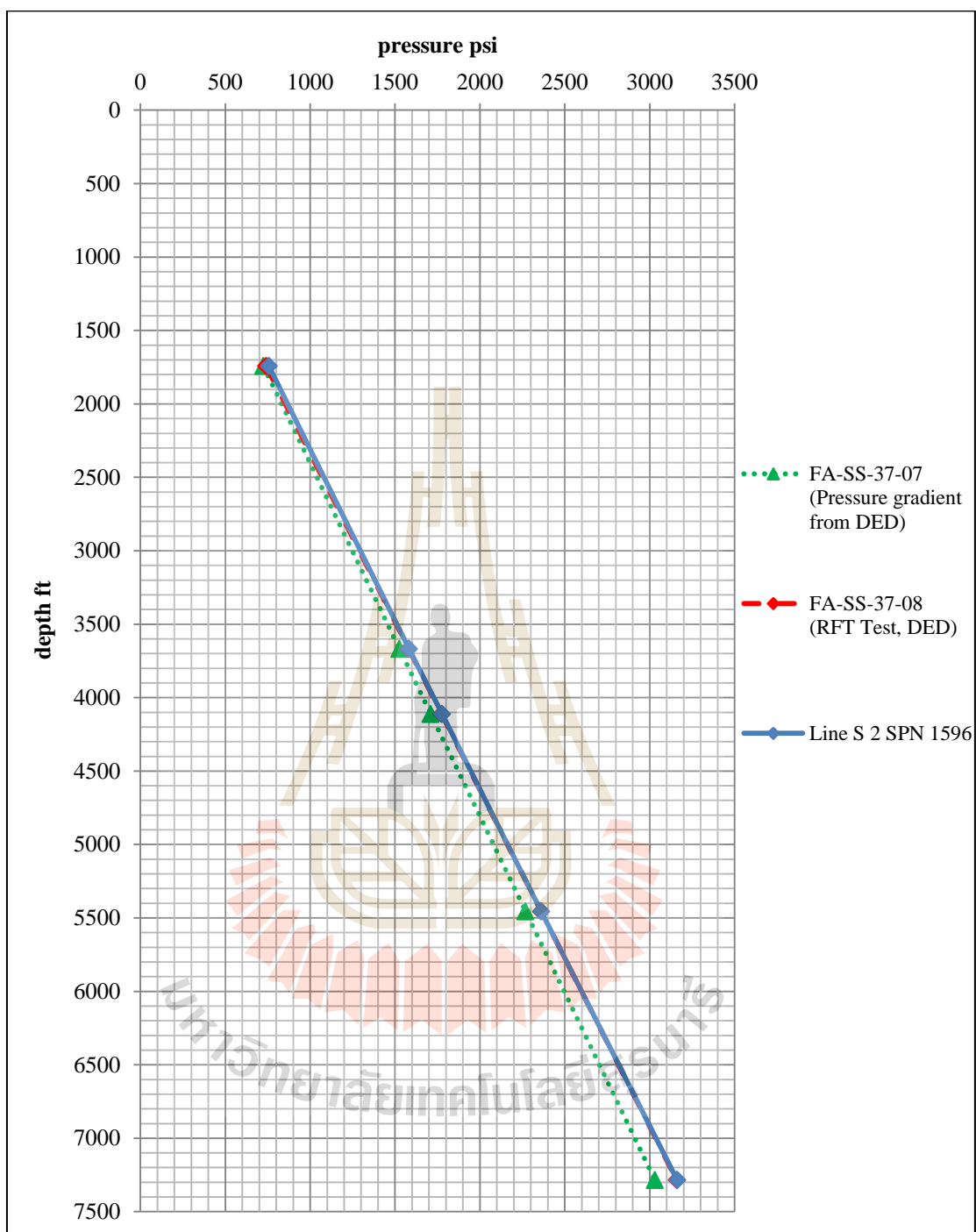
Figure 4.65 Comparison between reference pressure and calculated pressure of line

S-2 shot point number 1596

Table 4.33 Pore pressure calculated from Line S-2 shot point number 1596

compared with reference pressure

Depth point (ft)	Pressure psi		
	FA-SS-37-08	FA-SS-37-07	S-2 SPN 1596
1744	741	725	737
3670	1581	1527	1524
4113	1774	1711	1715
5456	2361	2270	2268
7287	3160	3031	2906

Table 4.34 Erroneous percentage of pore pressure calculated from Line S-2 shot

point number 1596 compared with reference pressure

Error From (%)	FA-SS-37-08	FA-SS-37-07
1744	0.53	1.57
3670	3.64	0.20
4113	3.34	0.25
5456	3.92	0.06
7287	8.03	4.14
Average Error (%)	3.89	1.24
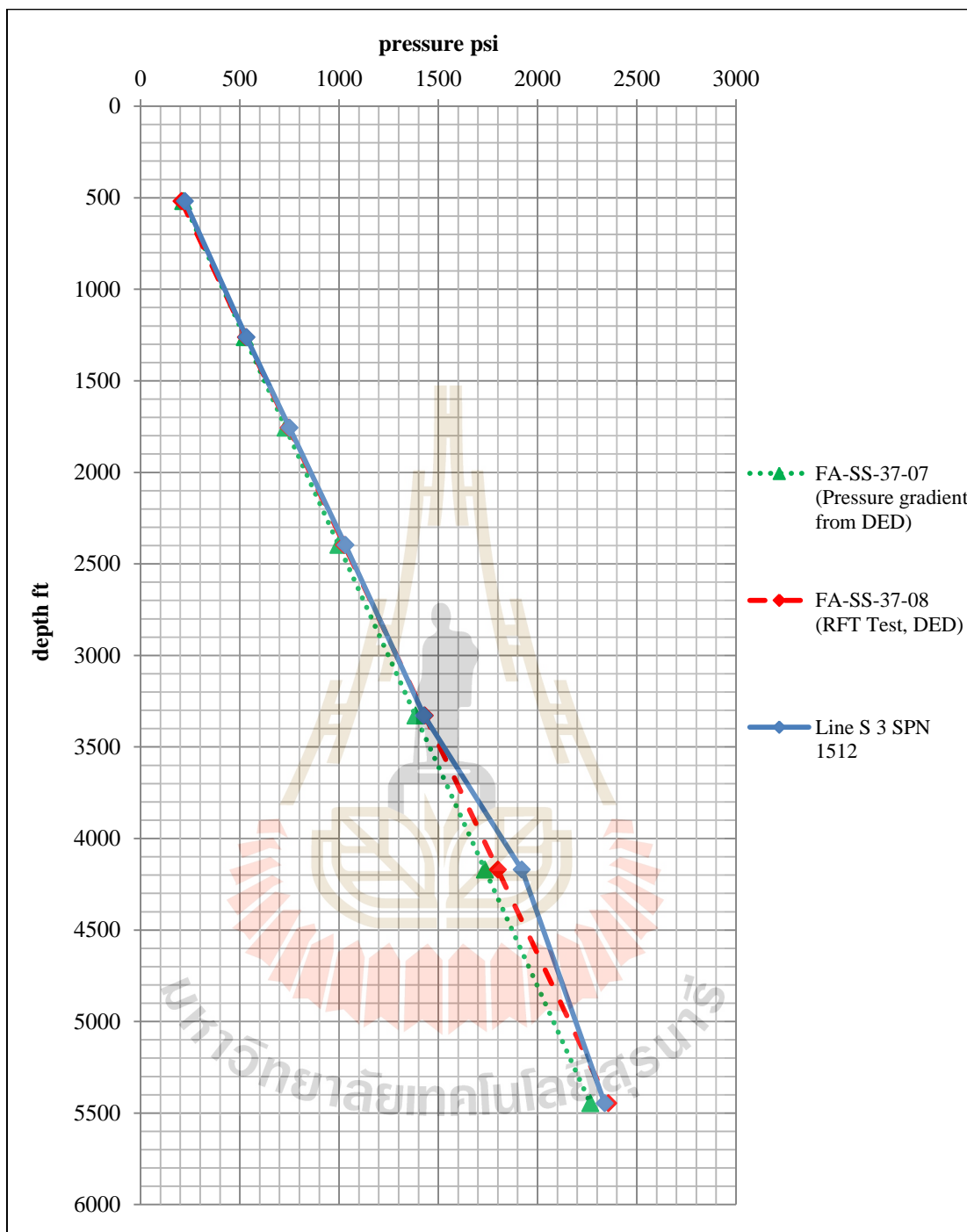
Figure 4.66 Comparison between reference pressure and calculated pressure of line

S-3 shot point number 1512

Table 4.35 Pore pressure calculated from Line S-3 shot point number 1512

compared with reference pressure

Depth point (ft)	pressure psi		
	FA-SS-37-08	FA-SS-37-07	S-3 SPN 1512
520	207	216	224
1263	531	525	534
1757	746	731	751
2398	1026	998	1033
3330	1433	1385	1428
4172	1800	1735	1922
5448	2357	2266	2339

Table 4.36 Erroneous percentage of pore pressure calculated from Line S-3 shot

point number 1512 compared with reference pressure

Error From (%)	FA-SS-37-08	FA-SS-37-07
520	8.36	3.51
1263	0.56	1.61
1757	0.59	2.73
2398	0.61	3.50
3330	0.32	3.11
4172	6.76	10.75
5448	0.77	3.21
Average Error (%)	2.57	4.06
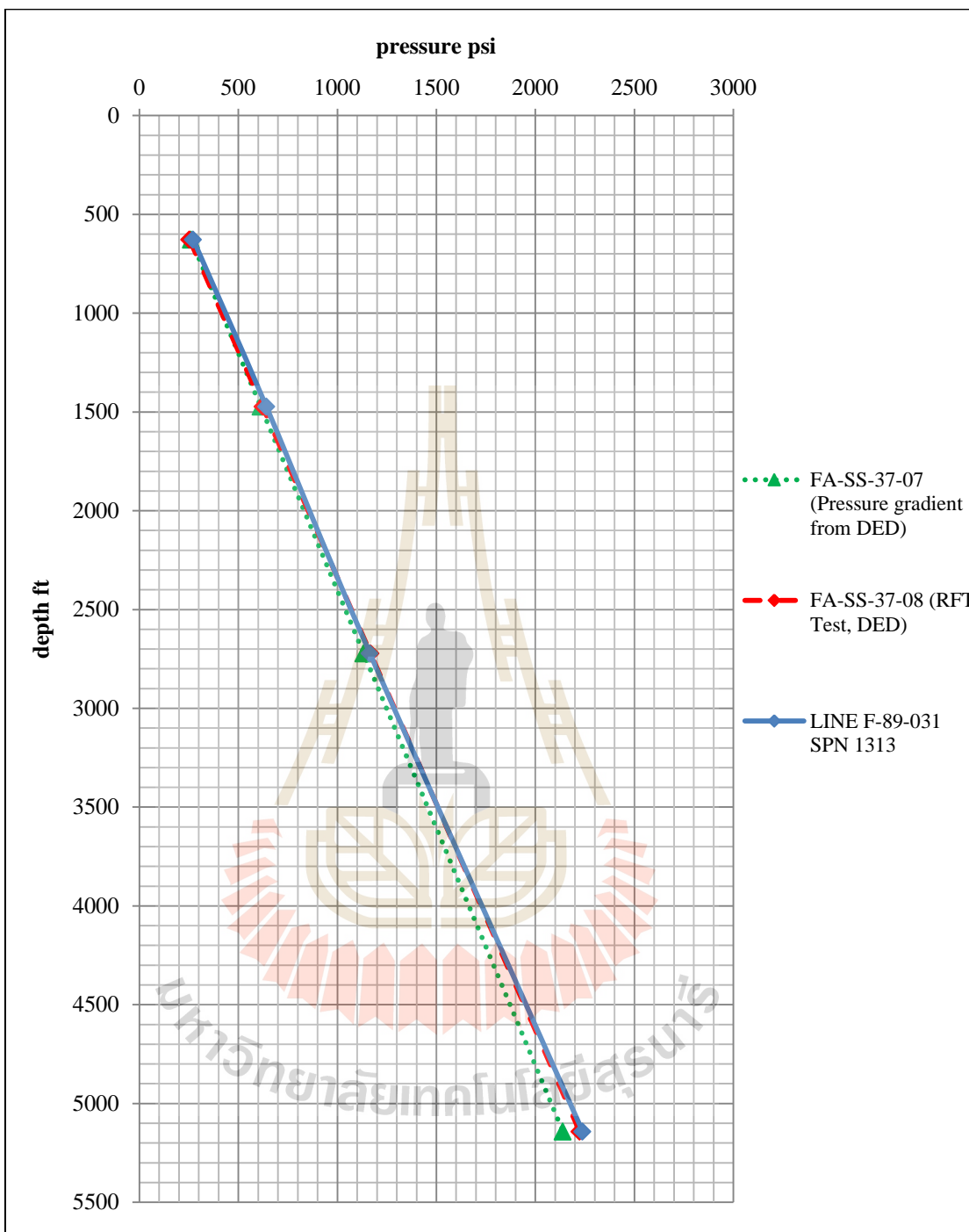
Figure 4.67 Comparison between reference pressure and calculated pressure of line

F-89-031 shot point number 1313

Table 4.37 Pore pressure calculated from Line F-89-031 shot point number

1313compared with reference pressure

Depth point (ft)	pressure psi		
	FA-SS-37-08	FA-SS-37-07	F-89-031 SPN 1313
628	254	261	272
1475	607	613	642
2723	1149	1133	1165
5143	2254	2139	2239

Table 4.38 Erroneous percentage of pore pressure calculated from Line F-89-031

shot point number 1313 compared with reference pressure

Error From (%)	FA-SS-37-08	FA-SS-37-07
628	7.25	4.18
1475	5.79	4.64
2723	1.34	2.83
5143	0.66	4.67
Average Error (%)	3.76	4.08
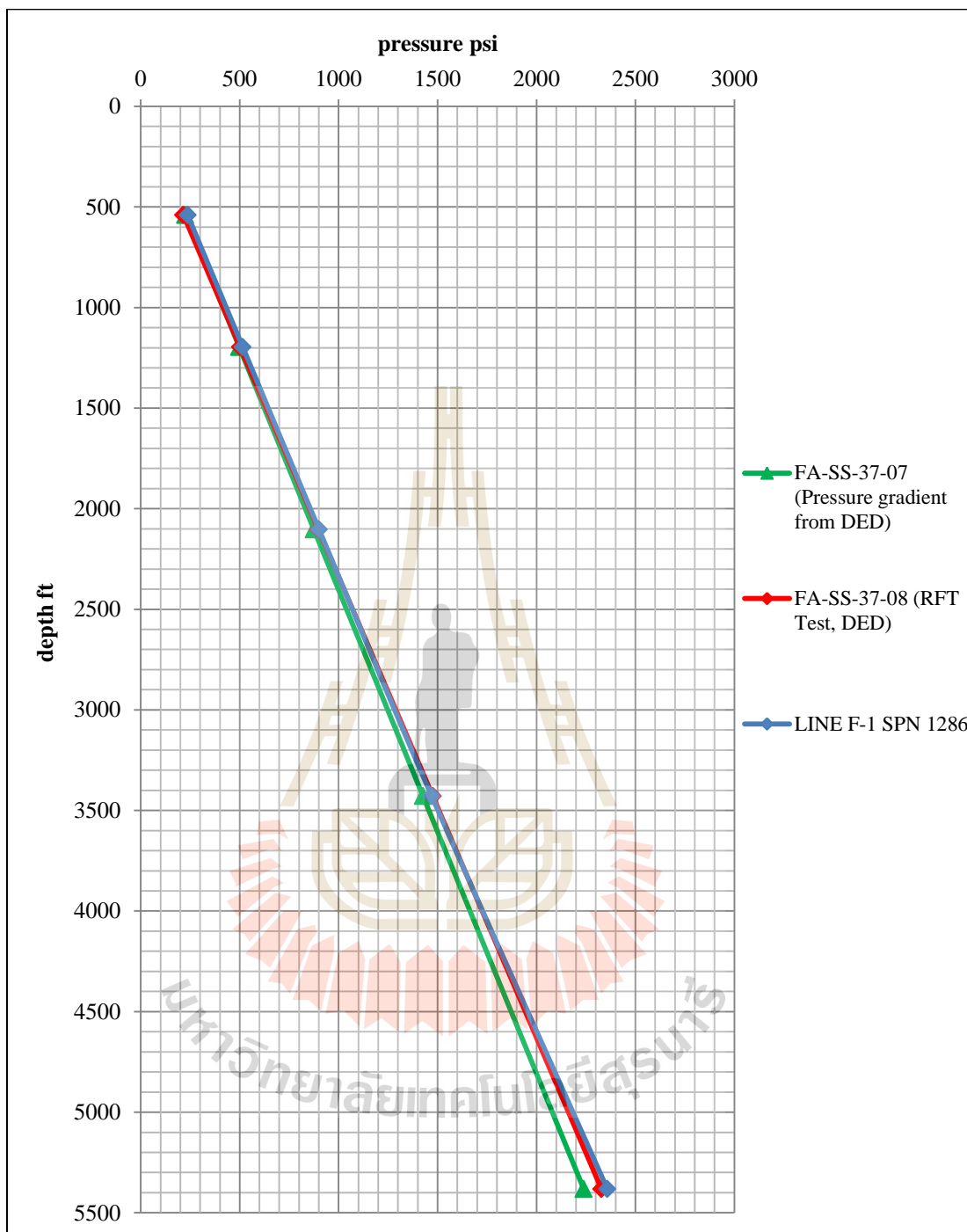
Figure 4.68 Comparison between reference pressure and calculated pressure of line

F-1 shot point number 1286

Table 4.39 Pore pressure calculated from Line F-1 shot point number 1286

compared with reference pressure

Depth point (ft)	pressure psi		
	FA-SS-37-08	FA-SS-37-07	F-1 SPN 1286
541	216	225	237
1197	502	498	516
2103	898	875	901
3429	1476	1426	1471
5383	2329	2239	2359

Table 4.40 Erroneous percentage of pore pressure calculated from Line F-1 shot

point number 1286 compared with reference pressure

Error From (%)	FA-SS-37-08	FA-SS-37-07
541	9.91	5.39
1197	2.71	3.56
2103	0.40	3.00
3429	0.37	3.10
5383	1.28	5.33
Average Error (%)	2.94	4.08
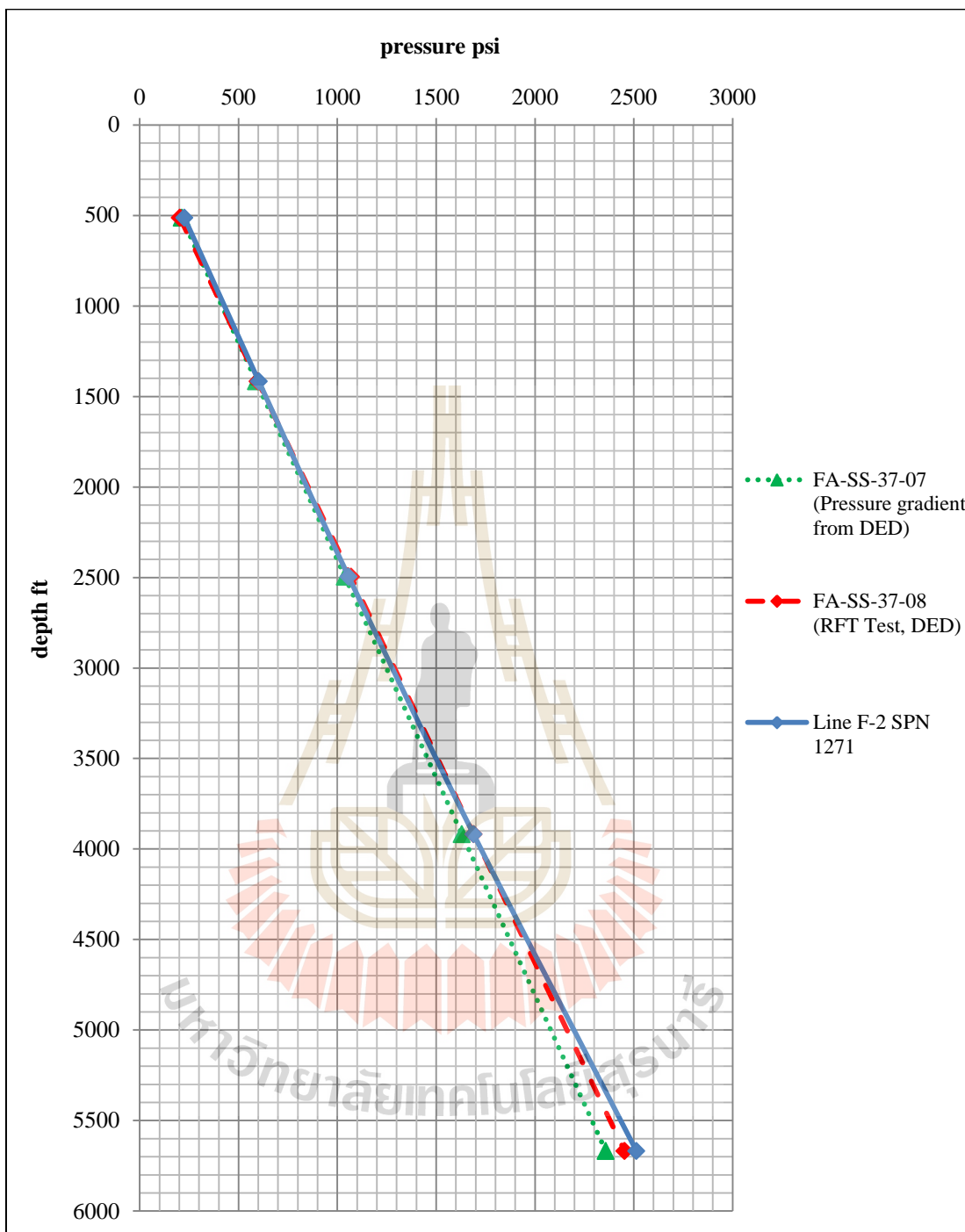
Figure 4.69 Comparison between reference pressure and calculated pressure of line

F-2 shot point number 1271

Table 4.41 Pore pressure calculated from Line F-2 shot point number 1271

compared with reference pressure

Depth point (ft)	pressure psi		
	FA-SS-37-08	FA-SS-37-07	F-2 SPN 1271
513	204	214	226
1417	598	590	603
2497	1069	1039	1058
3919	1690	1630	1689
5669	2454	2358	2514

Table 4.42 Erroneous percentage of pore pressure calculated from Line F-2 shot

point number 1271 compared with reference pressure

| Error From (%)	FA-SS-37-08	FA-SS-37-07
513	11.13	6.02
1417	0.82	2.29
2497	1.10	1.82
3919	0.03	3.63
5669	2.45	6.59
Average Error (%)	3.11	4.07
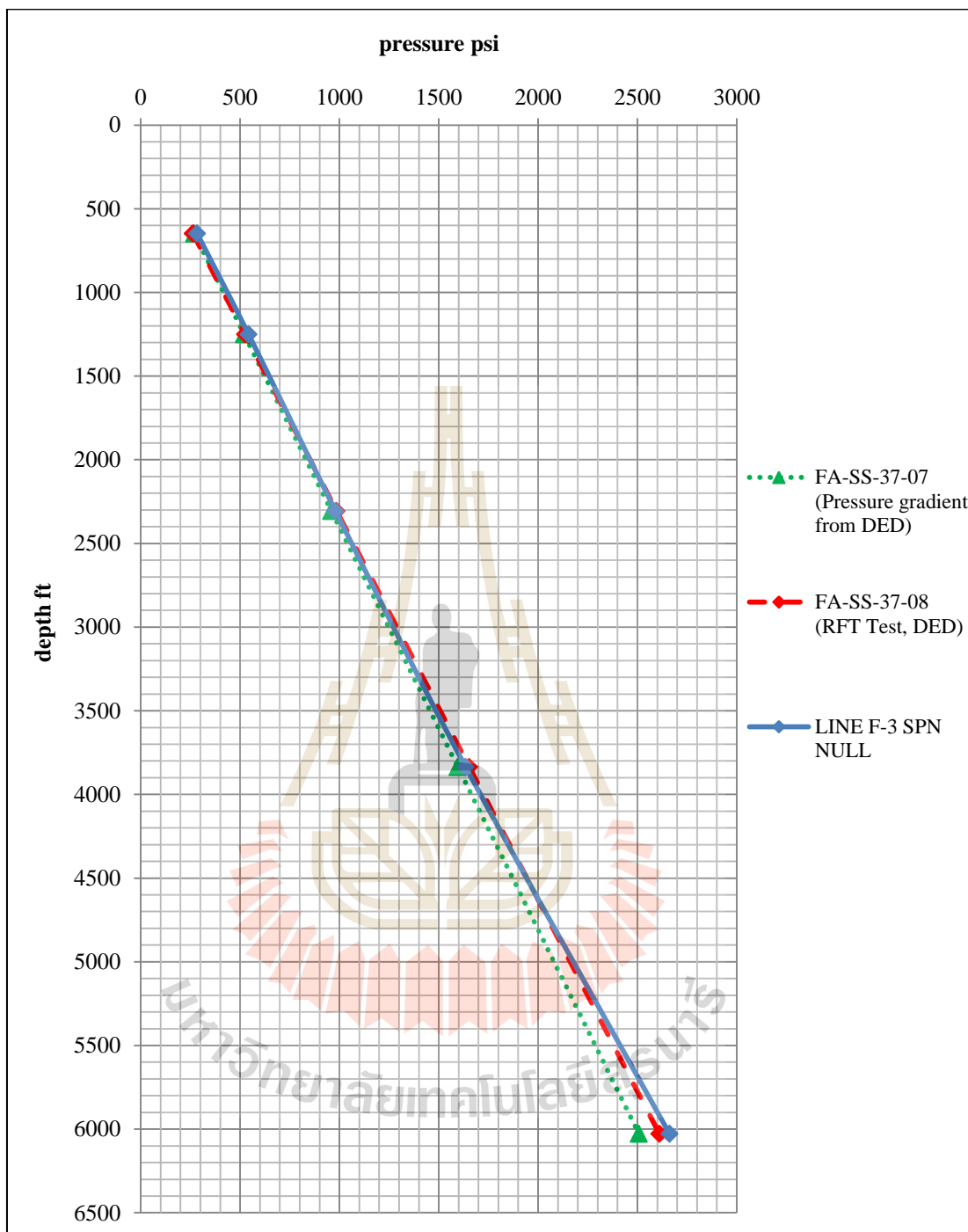
Figure 4.70 Comparison between reference pressure and calculated pressure of line

F-3 shot point number NULL

Table 4.43 Pore pressure calculated from Line F-3 shot point number NULL

compared with reference pressure

Depth point (ft)	pressure psi		
	FA-SS-37-08	FA-SS-37-07	F-3 SPN NULL
649	263	270	284
1251	526	520	543
2307	987	960	981
3836	1654	1596	1636
6029	2611	2508	2662

Table 4.44 Erroneous percentage of pore pressure calculated from Line F-3 shot

point number NULL compared with reference pressure

| Error From (%)	FA-SS-37-08	FA-SS-37-07
649	8.08	5.26
1251	3.27	4.31
2307	0.59	2.19
3836	1.11	2.48
6029	1.96	6.13
Average Error (%)	3.00	4.07
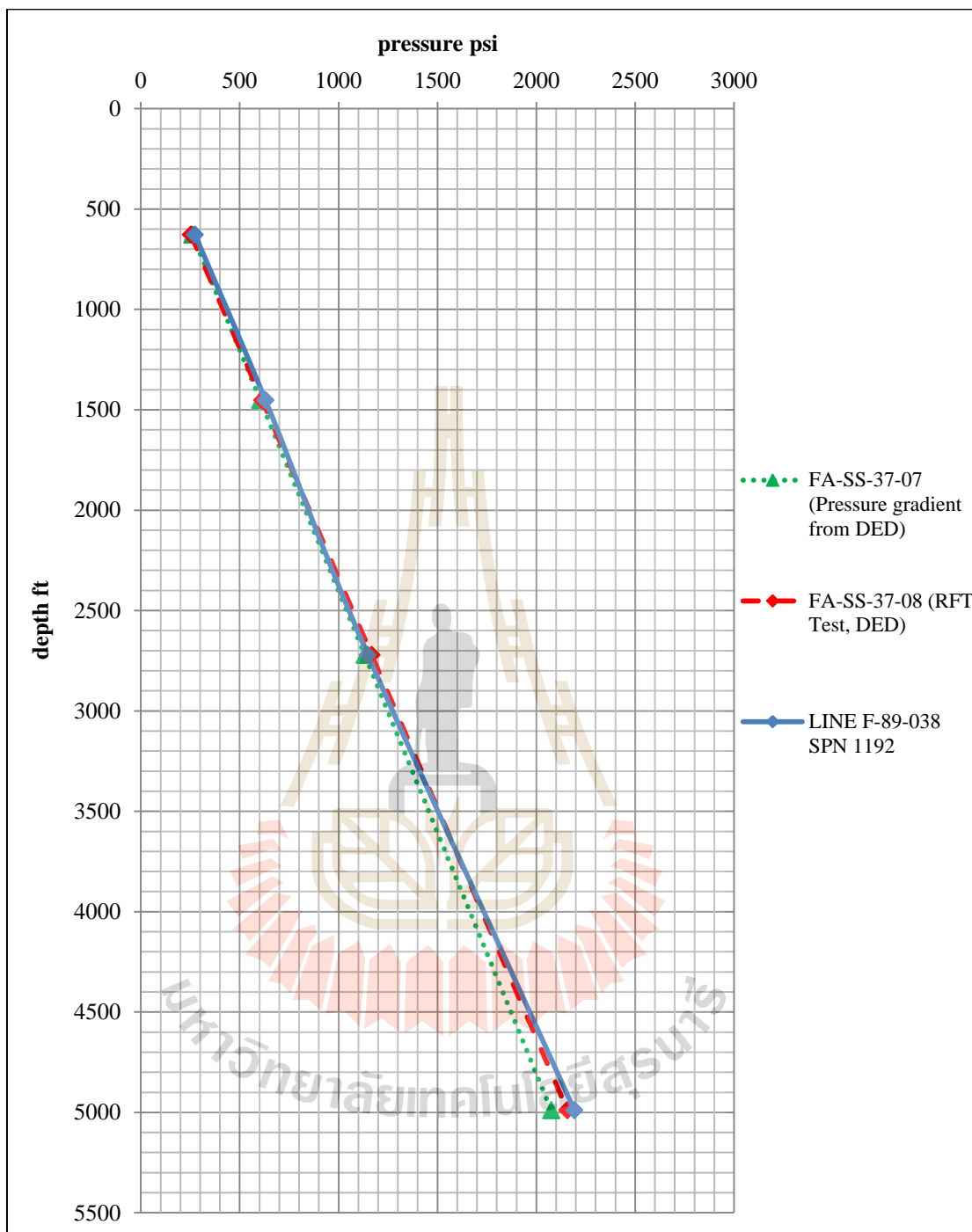
Figure 4.71 Comparison between reference pressure and calculated pressure of line

F-89-038 shot point number 1127

Table 4.45 Pore pressure calculated from Line F-89-038 shot point number 1192

compared with reference pressure

Depth point (ft)	pressure psi		
	FA-SS-37-08	**FA-SS-37-07**	**F-89-038 SPN 1192**
628	254	261	274
1453	614	605	631
2721	1167	1132	1149
4990	2157	2076	2193

Table 4.46 Erroneous percentage of pore pressure calculated from Line F-89-038

shot point number 1192 compared with reference pressure

| Error From (%)	FA-SS-37-08	FA-SS-37-07
628	7.94	4.85
1453	2.75	4.34
2721	1.60	1.46
4990	1.67	5.66
Average Error (%)	3.49	4.08
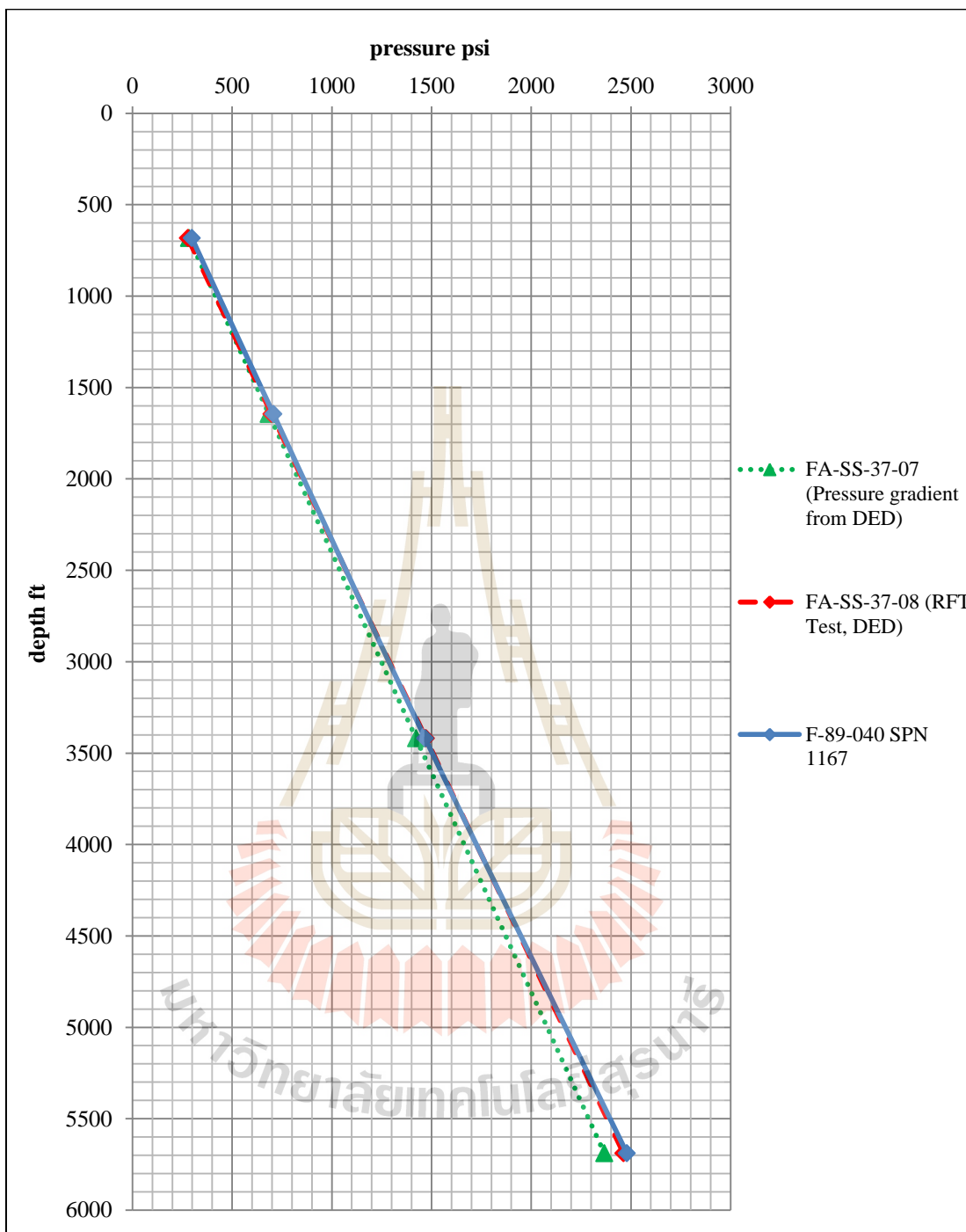
Figure 4.72 Comparison between reference pressure and calculated pressure of line

F-89-040 shot point number 1167

Table 4.47 Pore pressure calculated from Line F-89-040 shot point number 1167

compared with reference pressure

Depth point (ft)	pressure psi		
	FA-SS-37-08	FA-SS-37-07	F-89-040 SPN 1167
684	278	285	299
1645	698	684	707
3420	1472	1423	1469
5691	2463	2367	2481

Table 4.48 Erroneous percentage of pore pressure calculated from Line F-89-040

shot point number 1167 compared with reference pressure

Error From (%)	FA-SS-37-08	FA-SS-37-07
684	7.34	4.94
1645	1.40	3.37
3420	0.26	3.22
5691	0.71	4.78
Average Error (%)	2.42	4.08

Efficiency and accuracy of this method was displayed in erroneous percentage. From results above, maximum average error is 4.87 % whilst minimum average number is 1.24%. In general, these values are acceptable. This may prove and assure that prediction of pore pressure by using seismic data can use confidently in Fang basin.

CHAPTER V

CONCLUSION AND RECOMMENDATION

5.1   Conclusions

Pore pressure prediction by using seismic data based on Eaton's formula for pore pressure prediction and applied pore pressure transformation as 0.3 is applicable to San Sai oil field with acceptable accuracy. Number 0.3 was obtained from fitting graph between calculated pore pressure using sonic log from well FA-SS-37-08 and reference pressure obtained from RFT data at the same well.

Eaton's equation used to calculated pore pressure is

$$P_{pore} = OB_Z - [OB_Z - Pn_Z] \times \left(\frac{\Delta t_n}{\Delta t_O}\right)^{\alpha}$$

Therefore, in this study this equation was then modified to:

$$P_{pore} = (1 \times Z) - [(1 \times Z) - (0.433 \times Z)] \times \left(\frac{\Delta t_n}{\Delta t_O}\right)^{0.3}$$

where P_{pore} =   Predicted pore pressure (psi)

   OB =   Overburden pressure used 1 psi/ft

   Pn =   Normal pressure used 0.433 psi/ft

   Z =   Depth to point of measurement (ft)

Δt_n = The assumed normal sonic slowness at depth Z calculated from the Normal compaction trend line (μsec/ft)

Δt_o = The observed (measured) sonic slowness at depth Z (sec/ft)

α = Pore Pressure transformation exponent variable with age/basin location

Before calculate pore pressure, normal compaction trend line had to first generated by plot transit slowness (Δt, μsec/ft) and depth (ft) on semi-logarithmic graph. Corresponding linear equation that obtained from each shot point number in normal compaction trend line generating are showed in Table 5.1.

Table 5.1 Corresponding linear equation obtained from each shot point which is used to calculated normal sonic slowness (Δt_n, μsec/ft)

Seismic Line	Shot point number	Equation
S-2	1524	y = -17746ln(x) + 88174
	1560	y = -15831ln(x) + 78569
	1596	y = -11022ln(x) + 55376
S-3	1440	y = -10256ln(x) + 51632
	1476	y = -9385ln(x) + 47490
	1512	y = -9542ln(x) + 48565
F-89-031	1189	y = -8939ln(x) + 45445
	1257	y = -9497ln(x) + 48286
	1313	y = -9550ln(x) + 48837
F-1	1174	y = -10094ln(x) + 51173
	1231	y = -9091ln(x) + 46502
	1286	y = -8988ln(x) + 45983
F-2	1192	y = -10981ln(x) + 55766
	1227	y = -12927ln(x) + 65184
	1271	y = -11946ln(x) + 60269

Table 5.1 Corresponding linear equation obtained from each shot point which is used

to calculated normal sonic slowness (Δt_n, μsec/ft) (Continued)

Seismic Line	Shot point number	Equation
F-3	1228	y = -11713ln(x) + 59160
	1266	y = -10880ln(x) + 55103
	NULL	y = -10672ln(x) + 54104
F-89-038	1079	y = -8670ln(x) + 44086
	1127	y = -7176ln(x) + 36769
	1192	y = -6908ln(x) + 35341
F-89-040	1085	y = -9171ln(x) + 46598
	1131	y = -8361ln(x) + 42873
	1167	y = -8086ln(x) + 41330

Formation pore pressure gradient of study area is in range between 0.434 and

0.452 psi/ft. This is nearly close to the theoretical normal pressure 0.433 psi/ft.

Pressure gradient obtained from each shot point number are showed in Table 5.2.

Table 5.2 Pressure gradient obtained from each shot point calculated from its normal

sonic slowness (Δt_n, μsec/ft)

Seismic Line	Shot point number	Pressure Gradient (psi/ft)
S-2	1524	0.441
	1560	0.442
	1596	0.434
S-3	1440	0.452
	1476	0.452
	1512	0.442
F-89-031	1189	0.439
	1257	0.439
	1313	0.435

Table 5.2 Pressure gradient obtained from each shot point calculated from its normal

sonic slowness (Δt_n, $\mu sec/ft$) (Continued)

Seismic Line	Shot point number	Pressure Gradient (psi/ft)
F-1	1174	0.439
	1231	0.438
	1286	0.438
F-2	1192	0.449
	1227	0.443
	1271	0.450
F-3	1228	0.439
	1266	0.441
	NULL	0.441
F-89-038	1079	0.442
	1127	0.439
	1192	0.440
F-89-040	1085	0.442
	1131	0.436
	1167	0.436

Efficiency and accuracy of this method was showed in erroneous percentage. The erroneous percentage of pore pressure calculated from this method in study area compared with pressure obtained from well FA-SS-37-08 is in range between 1.42% and 4.87% and compared with well FA-SS 37-07 is in range between 1.24% and 4.81%. In general, these values are acceptable. This may prove and assure that prediction of pore pressure by using seismic data can use confidently in Fang basin.

Dependability of this research is in range with in depth between 1000 and 5000 ft. These because at depth over 1000 ft, it is in Mae Fang formation which is unconsolidated formation, P wave velocity is slow and affected to increase in

calculated pore pressure. On the other hand at depth below 5000 ft. calculated pore pressure tends to increase because it reaches the basement.

However, this relationship can only be applied to Fang basin due to its data source and geological characters of the study area.

5.2   Recommendations

In case of having more formation transit time data which obtained from seismic data, recorded and/or calculated from RFT or other well logging tools, this will enable to detect the area or depth that pressure alter from the normal pressure, both abnormal pressure zone and subnormal pressure zone, as illustrated in Figure 5.1 which is plotted from relationship of Δt and depth. From Figure 5.1 it can be notified that abnormal pressure zone depicts transit time higher than normal trend line whilst subnormal pressure zone depicts transit time lower than normal trend line.
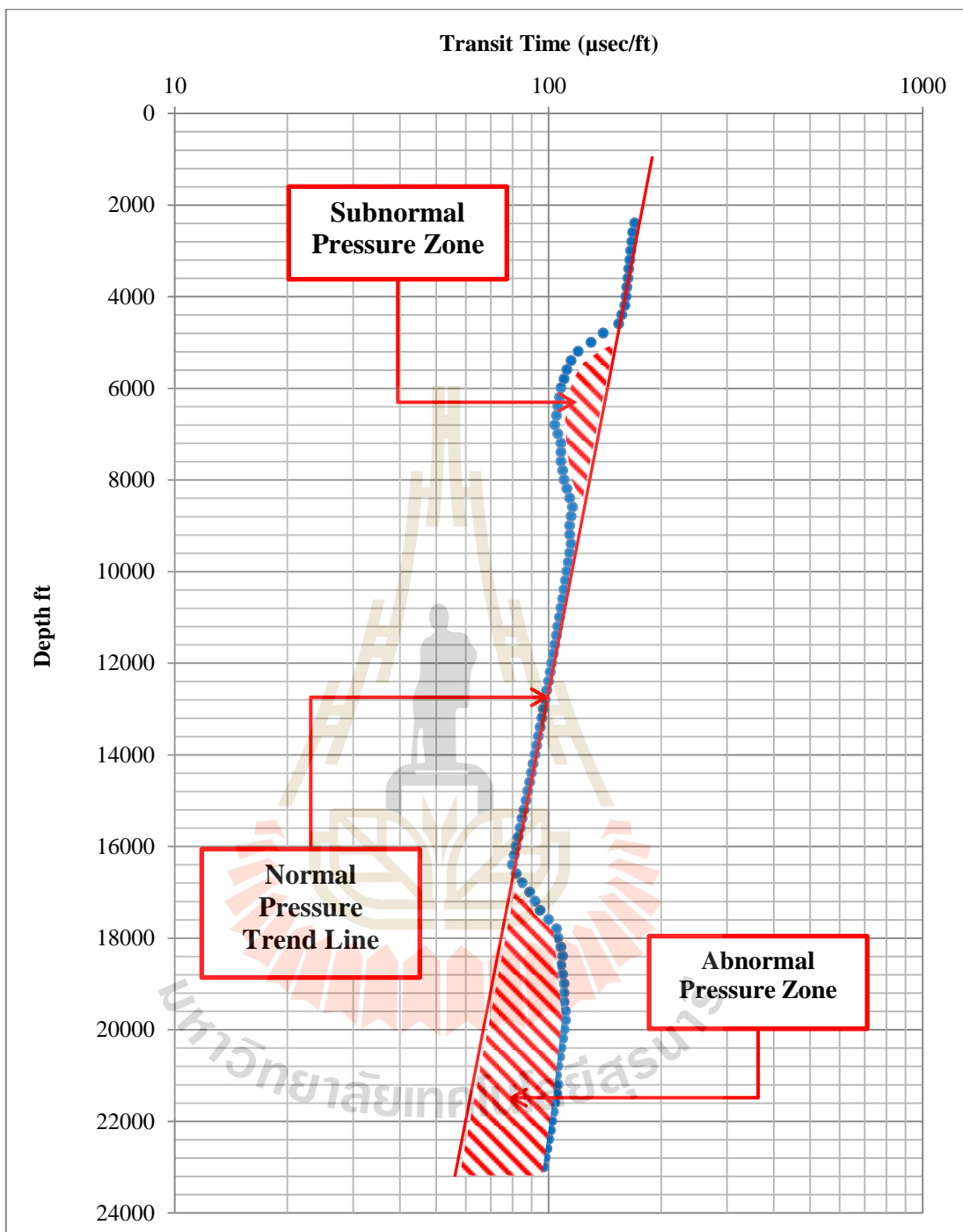
Figure 5.1 Relationships of transits time Δt and depth, that can be used for abnormal

and subnormal pressure zone detection

5.3 Further study

For the future work, there are some recommendations as listed below:

1. Calculated pore pressure should be modified if there are more seismic or other sonic data collected in same area.

2. Other electric wireline logs, e.g. sonic log, resistivity log and density log or other drilling data may be tried in the same way to calculated pore pressure.
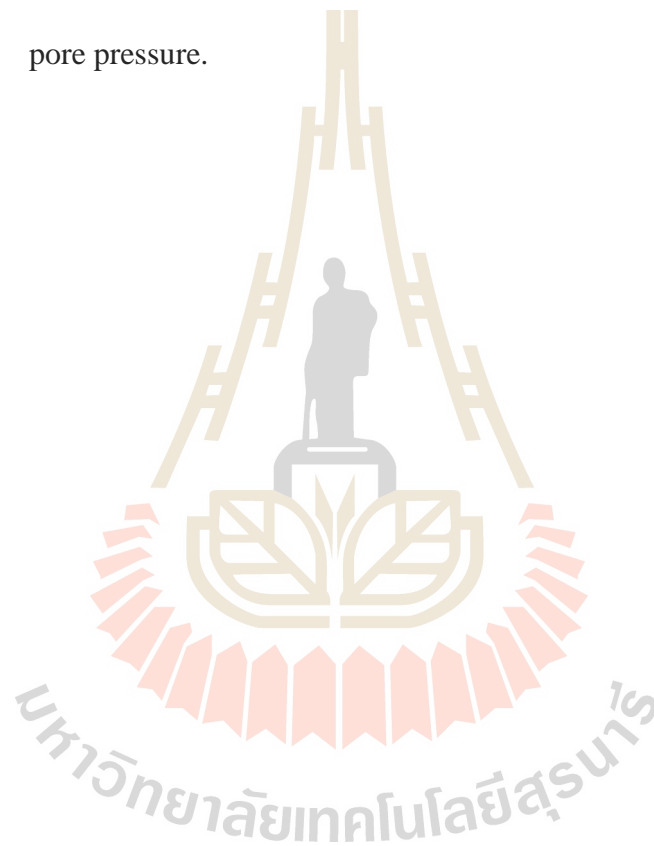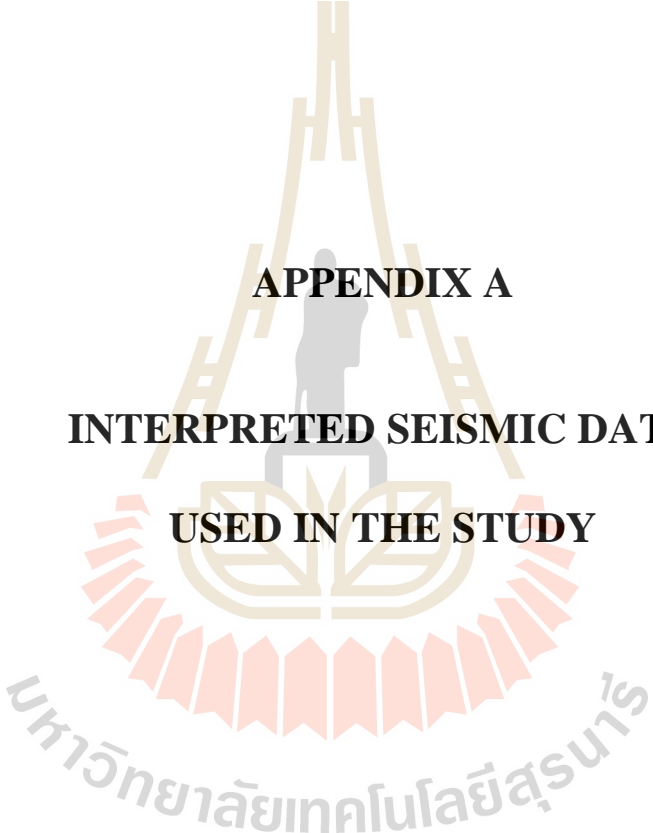
REFERENCES

Alexander E. Gurevich, George V. Chilingar, and Fred Aminzadeh (1994). Origin of the formation fluid pressure distribution and ways of improving pressure prediction methods. **Journal of Petroleum Science and Engineering.** 12(1): 67-77.

Aminzadeh, F., Chilingar, G.V., and Robertson Jr, J.O. (2002). Origin and Prediction of Abnormal Formation Pressures. **Developments in Petroleum Science** (vol. 50, pp. 169-190). Amsterdam: Elsevier Science Publishers.

Bourgoyne Jr, A.T., Millheim, K.K., Chenevert, M.E., and Young Jr, F.S. (1986). Formation pore pressure and fracture resistance. **Applied Drilling Engineering** (Vol. 2, pp. 246-299). Society of Petroleum Engineers publisher.

Bunapas, S., and Vella, P. (1983). Opening of the Gulf of Thailand Riffing of Continental S.E. Asia and Late Cenozoic Tectonics. **Journal of Thailand Geology Society**. 6(1): 1-12.

Daniel, R. B. (2001). Pressure prediction for a Central Graben wildcat well, UK North Sea. **Marine and Petroleum Geology.** 18(2): 235-250.

Domenico, S. N. (1977). Elastic properties of unconsolidated porous sand reservoirs. **Geophysics** (vol. 42, pp. 1339–1368).

Dutta, N. C. (1987). Geopressure. **Social of Exploration Geophysics reprint series** (Vol. 7, 365 p.)

Dutta, N.C. (1997). Pressure prediction from seismic data: implications for seal distribution and hydrocarbon exploration and exploitation in the deepwater Gulf of Mexico. **Norwegian Petroleum Society Special Publications** (vol.7, pp. 187-199). Amsterdam: Elsevier Science Publishers.

Dutta, N.C., and Khazanehdari, J. (2006). Estimation of formation fluid pressure using high-resolution velocity from inversion of seismic data and a rock physics model based on compaction and burial diagenesis of shales. **The Leading Edge.** 25(12): 1528-1539.

Dutta, N.C., Mukerji, T., Prasad, M., and Dvorkin, J. (2002). Seismic Detection and Estimation of Overpressures. Part I: the Rock Physics Basis. **Canadian Society of Exploration Geophysics (CSEG) Recorder.** 27(7): 34-57.

Dutta, N.C., Mukerji, T., Prasad, M., and Dvorkin, J. (2002). Seismic Detection and Estimation of Overpressures. Part II: Field Applications. **Canadian Society of Exploration Geophysics (CSEG) Recorder.** 27(7): 58-73.

Dvorkin, J., Mavko, G., and Nur, A. (1991). The effect of cementation on the elastic properties of granular material. **Mechanics of materials** (vol. 12, pp. 207–217).

Eaton, B. A. (1972). The effect of overburden stress on geopressure prediction from well Logs. **Journal of Petroleum Technology** 24(8): 929-934.

Fertl, W. H. (1976). Abnormal formation pressures. **Developments in Petroleum Science** (vol. 2, 382 p.). Amsterdam: Elsevier.

Fjær, E., Holt, R., Horsrud, P., Raaen, A. M., and Risnes, R., (1992), Petroleum related rock mechanics. **Developments in Petroleum Science** (vol. 1, 338 p.). Amsterdam: Elsevier.

Jeffrey Chung-Chen Kao (2009). **Deep Water Gulf of Mexico Pore Pressure Estimation Utilizing P-SV Waves from Multicomponent Seismic in Atlantis Field**. Master thesis, School of geological science, The University of Texas at Austin, United State.

Kumar, K.M., Ferguson, R.J., Ebrom, D., and Heppard, P. (2006). Pore pressure prediction using an Eaton's approach for PS waves**. Proceeding of 2006 Annual Meeting of Society of Exploration Geophysicists**. Louisiana, United State.

Magara, K. (1979). Calculation of pore pressure by shale compaction data. **Compaction and fluid migration: practical petroleum geology** (vol. 9, p. 66). Amsterdam: Elsevier Science Publishers.

Mindlin, R. D., and Deresiewicz, H. (1953). Elastic spheres in contact under varying oblique forces. **ASME Journal of Applied Mechanics** (vol. 20, pp. 327–344).

Øyvind Kvam (2005). **Pore pressure estimation from single and repeated seismic data sets**. Ph.D. Dissertation, Department of Petroleum Engineering and Applied Geophysics, Norwegian University of Science and Technology, Norway.

Pennebaker, E. S. (1968). An Engineering Interpretation of Seismic Data. **Proceeding of 43rd Annual Fall Meeting of Society of Petroleum Engineers.** SPE Paper no. 2165. 12 p.

Pennebaker, E. S. (1968). Seismic data indicate depth, magnitude of abnormal pressures. **World Oil** (vol. 166, pp. 73–78).

Reynolds, E. B. (1970). Predicting overpressured zones with seismic data. **World Oil** (vol. 171, pp. 78–82).

Rungsun Nuntajun (2008). **Seismic Stratigraphy of the Fang Basin, Chiang Mai, Thailand.** Master thesis, Department of Geological Sciences, Faculty of Science, Chiang Mai, Thailand.

Sayers, C., Johnson, G., and Denyer, G. (2002). Predrill pore-pressure prediction using seismic data. **Geophysics.** 67(4): 1286-1292.

Sayers C., Woodward, M., and Bartman, R. (2002). Seismic pore-pressure prediction using reflection tomography and 4-C seismic data**. The Leading Edge.** (21): 188-192.

Settakul, N. (1985). **Petroleum Geology of Fang Basin Part I**: Geology Section Division of Oil Exploration and Production, Defense Energy Department. (Unpublished Report).

Smith, J. E., (1971). The dynamics of shale compaction and evolution of pore-fluid pressures. **Mathematical Geology** (vol. 3, pp. 239–263).

Terzaghi, K. (1943) **Theoretical Soil Mechanics.** New York: John Wiley and Sons.

Yodton, K. (2009). **Hydrocarbon Seal Delineations by Pore Pressure Prediction from Reflection Seismic Data in an area of The Pattani Basin, The Gulf of Thailand**. Master thesis, Department of Geological Sciences, Faculty of Science, Chiang Mai, Thailand.

Zollner, E., and Moller, U. (1996). **3D Seismic Interpretation of Central Fang Basin, Thailand**: Geology Section Division of Oil Exploration and Production, Defense Energy Department. (Unpublished Report).

APPENDIX A

INTERPRETED SEISMIC DATA

USED IN THE STUDY

Table A 1 Seismic data of line S-2 modified from seismic migration stack data sheet

CDP 1113/ SPN 1109						
Time mSec	V_{rms} MT/Sec	V_{int} MT/Sec	Depth MT	Depth FT	Thickness MT	Travel Time mSec
0	1801		0	0		
265	1945	1945	258	846	258	133
344	1982	2102	341	1119	83	39
593	2139	2339	632	2073	291	124
758	2239	2567	844	2769	212	83
850	2261	2435	956	3136	112	46
1115	2413	2847	1333	4373	377	132
2348	2780	3075	3229	10594	1896	617
5000	4500	5598	10651	34944	7422	1326
CDP 1213/ SPN 1159						
Time mSec	V_{rms} MT/Sec	V_{int} MT/Sec	Depth MT	Depth FT	Thickness MT	Travel Time mSec
0	1801		0	0		
302	1992	1992	301	988	301	151
387	2042	2211	395	1296	94	43
603	2198	2453	660	2165	265	108
759	2254	2459	852	2795	192	78
906	2308	2569	1041	3415	189	74
1081	2365	2641	1272	4173	231	87
2351	2780	3090	3234	10610	1962	635
5000	4500	5601	10651	34944	7417	1324
CDP 1314/ SPN 1208						
Time mSec	V_{rms} MT/Sec	V_{int} MT/Sec	Depth MT	Depth FT	Thickness MT	Travel Time mSec
0	1801		0	0		
317	1946	1946	309	1014	309	159
414	1996	2152	413	1355	104	48
618	2219	2614	680	2231	267	102
849	2307	2528	972	3189	292	116
988	2372	2736	1162	3812	190	69
1141	2495	2177	1405	4610	243	112
2345	2893	2336	3346	10978	1941	831
5000	4500	5545	10707	35128	7361	1328

Table A 1 Seismic data of line S-2 modified from seismic migration stack data sheet

(Continued)

CDP 1414/ SPN 1259						
Time mSec	V_{rms} MT/Sec	V_{int} MT/Sec	Depth MT	Depth FT	Thickness MT	Travel Time mSec
0	1798		0	0		
304	1917	1917	292	958	292	152
459	1987	2118	456	1496	164	77
604	2110	2460	634	2080	178	72
939	2329	2679	1083	3553	449	168
1048	2385	2822	1237	4058	154	55
1304	2490	2881	1605	5266	368	128
2338	2843	3234	3277	10751	1672	517
5000	4500	5563	10680	35039	7403	1331
CDP 1513/ SPN 1308						
Time mSec	V_{rms} MT/Sec	V_{int} MT/Sec	Depth MT	Depth FT	Thickness MT	Travel Time mSec
0	1802		0	0		
299	1988	1988	298	978	298	150
404	2042	2189	413	1355	115	53
599	2191	2472	654	2146	241	97
982	2392	2677	1166	3825	512	191
1101	2472	3054	1348	4423	182	60
1412	2531	2730	1772	5814	424	155
2336	2858	3296	3295	10810	1523	462
5000	4500	5554	10692	35079	7397	1332
CDP 1585/ SPN 1344						
Time mSec	V_{rms} MT/Sec	V_{int} MT/Sec	Depth MT	Depth FT	Thickness MT	Travel Time mSec
0	1797		0	0		
329	1980	1980	326	1070	326	165
499	2082	2267	519	1703	193	85
702	2215	2513	774	2539	255	101
1082	2400	2709	1288	4226	514	190
1206	2454	2883	1467	4813	179	62
1566	2627	3138	2032	6667	565	180
2349	2844	3235	3298	10820	1266	391
5000	4500	5571	10682	35046	7384	1325

Table A 1 Seismic data of line S-2 modified from seismic migration stack data sheet

(Continued)

CDP 1657/ SPN 1380						
Time mSec	V_{rms} MT/Sec	V_{int} MT/Sec	Depth MT	Depth FT	Thickness MT	Travel Time mSec
0	1805		0	0		
494	2132	2132	527	1729	527	247
735	2285	2571	837	2746	310	121
955	2406	2773	1142	3747	305	110
1361	2576	2938	1738	5702	596	203
1446	2607	3061	1858	6096	120	39
1756	2704	3117	2351	7713	493	158
2320	2859	3269	3280	10761	929	284
5000	4500	5542	10706	35125	7426	1340
CDP 1730/ SPN 1417						
Time mSec	V_{rms} MT/Sec	V_{int} MT/Sec	Depth MT	Depth FT	Thickness MT	Travel Time mSec
0	1797		0	0		
626	2253	2253	706	2316	706	313
838	2361	2655	987	3238	281	106
1003	2436	2786	1217	3993	230	83
1386	2523	2738	1741	5712	524	191
1549	2567	2915	1979	6493	238	82
1775	2700	3478	2372	7782	393	113
2344	2868	3339	3321	10896	949	284
5000	4500	5556	10699	35102	7378	1328
CDP 1815/ SPN 1459						
Time mSec	V_{rms} MT/Sec	V_{int} MT/Sec	Depth MT	Depth FT	Thickness MT	Travel Time mSec
0	1799		0	0		
650	2220	2220	722	2369	722	325
906	2306	2512	1043	3422	321	128
1056	2384	2810	1254	4114	211	75
1421	2592	3117	1823	5981	569	183
1676	2670	3069	2214	7264	391	127
1954	2750	3191	2658	8720	444	139
2337	2850	3314	3292	10801	634	191
5000	4500	5559	10693	35082	7401	1331

Table A 1 Seismic data of line S-2 modified from seismic migration stack data sheet

(Continued)

Time mSec	V$_{rms}$ MT/Sec	V$_{int}$ MT/Sec	Depth MT	Depth FT	Thickness MT	Travel Time mSec
CDP 1874/ SPN 1488						
0	1800		0	0		
745	2264	2264	844	2769	844	373
994	2369	2659	1175	3855	331	124
1143	2443	2889	1390	4560	215	74
1538	2619	3072	1997	6552	607	198
1732	2754	2652	2351	7713	354	133
2064	2831	3203	2883	9459	532	166
2337	2877	3244	3320	10892	437	135
5000	4500	5546	10704	35118	7384	1331
CDP 1945/ SPN 1524						
0	1800		0	0		
778	2254	2254	877	2877	877	389
943	2332	2670	1098	3602	221	83
1046	2472	2811	1237	4058	139	49
1480	2482	2729	1829	6001	592	217
1690	2548	2972	2141	7024	312	105
2108	2782	3576	2889	9478	748	209
2345	2865	3519	3305	10843	416	118
5000	4500	5558	10683	35049	7378	1327
CDP 2017/ SPN 1560						
0	1798		0	0		
878	2316	2316	1017	3337	1017	439
978	2364	2750	1155	3789	138	50
1088	2421	2879	1313	4308	158	55
1487	2565	2922	1896	6220	583	200
1695	2644	3152	2224	7297	328	104
2137	2789	3287	2950	9678	726	221
2368	2867	3508	3355	11007	405	115
5000	4500	5575	10691	35075	7336	1316

Table A 1 Seismic data of line S-2 modified from seismic migration stack data sheet

(Continued)

CDP 2090/ SPN 1596						
Time mSec	V_{rms} MT/Sec	V_{int} MT/Sec	Depth MT	Depth FT	Thickness MT	Travel Time mSec
0	1800		0	0		
912	2329	2329	1063	3488	1063	456
991	2372	2822	1174	3852	111	39
1100	2432	2922	1333	4373	159	54
1501	2689	3293	1993	6539	660	200
1737	2876	3859	2449	8035	456	118
2302	3185	3988	3575	11729	1126	282
2427	3266	4505	3857	12654	282	63
5000	4500	5412	10819	35495	6962	1286

Table A 2 Seismic data of line S-3 modified from seismic migration stack data sheet

Time mSec	V$_{rms}$ MT/Sec	V$_{int}$ MT/Sec	Depth MT	Depth FT	Thickness MT	Travel Time mSec
CDP 1114/ SPN 1058						
0	1801		0	0		
158	1894	1894	150	492	150	79
285	1941	1998	277	909	127	64
373	1986	2126	371	1217	94	44
455	2044	2290	464	1522	93	41
774	2268	2554	872	2861	408	160
1001	2495	3149	1229	4032	357	113
1416	2658	3016	1855	6086	626	208
5000	4500	5046	10897	35751	9042	1792
CDP 1215/ SPN 1110						
0	1799		0	0		
176	1903	1903	168	551	168	88
301	980	2084	298	978	130	62
393	1995	2044	392	1286	94	46
535	2070	2265	553	1814	161	71
802	2213	2475	883	2897	330	133
1079	2547	3331	1345	4413	462	139
1411	2674	3051	1851	6073	506	166
5000	4500	5040	10895	35745	9044	1794
CDP 1319/ SPN 1162						
0	1801		0	0		
203	1895	1895	193	633	193	102
319	1932	1996	309	1014	116	58
419	1972	2095	413	1355	104	50
594	2105	2394	623	2044	210	88
829	2211	2459	912	2992	289	118
1072	2402	2963	1272	4173	360	121
1453	2676	3329	1906	6253	634	190
5000	4500	5061	10881	35699	8975	1773

Table A 2 Seismic data of line S-3 modified from seismic migration stack data sheet

(Continued)

CDP 1428/ SPN 1216						
Time mSec	V$_{rms}$ MT/Sec	V$_{int}$ MT/Sec	Depth MT	Depth FT	Thickness MT	Travel Time mSec
0	1797		0	0		
194	1910	1910	186	610	186	97
350	1972	2047	345	1132	159	78
490	2050	2234	502	1647	157	70
656	2144	2401	701	2300	199	83
865	2290	2698	983	3225	282	105
1098	2549	3340	1372	4501	389	116
1449	2659	2977	1894	6214	522	175
5000	4500	5063	10883	35705	8989	1775
CDP 1517/ SPN 1265						
Time mSec	V$_{rms}$ MT/Sec	V$_{int}$ MT/Sec	Depth MT	Depth FT	Thickness MT	Travel Time mSec
0	1795		0	0		
252	1980	1980	250	820	250	126
385	2063	2212	397	1302	147	66
493	2109	2266	519	1703	122	54
623	2124	2180	661	2169	142	65
828	2204	2432	910	2986	249	102
1100	2432	3022	1321	4334	411	136
1492	2605	3039	1917	6289	596	196
5000	4500	5097	10856	35617	8939	1754
CDP 1590/ SPN 1299						
Time mSec	V$_{rms}$ MT/Sec	V$_{int}$ MT/Sec	Depth MT	Depth FT	Thickness MT	Travel Time mSec
0	1798		0	0		
231	1936	1936	224	735	224	116
377	1994	2083	376	1234	152	73
593	2145	2386	634	2080	258	108
804	2269	2586	907	2976	273	106
917	2348	2848	1067	3501	160	56
1213	2601	3263	1550	5085	483	148
1581	3710	3042	2110	6923	560	184
5000	4500	5121	10863	35640	8753	1709

Table A 2 Seismic data of line S-3 modified from seismic migration stack data sheet

(Continued)

CDP 1662/ SPN 1332						
Time mSec	V_{rms} MT/Sec	V_{int} MT/Sec	Depth MT	Depth FT	Thickness MT	Travel Time mSec
0	1798		0	0		
263	1994	1994	263	863	263	132
403	2117	2331	426	1398	163	70
601	2238	2467	670	2198	244	99
855	2297	2431	979	3212	309	127
1068	2439	2941	1292	4239	313	106
1233	2577	3335	1567	5141	275	82
1528	2684	3092	2023	6637	456	147
5000	4500	5099	5099	16729	3076	603
CDP 1733/ SPN 1367						
Time mSec	V_{rms} MT/Sec	V_{int} MT/Sec	Depth MT	Depth FT	Thickness MT	Travel Time mSec
0	1806		0	0		
286	1987	1987	285	935	285	143
447	2072	2215	463	1519	178	80
564	2164	2485	608	1995	145	58
789	2306	2629	904	2966	296	113
1050	2545	3160	1316	4318	412	130
1210	2605	2969	1554	5098	238	80
1447	2681	3040	1914	6280	360	118
5000	4500	5057	10897	35751	8983	1776
CDP 1805/ SPN 1404						
Time mSec	V_{rms} MT/Sec	V_{int} MT/Sec	Depth MT	Depth FT	Thickness MT	Travel Time mSec
0	1803		0	0		
272	1952	1952	266	873	266	136
454	2055	2200	466	1529	200	91
614	2121	2298	650	2133	184	80
803	2273	2709	906	2972	256	94
999	2477	3179	1217	3993	311	98
1126	2570	3209	1421	4662	204	64
1491	2652	2891	1949	6394	528	183
5000	4500	5086	10872	35669	8923	1754

Table A 2 Seismic data of line S-3 modifiedfrom seismic migration stack data sheet

(Continued)

CDP 1876/ SPN 1440						
Time mSec	V$_{rms}$ MT/Sec	V$_{int}$ MT/Sec	Depth MT	Depth FT	Thickness MT	Travel Time mSec
0	1802		0	0		
307	2006	2006	308	1010	308	154
481	2117	2313	510	1673	202	87
581	2195	2568	638	2093	128	50
776	2270	3454	877	2877	239	69
1017	2464	3205	1239	4065	362	113
1106	2500	2880	1367	4485	128	44
1385	2609	3003	1786	5860	419	140
5000	4500	5040	10896	35748	9110	1808
CDP 1948/ SPN 1476						
Time mSec	V$_{rms}$ MT/Sec	V$_{int}$ MT/Sec	Depth MT	Depth FT	Thickness MT	Travel Time mSec
0	1801		0	0		
333	1977	1977	330	1083	330	167
498	2095	2315	521	1709	191	83
628	2202	2572	688	2257	167	65
770	2258	2491	865	2838	177	71
992	2432	2958	1193	3914	328	111
1127	2523	3112	1403	4603	210	67
1426	2623	2970	1847	6060	444	149
5000	4500	5059	10886	35715	9039	1787
CDP 2020/ SPN 1512						
Time mSec	V$_{rms}$ MT/Sec	V$_{int}$ MT/Sec	Depth MT	Depth FT	Thickness MT	Travel Time mSec
0	1802		0	0		
315	2011	2011	317	1040	317	158
434	2087	2276	453	1486	136	60
576	2150	2333	618	2028	165	71
760	2226	2449	844	2769	226	92
1011	2360	2926	1186	3891	342	117
1110	2478	2460	1357	4452	171	70
1468	2730	3395	1964	6444	607	179
5000	4500	5057	10894	35741	8930	1766

Table A 2 Seismic data of line S-3 modified from seismic migration stack data sheet

(Continued)

Time mSec	V$_{rms}$ MT/Sec	V$_{int}$ MT/Sec	Depth MT	Depth FT	Thickness MT	Travel Time mSec
CDP 2093/ SPN 1548						
0	1802		0	0		
295	1993	1993	294	965	294	148
442	2085	2259	460	1509	166	73
579	2145	2329	620	2034	160	69
766	2221	2442	848	2782	228	93
1004	2317	2603	1158	3799	310	119
1126	2369	2760	1326	4350	168	61
1926	2682	3277	2150	7054	824	251
5000	4500	5154	10836	35551	8686	1685
CDP 2165/ SPN 1584						
Time mSec	V$_{rms}$ MT/Sec	V$_{int}$ MT/Sec	Depth MT	Depth FT	Thickness MT	Travel Time mSec
0	1801		0	0		
274	2025	2025	278	912	278	137
484	2086	2164	505	1657	227	105
594	2135	2339	634	2080	129	55
793	2253	2574	890	2920	256	99
999	2516	3341	1234	4049	344	103
1250	2632	3051	1617	5305	383	126
1630	2750	3107	2207	7241	590	190
5000	4500	5137	10862	35636	8655	1685

Table A 3 Seismic data of line F-1 modified from seismic migration stack data sheet

CDP 1550/ SPN 1074						
Time mSec	V_{rms} MT/Sec	V_{int} MT/Sec	Thickness MT	Depth MT	Depth FT	Travel Time mSec
0	1800		0		0	
77	1800	1800	69	69	227	39
194	1875	1923	112	182	596	59
466	2097	2242	305	487	1597	136
813	2355	2663	462	949	3113	174
1160	2581	3046	528	1477	4847	174
1683	2909	3530	923	2400	7875	262
2428	3245	3899	1452	3853	12640	373
3304	3467	4019	1760	5613	18415	438
5000	3651	3986	3380	8993	29505	848
CDP 1447/ SPN 1124						
Time mSec	V_{rms} MT/Sec	V_{int} MT/Sec	Thickness MT	Depth MT	Depth FT	Travel Time mSec
0	1800		0			
99	1800	1800	89	89	292	50
211	1878	1945	109	198	650	56
503	2066	2192	320	518	1700	146
905	2307	2577	518	1036	3399	201
1203	2494	2992	446	1482	4862	149
1752	2856	3522	967	2449	8034	275
2429	3193	3934	1332	3780	12403	339
3317	3434	4021	1785	5566	18260	444
5000	3629	3986	3354	8920	29265	842
CDP 1348/ SPN 1174						
Time mSec	V_{rms} MT/Sec	V_{int} MT/Sec	Thickness MT	Depth MT	Depth FT	Travel Time mSec
0	1800		0			
103	1800	1800	93	93	304	52
219	1878	1945	113	206	674	58
519	2056	2177	327	532	1746	150
929	2294	2564	526	1058	3470	205
1261	2506	3022	502	1559	5116	166
1780	2850	3550	921	2481	8138	260
2424	3153	3869	1246	3726	12226	322
3320	3394	3974	1780	5507	18067	448
5000	3638	4078	3426	8932	29305	840

Table A 3 Seismic data of line F-1 modified from seismic migration stack data sheet

(Continued)

Time mSec	V$_{rms}$ MT/Sec	V$_{int}$ MT/Sec	Thickness MT	Depth MT	Depth FT	Travel Time mSec
CDP 1236/ SPN 1231
0	1800		0		0	
80	1800	1800	72	72	236	40
245	1855	1882	155	227	746	83
538	1996	2107	309	536	1758	147
807	2138	2397	322	858	2816	135
1230	2432	2912	616	1474	4837	212
1721	2780	3504	860	2334	7659	246
2434	3195	4025	1435	3769	12367	357
3302	3434	4030	1749	5518	18105	434
5000	3648	4032	3423	8942	29336	849

Time mSec	V$_{rms}$ MT/Sec	V$_{int}$ MT/Sec	Thickness MT	Depth MT	Depth FT	Travel Time mSec
CDP 1125/ SPN 1286
0	1800		0		0	
98	1800	1800	88	88	289	49
261	1851	1881	153	242	792	82
494	1980	2116	247	488	1601	117
752	2123	2373	306	794	2605	129
1118	2344	2743	502	1296	4252	183
1545	2618	3228	689	1985	6513	214
2363	3096	3840	1571	3556	11666	409
3314	3417	4108	1953	5509	18075	476
5000	3662	4102	3458	8967	29420	843

Time mSec	V$_{rms}$ $_M$T/Sec	V$_{int}$ MT/Sec	Thickness MT	Depth MT	Depth FT	Travel Time mSec
CDP 1348/ SPN 1174
0	1800		0		0	
88	1800	1800	79	79	260	44
262	1854	1881	164	243	797	87
492	1985	2125	244	487	1598	115
744	2121	2365	298	785	2576	126
1112	2347	2748	506	1291	4235	184
1545	2622	3223	698	1989	6524	217
2366	3091	3821	1569	3557	11670	411
3315	3408	4093	1942	5499	18042	475
5000	3646	4074	3432	8932	29303	843

Table A 4 Seismic data of line F-2 modified from seismic migration stack data sheet

Time mSec	V_{rms} MT/Sec	V_{int} MT/Sec	Depth MT	Depth FT	Thickness MT	Travel Time mSec
CDP 1155/ SPN 1112						
0	1750		0	0		
268	1882	1882	253	830	253	134
509	2015	2154	512	1680	259	120
756	2197	2532	825	2707	313	124
1167	2380	2685	1376	4514	551	205
1747	2626	3062	2264	7428	888	290
2350	2822	3326	3267	10719	1003	302
5000	3700	4333	9007	29551	5740	1325
CDP 1235/ SPN 1152						
0	1750		0	0		
239	1856	1856	222	728	222	120
471	1979	2099	466	1529	244	116
702	2169	2513	756	2480	290	115
1152	2415	2756	1376	4514	620	225
1724	2616	2980	2228	7310	852	286
2330	2814	3314	3232	10604	1004	303
5000	3700	4328	9009	29557	5777	1335
CDP 1315/ SPN 1192						
0	1750		0	0		
257	1878	1878	242	794	242	129
504	2024	2166	509	1670	267	123
800	2247	2583	892	2927	383	148
1215	2433	2757	1463	4800	571	207
1685	2597	2980	2164	7100	701	235
2292	2796	3286	3161	10371	997	303
5000	3700	4320	9010	29560	5849	1354

Table A 4 Seismic data of line F-2 modified from seismic migration stack data sheet

(Continued)

Time mSec	V_{rms} MT/Sec	V_{int} MT/Sec	Depth MT	Depth FT	Thickness MT	Travel Time mSec
CDP 1395/ SPN 1227						
0	1750		0	0		
349	1967	1967	344	1129	344	175
636	2142	2338	679	2228	335	143
923	2295	2603	1053	3455	374	144
1280	2422	2724	1539	5049	486	178
1736	2589	3009	2225	7300	686	228
2279	2782	3325	3127	10259	902	271
5000	3700	4322	9006	29547	5879	1360
CDP 1475/ SPN 1271						
0	1750		0	0		
320	1954	1954	313	1027	313	160
526	2100	239	551	1808	238	996
855	2286	2556	971	3186	420	164
1179	2424	2756	1418	4652	447	162
1598	2577	2966	2038	6686	620	209
2228	2787	3260	3066	10059	1028	315
5000	3700	4296	9019	29590	5953	1386
CDP 1555/ SPN 1312						
0	1750		0	0		
264	1916	1916	253	830	253	132
444	2023	2171	449	1473	196	90
727	2189	2427	792	2598	343	141
1003	2329	2663	1160	3806	368	138
1374	2491	2884	1695	5561	535	186
2153	2764	3190	2937	9636	1242	389
5000	3700	4274	9020	29593	6083	1423

Table A 4 Seismic data of line F-2 modified from seismic migration stack data sheet

(Continued)

CDP 1635/ SPN 1352						
Time mSec	V_{rms} MT/Sec	V_{int} MT/Sec	Depth MT	Depth FT	Thickness MT	Travel Time mSec
0	1750		0	0		
278	1924	1924	268	879	268	139
422	2008	2161	424	1391	156	72
701	2174	2404	759	2490	335	139
977	2325	2671	1127	3698	368	138
1201	2424	2816	1443	4734	316	112
2093	2744	3124	2836	9304	1393	446
5000	3700	4258	9024	29606	6188	1453

Table A 5 Seismic data of line F-3 modified from seismic migration stack data sheet

CDP 1546/ SPN 1046						
Time mSec	V_{rms} MT/Sec	V_{int} MT/Sec	Thickness MT	Depth MT	Depth FT	Travel Time mSec
0	1800		0		0	
104	1800	1800	94	94	307	52
316	1975	2056	218	312	1022	106
707	2271	2485	486	797	2616	196
1137	2537	2923	628	1426	4678	215
1582	2751	3235	720	2146	7039	223
2154	2990	3569	1021	3166	10388	286
2823	3188	3756	1256	4423	14510	335
3656	3394	4015	1672	6095	19997	417
5000	3533	3887	2612	8707	28566	672
CDP 1440/ SPN 1098						
Time mSec	V_{rms} MT/Sec	V_{int} MT/Sec	Thickness MT	Depth MT	Depth FT	Travel Time mSec
0	1800		0			
104	1800	1800	94	94	307	52
293	1929	1997	189	282	926	95
717	2178	2335	495	777	2550	212
1197	2462	2834	680	1457	4782	240
1661	2735	3338	774	2232	7323	232
2229	2997	3658	1039	3271	10731	284
2908	3239	3931	1335	4605	15109	340
3656	3368	3829	1432	6037	19808	374
5000	3519	3901	2621	8659	28408	672
CDP 1366/ SPN 1136						
Time mSec	V_{rms} MT/Sec	V_{int} MT/Sec	Thickness MT	Depth MT	Depth FT	Travel Time mSec
0	1800		0			
104	1800	1800	94	94	307	52
308	1942	2011	205	299	980	102
715	2213	2398	488	787	2581	204
1197	2504	2883	695	1482	4861	241
1686	2779	3359	821	2303	7555	245
2206	3008	3654	950	3253	10672	260
2906	3234	3861	1351	4604	15106	350
3631	3363	3837	1391	5995	19669	363
5000	3510	3873	2651	8646	28367	685

Table A 5 Seismic data of line F-3 modified from seismic migration stack data sheet

(Continued)

Time mSec	V_{rms} MT/Sec	V_{int} MT/Sec	Thickness MT	Depth MT	Depth FT	Travel Time mSec
CDP 1292/ SPN 1172						
0	1800		0		0	
97	1804	1804	87	87	287	49
311	1938	1996	214	301	988	107
721	2194	2370	486	787	2582	205
1126	2386	2695	546	1333	4372	203
1595	2606	3071	720	2053	6735	235
2052	2818	2458	562	2614	8578	229
2819	3100	3752	1439	4053	13298	384
3606	3327	4037	1589	5642	18510	394
5000	3505	3929	2739	8380	27495	697
CDP 1180/ SPN 1228						
0	1800		0		0	
94	1800	1800	85	85	278	47
294	1917	1970	197	282	924	100
525	2064	2238	258	540	1772	116
956	2297	2553	550	1090	3577	216
1335	2491	2924	554	1644	5395	190
1821	2738	3324	808	2452	8045	243
2590	3020	3601	1385	3837	12588	385
3505	3285	3940	1803	5639	18501	458
5000	3494	3941	2946	8585	28166	748
CDP 1106/ SPN 1266						
0	1800		0			
141	1800	1800	127	127	416	71
283	1897	1989	141	268	880	71
490	2012	2160	224	492	1613	104
839	2206	2453	428	920	3017	175
1192	2426	2883	509	1429	4687	177
1702	2672	3174	809	2238	7342	255
2444	2976	3578	1327	3565	11697	371
3415	3240	3825	1857	5422	17790	486
5000	3494	3987	3160	8582	28157	793

Table A 5 Seismic data of line F-3 modified from seismic migration stack data sheet

(Continued)

CDP 1001/ SPN NULL						
Time mSec	V_{rms} MT/Sec	V_{int} MT/Sec	Thickness MT	Depth MT	Depth FT	Travel Time mSec
0	1800		0			
143	1800	1800	129	129	422	72
283	1890	1978	138	267	877	70
496	2002	2142	228	495	1625	107
830	2211	2490	416	911	2989	167
1192	2424	2853	516	1428	4683	181
1704	2682	3204	820	2248	7374	256
2446	2971	3547	1316	3564	11692	371
3421	3239	3830	1867	5431	17818	488
5000	3484	3964	3130	8560	28085	790

Table A 6 Seismic data of line F-89-031 modified from seismic migration stack data

sheet

CDP 1753/ SPN NULL						
Time mSec	V$_{rms}$ MT/Sec	V$_{int}$ MT/Sec	Depth MT	Depth FT	Thickness MT	Travel Time mSec
0	1800		0	0		
61	1800	1800	55	180	55	31
189	1882	1920	178	584	123	64
366	1792	2064	361	1184	183	89
649	2099	2253	680	2231	319	142
1160	2409	2753	1383	4537	703	255
1737	2835	3540	2404	7887	1021	288
2511	3246	4019	3959	12989	1555	387
3416	3448	3955	5749	18862	1790	453
5000	3594	3891	8830	28970	3081	792
CDP 1692/ SPN 1061						
Time mSec	V$_{rms}$ MT/Sec	V$_{int}$ MT/Sec	Depth MT	Depth FT	Thickness MT	Travel Time mSec
0	1800		0	0		
61	1800	1800	55	180	55	31
189	1882	1920	178	584	123	64
366	1792	2064	361	1184	183	89
649	2099	2253	680	2231	319	142
1160	2409	2753	1383	4537	703	255
1737	2835	3540	2404	7887	1021	288
2511	3246	4019	3959	12989	1555	387
3416	3448	3955	5749	18862	1790	453
5000	3594	3891	8830	28970	3081	792
CDP 1615/ SPN 1101						
Time mSec	V$_{rms}$ MT/Sec	V$_{int}$ MT/Sec	Depth MT	Depth FT	Thickness MT	Travel Time mSec
0	1800		0	0		
82	1800	1800	74	243	74	41
181	1936	2042	175	574	101	49
342	2090	2251	357	1171	182	81
639	2216	2353	706	2316	349	148
1145	2502	2823	1420	4659	714	253
1747	2966	3691	2531	8304	1111	301
2508	3306	3979	4045	13271	1514	380
3399	3483	3939	5799	19026	1754	445
5000	3591	3811	8849	29032	3050	800

Table A 6 Seismic data of line F-89-031 modified from seismic migration stack data

sheet (Continued)

CDP 1550/ SPN 1132						
Time mSec	V_{rms} MT/Sec	V_{int} MT/Sec	Depth MT	Depth FT	Thickness MT	Travel Time mSec
0	1800		0	0		
70	1800	1800	63	207	63	35
211	1917	1973	203	666	140	71
609	2151	2303	546	1791	343	149
789	2342	2655	917	3009	371	140
1362	2664	3053	1792	5879	875	287
1890	2929	3552	2729	8953	937	264
2698	3330	4102	4386	14390	1657	404
3485	3493	4002	5961	19557	1575	394
5000	3708	4161	9113	29898	3152	758
CDP 1436/ SPN 1189						
Time mSec	V_{rms} MT/Sec	V_{int} MT/Sec	Depth MT	Depth FT	Thickness MT	Travel Time mSec
0	1800		0	0		
96	1800	1800	87	285	87	48
310	1929	1985	299	981	212	107
576	2126	2235	610	2001	311	139
899	2344	2690	1044	3425	434	161
1551	2768	3264	2108	6916	1064	326
2013	3009	3706	2964	9724	856	231
2705	3324	4106	4384	14383	1420	346
3592	3520	4060	6185	20292	1801	444
5000	3734	4232	9163	30062	2978	704
CDP 1300/ SPN 1257						
Time mSec	V_{rms} MT/Sec	V_{int} MT/Sec	Depth MT	Depth FT	Thickness MT	Travel Time mSec
0	1800		0	0		
90	1800	1800	81	266	81	45
281	1894	1937	266	873	185	96
585	2091	2258	610	2001	344	152
904	2283	2599	1024	3360	414	159
1617	2709	3168	2153	7064	1129	356
2094	3016	3880	3076	10092	923	238
2720	3296	4096	4361	14308	1285	314
3569	3516	4125	6168	20236	1807	438
5000	3698	4128	9055	29708	2887	699

Table A 6 Seismic data of line F-89-031 modified from seismic migration stack data

sheet (Continued)

Time mSec	V$_{rms}$ MT/Sec	V$_{int}$ MT/Sec	Depth MT	Depth FT	Thickness MT	Travel Time mSec
CDP 1190/ SPN 1313						
0	1800		0	0		
109	1800	1800	99	325	99	55
299	1898	1953	284	932	185	95
599	2060	2110	615	2018	331	157
941	2235	2513	1045	3428	430	171
4616	2629	3096	2090	6857	1045	338
2182	2957	3739	3148	10328	1058	283
2777	3210	4004	4339	14236	1191	297
3649	3422	4024	6093	19990	1754	436
5000	3601	4026	8825	28953	2732	679
CDP 1090/ SPN 1363						
0	1800		0	0		
98	1800	1800	89	292	89	49
293	1890	1934	277	909	188	97
658	2086	2231	684	2244	407	182
984	2251	2552	1100	3609	416	163
1664	2616	3069	2144	7034	1044	340
2206	2929	3730	3154	10348	1010	271
2814	3169	3919	4345	14255	1191	304
3699	3394	4027	6127	20102	1782	443
5000	3557	3985	8719	28606	2592	650
CDP 1002/ SPN NULL						
0	1800		0	0		
97	1800	1800	88	289	88	49
299	1909	1960	286	938	198	101
657	2098	2244	687	2254	401	179
983	2256	2545	1102	3615	415	163
1661	2615	3062	2140	7021	1038	339
2204	2926	3720	3150	10335	1010	272
2818	3162	3894	4345	14255	1195	307
3705	3387	4020	6127	20102	1782	443
5000	3541	3949	8684	28491	2557	648

Table A 7 Seismic data of line F-89-038 modified from seismic migration stack data

sheet

CDP 1097/ SPN 1079						
Time mSec	V_{rms} MT/Sec	V_{int} MT/Sec	Depth MT	Depth FT	Thickness MT	Travel Time mSec
0	1800		0	0		
1047	1800	1800	94	308	94	52
293	1891	1940	277	909	183	94
699	2188	2380	760	2493	483	203
1128	2528	3001	1404	4606	644	215
1654	2937	3664	2367	7766	963	263
2343	3366	4222	3822	12539	1455	345
3097	3627	4339	5458	17907	1636	377
4002	3838	4486	7487	24564	2029	452
5000	4039	4761	9863	32359	2376	499
CDP 1195/ SPN 1127						
Time mSec	V_{rms} MT/Sec	V_{int} MT/Sec	Depth MT	Depth FT	Thickness MT	Travel Time mSec
0	1800		0	0		
103	1800	1800	93	305	93	52
298	1879	1920	280	919	187	97
573	2064	2248	589	1932	309	137
945	2371	2779	1106	3629	517	186
1504	2822	3653	2071	6795	965	264
2223	3307	4142	3560	11680	1489	359
3087	3641	4385	5454	17894	1894	432
3983	3844	4474	7459	24472	2005	448
5000	4067	4843	9921	32549	2462	508
CDP 1324/ SPN 1192						
Time mSec	V_{rms} MT/Sec	V_{int} MT/Sec	Depth MT	Depth FT	Thickness MT	Travel Time mSec
0	1800		0	0		
91	1800	1800	82	269	82	46
313	1919	1966	301	988	219	111
567	2070	2243	585	1919	284	127
905	2409	2890	1074	3524	489	169
1399	2896	3623	1968	6457	894	247
2177	3419	4199	3602	11818	1634	389
3090	3723	4364	5593	18350	1991	456
3995	3904	4468	7615	24984	2022	453
5000	4104	4818	10036	32927	2421	502

Table A 8 Seismic data of line F-89-040 modified from seismic migration stack data

sheet

CDP 1831/ SPN 911						
Time mSec	V_{rms} MT/Sec	V_{int} MT/Sec	Depth MT	Depth FT	Thickness MT	Travel Time mSec
0	1800		0	0		
67	1800	1800	61	200	61	34
296	1945	1990	289	948	228	115
805	2292	2471	917	3009	628	254
1580	2990	3574	2302	7552	1385	388
2287	3446	4294	3820	12533	1518	354
2985	3636	4197	5391	17687	1571	374
3594	3749	4263	6682	21923	1291	303
4297	3851	4356	8048	26404	1366	314
5000	3940	4423	9669	31722	1621	366
CDP 1747/ SPN 953						
Time mSec	V_{rms} MT/Sec	V_{int} MT/Sec	Depth MT	Depth FT	Thickness MT	Travel Time mSec
0	1800		0	0		
72	1800	1800	65	213	65	36
301	1952	1998	294	965	229	115
834	2317	2500	901	2956	607	243
1511	2952	3583	2173	7129	1272	355
2168	3397	4248	3568	11706	1395	328
2839	3591	4157	4963	16283	1395	336
3500	3732	4286	6379	20928	1416	330
4202	3845	4365	7911	25955	1532	351
5000	3952	4474	9696	31811	1785	399
CDP 1657/ SPN 998						
Time mSec	V_{rms} MT/Sec	V_{int} MT/Sec	Depth MT	Depth FT	Thickness MT	Travel Time mSec
0	1800		0	0		
65	1800	1800	59	194	59	33
299	1896	1922	284	932	225	117
805	2270	2466	907	2976	623	253
1503	2875	3444	2109	6919	1202	349
2005	3255	4192	3161	10371	1052	251
2701	3556	4308	4660	15289	1499	348
3304	3706	4315	5961	19557	1301	302
4185	3862	4399	7898	25912	1937	440
5000	3982	4549	9752	31995	1854	408

Table A 8 Seismic data of line F-89-040 modified from seismic migration stack data

sheet (Continued)

CDP 1562/ SPN 1046						
Time mSec	V$_{rms}$ MT/Sec	V$_{int}$ MT/Sec	Depth MT	Depth FT	Thickness MT	Travel Time mSec
0	1800		0	0		
96	1800	1800	87	285	87	48
289	1947	2017	281	922	194	96
724	2179	2321	784	2572	503	217
1397	2788	3321	1904	6247	1120	337
1898	3177	4070	2923	9590	1019	250
2600	3542	4380	4460	14633	1537	351
3196	3684	4250	5724	18780	1264	297
4102	3849	4382	7711	25299	1987	453
5000	3973	4497	9730	31923	2019	449
CDP 1485/ SPN 1085						
Time mSec	V$_{rms}$ MT/Sec	V$_{int}$ MT/Sec	Depth MT	Depth FT	Thickness MT	Travel Time mSec
0	1800		0	0		
105	1800	1800	95	312	95	53
274	1885	1936	259	850	164	85
671	2148	2313	718	2356	459	198
1287	2648	3103	1673	5489	955	308
1806	3072	3931	2693	8835	1020	259
2496	3481	4375	4202	13786	1509	345
3702	3664	4338	5516	18097	1314	303
4008	3818	4304	7466	24495	1950	453
5000	3988	4612	9753	31998	2287	496
CDP 1392/ SPN 1131						
Time mSec	V$_{rms}$ MT/Sec	V$_{int}$ MT/Sec	Depth MT	Depth FT	Thickness MT	Travel Time mSec
0	1800		0	0		
93	1800	1800	84	276	84	47
292	1882	1920	275	902	191	99
642	2035	2155	652	2139	377	175
1216	2456	2855	1479	4852	827	290
1653	2836	3694	2278	7474	799	216
2393	3351	4284	3863	12674	1585	370
3037	3596	4389	5276	17310	1413	322
3940	3769	4301	7218	23681	1942	452
5000	3936	4503	9604	31509	2386	530

Table A 8 Seismic data of line F-89-040 modified from seismic migration stack data

sheet (Continued)

CDP 1318/ SPN 1167						
Time mSec	V$_{rms}$ MT/Sec	V$_{int}$ MT/Sec	Depth MT	Depth FT	Thickness MT	Travel Time mSec
0	1800		0	0		
101	1800	1800	91	299	91	51
341	1912	1958	326	1070	235	120
647	2100	2292	677	2221	351	153
1152	2480	2865	1408	4619	731	255
1510	2802	3651	2061	6762	653	179
2269	3344	4221	3663	12018	1602	380
3011	3634	4404	5297	17379	1634	371
3891	3776	4226	7156	23478	1859	440
5000	3961	4551	9679	31755	2523	554
CDP 1232/ SPN 1211						
Time mSec	V$_{rms}$ MT/Sec	V$_{int}$ MT/Sec	Depth MT	Depth FT	Thickness MT	Travel Time mSec
0	1800		0	0		
94	1800	1800	85	279	85	47
317	1949	2009	309	1014	224	111
654	2140	2306	697	2287	388	168
1094	2474	2901	1336	4383	639	220
1398	2794	3725	1902	6240	566	152
2218	3396	4230	3639	11939	1737	411
2978	3648	4300	5270	17290	1631	379
3893	3811	4299	7236	23740	1966	457
5000	4000	4604	9784	32100	2548	553
CDP 1108/ SPN 1273						
Time mSec	V$_{rms}$ MT/Sec	V$_{int}$ MT/Sec	Depth MT	Depth FT	Thickness MT	Travel Time mSec
0	1800		0	0		
101	1800	1800	91	299	91	51
306	1950	2020	298	978	207	102
612	2232	2453	678	2224	380	155
1019	2623	2127	1313	4308	635	299
1327	2891	2640	1874	6148	561	213
2134	3427	4061	3553	11657	1679	413
2943	3655	4198	5250	17224	1697	404
3865	3794	4208	7190	23589	1940	461
5000	3967	4502	9757	32011	2567	570

Table A 8 Seismic data of line F-89-040 modified from seismic migration stack data

sheet (Continued)

CDP 1001/ SPN null						
Time mSec	V$_{rms}$ MT/Sec	V$_{int}$ MT/Sec	Depth MT	Depth FT	Thickness MT	Travel Time mSec
0	1800		0	0		
101	1800	1800	91	299	91	51
306	1950	2020	298	978	207	102
312	2232	2483	678	2224	380	153
1019	2623	3121	1313	4308	635	203
1327	2891	3640	1874	6148	561	154
2134	3427	4161	3553	11657	1679	404
2943	3656	4198	5250	17224	1697	404
3855	3794	4208	7190	23589	1940	461
5000	3967	4507	9747	31978	2557	567

BIOGRAPHY

Mr. Adisorn Sridej was born on March 30, 1985 in Nakhon Sawan, Thailand. He earned his Bachelor's Degree in Engineering in Petrochemical and polymeric materials from Silpakorn University in 2008. After that, he then continued his Master's degree in Geotechnology at School of Geotechnology, Institute of Engineering, Suranaree University of Technology. He interested in drilling engineering and formation evaluation.